Molecular Dynamics Simulation Study of Lipid Membranes using Coarse-Grained Models

Yawen Zhang

Department of Chemistry

Imperial College London

September 30, 2014

Submitted in partial fulfilment of the requirements for the degree of Doctor of Philosophy of Imperial College London and the Diploma of Imperial College London

Declaration

I hereby declare that this thesis is a presentation of my original research work. Wherever contributions of other sources are involved, I confirm that this has been indicated to the best of my knowledge.

The copyright of this thesis rests with the author and is made available under a Creative Commons Attribution Non-Commercial No Derivatives licence. Researchers are free to copy, distribute or transmit the thesis on the condition that they attribute it, that they do not use it for commercial purposes and that they do not alter, transform or build upon it. For any reuse or redistribution, researchers must make clear to others the licence terms of this work.

Abstract

In this work we use coarse-grained molecular dynamics simulations to investigate how lipid composition affects the phase transition of phospholipid bilayers. We consider a fully hydrated membrane consisting of saturated 1,2-dipalmitoyl-*sn*-glycero-3-phosphocholine (DPPC) and cholesterol or unsaturated 1,2-dioleoyol-*sn*-glycero-3-phosphocholine (DOPC). We report structural, dynamic changes occurring in the model bilayer mixtures with varying temperature and composition.
Firstly we study the effect of cholesterol on the properties of a DPPC bilayer. We have combined the computations of area per lipid, radial distribution function, chain order parameter and Voronoi construction to quantify the phase transitions, and the coarse-grained (CG) model is found to quantitatively reproduce most of the experimental observations. Based on the changes in the structural and dynamic properties, a temperature-composition phase diagram of DPPC/cholesterol is proposed and compared with the experiments.
'Thread-like' cholesterol clusters in the bilayer at high cholesterol concentrations are observed and the origin of this specific lateral organisation is discussed. To explore the role of the CG bead size, a series of simulations varying the cholesterol cross sectional areas were performed. Parameters obtained from simulation of the different cholesterol isomorphs provide important insight into the microscopic degrees of freedom determining the cholesterol arrangement in the bilayer. The results for the modified cholesterols are further discussed in relation to naturally occurring sterols.
Finally, the effect of a mono-unsaturated phospholipid (DOPC) on the main melting phase transition is investigated. This analysis is performed by simulating bilayer systems which were constructed by

combining a gel phase DPPC bilayer and a fluid phase DOPC bilayer. The visual observations of the bilayers show that the gel and fluid phases coexist within a wide range of temperature and composition. A temperature-composition phase diagram with phase coexistences is proposed using the information extracted from structural and local composition analysis.

To my beloved parents, M. Zhang and S. Chen. Thank you for their endless love, belief, support and sacrifices.

And to my lovely grandparents, who will always hold a special place in my heart.

好雨知时节，当春乃发生。
随风潜入夜，润物细无声。

—杜甫

Acknowledgements

This thesis would not have been possible without the help and support from a host of people around me, and for this reason I would like to take this opportunity to express my gratitude to them.
First and foremost, I would like to express my deepest appreciation to my supervisors, Professor Fernando Bresme and Professor John Seddon. It is such a blessing and a great honour to have their constant guidance, endless advices and persistent help. Since I started to work in the group as an undergraduate, Fernando has supported me not only by providing an excellent research assistantship for almost five years, but also academically and emotionally through the hard time in my life. I am extremely grateful to have had all his guidance from my Master project up to this Ph.D thesis manuscript. John, who is an undoubtedly world renowned expert in Biophysics, has always been supportive since the days I began my working with this project. His sheer breadth and depth of understanding in Biophysics is a truly precious contribution to this work.
Next, I would like give my warmest thanks to Dr Anders Lervik, the former group member and an absolutely awesome scientist. Thank you for spending countless hours answering my endless questions. Many parts of the thesis would not have been possible without the valuable resource provided by him.
Also thank you to everyone in the Bresme group. Thank you to Jeff and Niall for proofreading and listening to me talk about my research. Thank you to Irene, Silvia, Anna-sofia for joining the ladies faction of the group. Thank you to James for expending the membrane subgroup. And thank you to my former neighbour, the 'permanent residence' Stefano, for helping me with all the MAC and Latex issues.

Thank you to all of you for being the best colleagues. It is a truly enjoyable experience for me to work with everyone of you.
Finally, I would like to acknowledge my family. Thank you for being the most supportive family. I feel so blessed to have all of you in my life. In particular my mother and father, Shufen Chen and Maolin Zhang, have given me the countless support, the greatest trust, lots of love and the determination required to move to the other side of the earth, with their endless sacrifices. I would also like to express my deep thanks the Week's family, Lily, Chris, Fei and Yan, for providing me with a home in Britain.

Contents

Contents 11

List of Figures 14

List of Tables 18

1 Introduction 19

References 32

2 Methodology 38

2.1 Molecular Dynamics (MD) simulation 38

2.1.1 The idea 39

2.1.2 Integrator 41

2.1.3 Initial conditions 42

2.1.4 Force calculation 44

2.1.4.1 Non-bonded interactions 44

2.1.4.2 Bonded interactions 45

2.1.5 Ensembles 46

2.1.6 Berendsen thermostat and barostat 47

2.1.7 Periodic Boundary Condition 49

2.1.8 Modified non-bonded and bonded interactions 50

2.2 MARTINI Coarse-Grained Force-field 53

2.2.1 Atom type and interactions 54

2.2.1.1 Non-bonded interactions 55

2.2.1.2 Bonded interactions 57

2.2.2 Interpretation of Time Scale . . . 59
2.3 Analysis . . . 62
2.3.1 Area per molecule . . . 62
2.3.2 Chain order parameter . . . 64
2.3.3 Radial distribution function . . . 65
2.3.4 Lateral diffusion coefficient . . . 66

References **68**

3 Phase behavior of DPPC/Cholesterol mixtures **73**
3.1 Introduction . . . 73
3.2 Simulation Methods . . . 76
3.2.1 Force-field and simulation details . . . 76
3.2.2 Analysis . . . 77
3.3 Results and discussion . . . 78
3.3.1 Phase transition in pure DPPC bilayers . . . 78
3.3.1.1 Gel formation . . . 79
3.3.1.2 Solid-liquid phase transition . . . 81
3.3.2 Impact of cholesterol on phase transition . . . 84
3.3.2.1 $S_o \rightarrow L_d$ transition and formation of L_o phase . . . 84
3.3.2.2 Phase transition across x_{chol} . . . 89
3.3.3 Lipid dynamics . . . 92
3.3.4 Investigation of possible S_o/L_o and L_o/L_d coexistences . . . 94
3.4 Conclusion . . . 98

References **100**

4 Effect of cholesterol modification on DPPC/Cholesterol bilayers **105**
4.1 Introduction . . . 105
4.2 Methods . . . 107
4.2.1 Force-field and simulation details . . . 107
4.2.2 Analysis . . . 109
4.3 Results and discussion . . . 110
4.3.1 Cholesterol cluster formation at $x_{CHOL} = 0.5$ . . . 110

4.3.2 Effect on phase transition at $x_{CHOL} = 0.2$ 118
4.4 Discussion and Conclusion 123

References **127**

5 Phase transition in DPPC/DOPC bilayers **131**
5.1 Introduction 131
5.2 Methodology 135
5.2.1 Force-field and simulation details 135
5.3 Results and Discussions 138
5.3.1 Phase behaviour of pure DOPC bilayers 138
5.3.2 Phase behaviour of asymmetric DPPC/DOPC bilayers . . 141
5.3.2.1 Lipid dynamics of asymmetric DPPC/DOPC bilayers 147
5.3.3 Self-assembled DPPC/DOPC bilayer at $x_{DOPC} = 0.5$ . . . 149
5.3.4 Phase behaviour of symmetric DPPC/DOPC bilayers . . . 150
5.3.4.1 $S_o \rightarrow L_d$ transition and domain formation 152
5.3.4.2 Exploring the S_o/L_d coexistence regions 157
5.4 Conclusions 160

References **162**

6 Conclusions **166**
6.1 DPPC/cholesterol bilayer 166
6.2 Modified MARTINI cholesterol model 168
6.3 DPPC/DOPC bilayer 169
6.4 Limitations 170
6.5 Future work 170

List of Figures

1.1 An example of a plant cell 20
1.2 Representations of model and real membranes 21
1.3 Comparison of chemical structure, 3D structure and cartoon of DPPC molecule 22
1.4 The chemical structure (left) and Van der waals representation (right) of a cholesterol molecule. 22
1.5 Illustration of a micelle, a lipid bilayer and a vesicle composed of two lipid layers exposed to water. 23
1.6 Dependence of phase transitions of lipid-water mixtures on hydration and temperature 24
1.7 An example of a binary phase diagram 26
1.8 An example of a schematic phase diagram of a phospholipid/cholesterol bilayer. Figure taken from reference [28] 27
1.9 The chemical structure of the unsaturated phospholipid DOPC, with the unsaturated *cis* bonds shown in the lipid tails. 29
1.10 An example of a schematic phase diagram for a binary mixture bilayer 29

2.1 Illustration of the MD simulation approach. 39
2.2 Schematic diagram showing an MD simulation stepwise 41
2.3 An example of the Maxwell-Boltzmann velocity distribution . . . 43
2.4 Periodic boundary conditions shown in two-dimensions. 50
2.5 The minimum image convention in two-dimensions. 52
2.6 Mapping between the real chemical structure and the CG sites . . 54
2.7 Coarse grained molecular models 55

2.8 Example plot of the Lennard-Jones potential function 56
2.9 Example plot of Coulombic potential function 58
2.10 A example plot of improper dihedral potential 59
2.11 Illustration of how Voronoi diagram is constructed 63
2.12 Voronoi construction applied to partition bilayer cross-sectional area 64
2.13 Representation of the observation of order parameter S_{chain} 65
2.14 Example plots of MSD vs. time 67

3.1 Snapshots showing the vertical positions C2A/C2B and R3 sites . 78
3.2 Time evolution of equilibration process and growth of gel phase DPPC 79
3.3 Time evolution showing the liquid-gel phase transformation of DPPC 80
3.4 Simulation results for a pure DPPC bilayer at various temperatures 82
3.5 Snapshot of pure DPPC bilayer (side view) showing the straightened lipid acyl chains at 285 K. 82
3.6 Time evolution of the half bilayer showing the gel-liquid phase transformation 84
3.7 Time evolution of equlibration process 84
3.8 Simulation results for DPPC/cholesterol bilayers at various temperatures 86
3.9 2D RDFs and snapshots of bilayers at various cholesterol compositions and temperatures 88
3.10 Simulation results for DPPC/cholesterol bilayers at various cholesterol compositions 89
3.11 2D RDFs showing the effect of cholesterol addition at constant temperatures 91
3.12 Mean square displacement (MSD) of DPPC/CHOL bilayers as a function of cholesterol content and temperature 93
3.13 Voronoi construction of the initial configuration (top-left) and configurations obtained after 10 μs at different temperatures 95
3.14 Histogram of cholesterol concentration at various temperatures . . 96
3.15 DPPC/CHOL phase diagram proposed in this work 97

4.1 Representations of CG DPPC/CHOL/water 108

4.2 Simulation results of DPPC/50% bilayer at various temperatures . 111
4.3 Probability distribution of cluster size found in lipid bilayers . . . 113
4.4 Snapshots of half bilayers show the asphericity of cholesterol clusters 114
4.5 Probablity of finding N nearest neighbours around a given cholesterol molecule 115
4.6 2D RDFs of cholesterol-cholesterol and cholesterol-DPPC 115
4.7 Number density functions of DPPC and cholesterol molecules . . 117
4.8 Tilt angle distribution between the bilayer normal and cholesterol 118
4.9 Simulation results of DPPC/20%cholestrol bilayers at various temperatures 119
4.10 2D RDF of DPPC-DPPC pair correlation and Voronoi construction of one monolayer for DPPC/CHO2 120
4.11 Voronoi construction of one monolayer for DPPC/CHOL ($x_{CHOL} = 0.2$) 121
4.12 Schematic diagram showing the interaction between DPPC and CHO1 or CHO2 124
4.13 Chemical structures of ergosterol, cholesterol and lanosterol. . . . 125

5.1 Comparison of CG DPPC and DOPC molecules 132
5.2 Representative phase diagrams for DPPC/DOPC bilayer reported from previous studies. 134
5.3 Time evolution showing the equlibration process 138
5.4 Simulation results for a pure DOPC bilayer at various temperatures. 139
5.5 The orientational order parameter of intra-molecular bonds 140
5.6 Asymmetric equi-molar DPPC/DOPC bilayer 142
5.7 Area per DPPC(A) and DOPC(B) lipid versus temperature for different molar fractions of DOPC from 0 to 1. 142
5.8 Average chain order parameter of DOPC(A) and DPPC(B) as a function of DOPC molar fraction and temperature. 143
5.9 Probability of the average chain order parameter in pure bilayers . 144
5.10 Probability of the average chain order parameter of mixture bilayers at $x_{\mathrm{DOPC}} = 0.05$ 144

5.11 Probability of the average chain order parameter of mixture bilayers at $x_{\mathrm{DOPC}} = 0.25$ 145
5.12 RDFs of lipids at various temperatures and compositions 145
5.13 Snapshots represent the corresponding Voronoi construction plots 146
5.14 Lateral mean square displacement as a function of temperature at $x_{\mathrm{DOPC}} = 0.05$ 147
5.15 Temperature dependence of the MSD at $x_{\mathrm{DOPC}} = 0.5$ 148
5.16 Self-assembled equi-molar DPPC/DOPC bilayer 149
5.17 RDFs and area per lipid of self-assembly bilayers at $x_{\mathrm{DOPC}} = 0.5$ 150
5.18 Probability of the average chain order parameter of DPPC in asymmetric bilayer and self-assembly bilayer 150
5.19 Symmetric equi-molar DPPC/DOPC bilayer 151
5.20 Time evolution showing the equlibration process with $x_{DOPC} = 0.5$ 151
5.21 Area per lipid and average chain order parameter versus temperature with different compositions of DOPC 152
5.22 Probability distribution S_{chain} with $x_{DOPC} = 0.25$ 153
5.23 2D RDFs and snapshots of asymmetric DPPC/DOPC bilayers at various temperatures and DOPC compositions 154
5.24 2D RDFs of lipids with different concentrations and temperatures. 155
5.25 Histograms of DOPC concentration and Voronoi constructions of the corresponding monolayers 158
5.26 Proposed DPPC/DOPC phase diagram 159
5.27 A calculated phase digram of DPPC/DOPC bilayer 159

List of Tables

2.1 CG topology of Cholesterol 60
2.2 CG topology of DPPC 61

3.1 Parameters obtained from Voronoi analysis show the growth of gel domain 81
3.2 Lateral diffusion coefficient of DPPC 93

4.1 Total number of clusters within the bilayer and average cluster size 112
4.2 Thickness of DPPC/cholesterol monolayers 116
4.3 Relative z position of head group and centre of mass (COM) of cholesterol with respect to the headgroup and COM of DPPC. . . 117
4.4 Lateral diffusion coefficient of DPPC 122

5.1 Asymmetric bilayers obtained with different concentrations of DOPC 136
5.2 Equi-molar DPPC/DOPC bilayer obtained by self-assembly. . . . 136
5.3 Symmetric bilayers constructed by combining gel phase DPPC bilyer and fluid phase DOPC bilayers 137
5.4 Lateral diffusion coefficient of DPPC 147
5.5 Lateral diffusion coefficient of DOPC 148
5.6 Properties of lipid bilayers with phase coexistence. 156

Chapter 1

Introduction

Our bodies work as very sophisticated and complicated machines. All living matter, including our bodies, are built up from simple and small units - cells. Cells contain a large class of organelles which are structurally soft and complex. An understanding of the dynamics and structure of cells was not well developed till a long time after the first description of cells by Robert Hooke in 1665 with the invention of the microscope [1]. It is 200 years since the importance of the cell was proposed by Henri Dutrochet [2]. He stated that the cell was more than just a structure; instead, the cell was a physiological unit, and everything was ultimately derived from it. By now, it is clear that each cell functions differently and contributes to all living organisms. The internal compartments of a living cell (organelles) are surrounded by membranes, and the cell itself is also separated from the outer environment by cell or plasma membranes (see figure 1.1). These thin, fragile, soft and complex biological membranes act as semi-permeable barriers that "control" the in- and out- flow of molecules in the cell or the internal compartments [3]. The cell membrane is involved in maintaining the shape of the cell and many other cell functions such cell adhesion, in endo- and exocytosis, in signaling, etc.

Biological membranes consist of multicomponent mixtures, and include a wide variety of lipids and proteins. The composition within the lipid membrane varies from cell to cell (see Figure 1.2A for the mosaic model for cell membranes, Figure 1.2B shows the plasma membrane structure obtained with transmission elec-

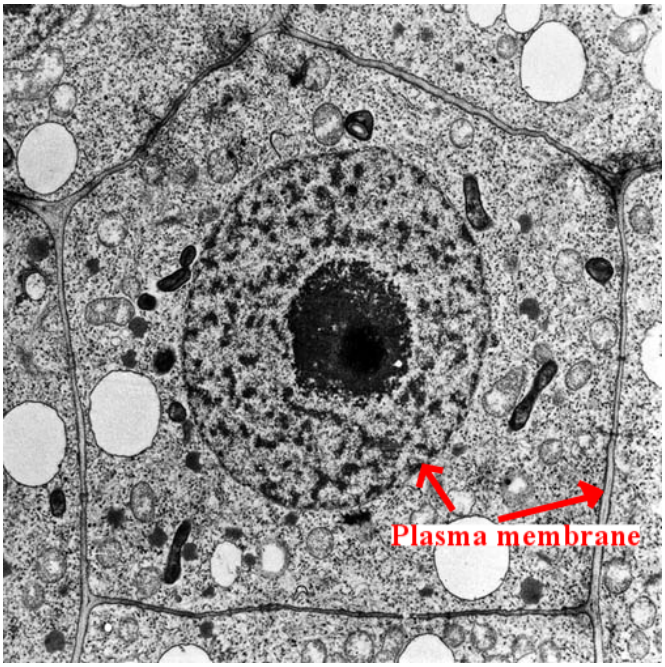

Figure 1.1: An example of a plant cell (root tip cell) imaged with a Transmission Electron Microscope showing the internal compartment and the cell itself are separated from the outer environment by plasma membranes. Imaging: A.M. Wolters-Arts, Radboud University Nijmegen.

tron microscopy [4] and Figure 1.2C gives a snapshot of a protein immersed bilayer from an atomistic simulation). Two of the most common lipid classes are phospholipids and sterol lipids. Some major derivatives of phospholipids are phosphatidylcholine (PC), phosphatidylethanolamine (PE) and phosphatidylserine (PS).

Approximately 25% of the phospholipids found in human red cell membranes are phosphatidylcholine [6]. A common example of phosphatidylcholine is shown in figure 1.3, 1,2-dipalmitoyl-*sn*-glycero-3-phosphocholine (DPPC) that accounts for approximately 50% of the surfactants in the alveoli of the lungs [7]. The top region of DPPC begins with a choline, a quaternary saturated amine, connected to two dipalmitoyl tails of 16 carbon atoms by an electron-rich phosphate group, a glycerol backbone and two esters (see Figure 1.3). The phosphatidylcholine group is defined as the headgroup of the lipid, and it is zwitterionic that is it

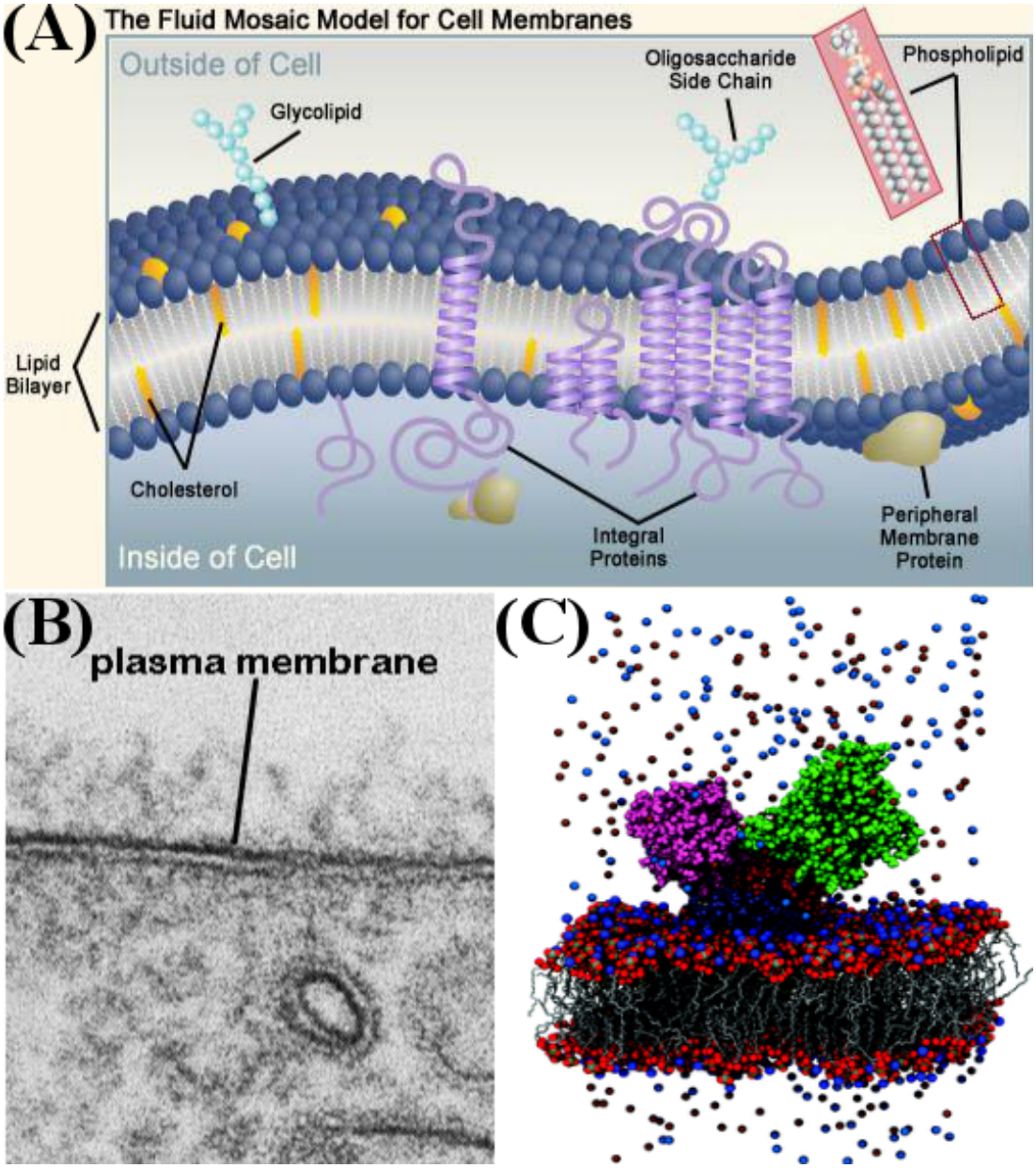

Figure 1.2: (A) Cartoon of a model membrane showing the multicomponent structure of cell membrane, picture taken from http://www.biology.arizona.edu. (B) A transmission electron microscopy image of a membrane, which clearly show the two leaflets of the bilayer, picture taken from reference [4]. (C) Atomistic model of a lipid bilayer containing the a Ca^{2+}-ATPase protein which acts as Ca^{2+} pump. Picture taken from reference [5].

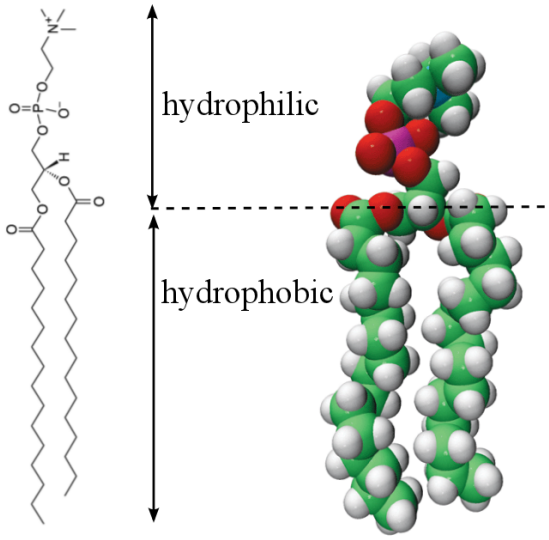

Figure 1.3: Chemical structure (left) and 3D structure (right) of a DPPC molecule.

consists a positively charged amine and a negatively charged phosphatidic acid. This part of the lipid is hydrophilic, while the two tails are hydrophobic.
One of the most common sterols is cholesterol (see figure 1.4). Cholesterol can reach concentrations of over 50 mol% of total lipids in mammalian cell membranes [8]. It acts as an essential structural component to maintain the proper membrane permeability and fluidity [9]. The cholesterol molecule has a rigid ring system and a branched hydrocarbon tail which makes it hydrophobic. However, there is also a weakly polar hydroxyl group attached on the other side of the ring system.

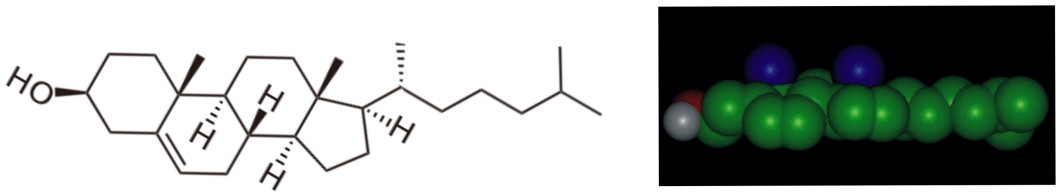

Figure 1.4: The chemical structure (left) and Van der waals representation (right) of a cholesterol molecule.

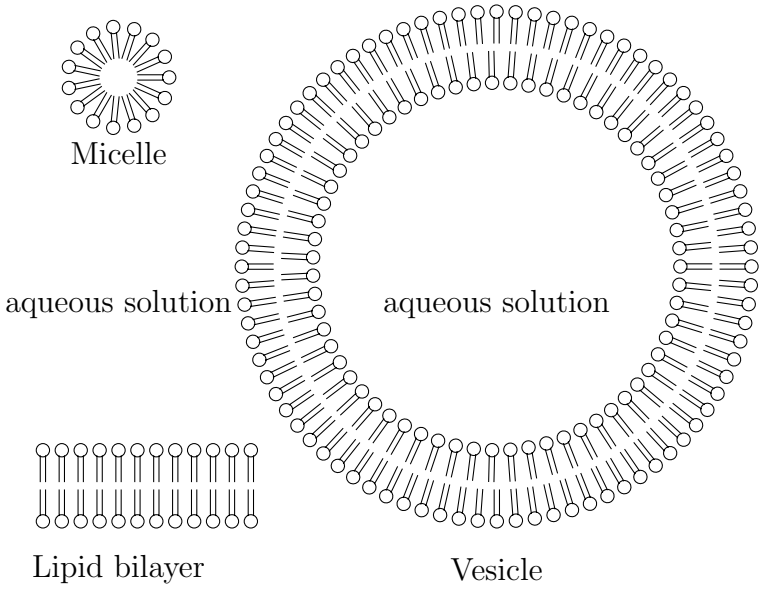

Figure 1.5: Illustration of a micelle, a lipid bilayer and a vesicle composed of two lipid layers exposed to water.

As lipids have both hydrophobic and hydrophilic parts, they are known as amphiphilic molecules. When exposed to water, phospholipids spontaneously form more complex structures to minimize the contact between water and their hydrophobic tails due to their amphiphilic nature (see figures 1.3 for the structure of an amphiphilic molecule and figure 1.5 for some examples of self-assembled lipid structures). This hydrophobic nature is reflected experimentally for water with non-polar (or uncharged) molecules [10, 11, 12, 13]. As a function of water content and temperature, different aggregate structures can form (see figure 1.6). In bilayers, lipids pack as a 2-dimensional flat sheet, where hydrophobic tails direct inwardly and the hydrophilic headgroups align on the outside in contact with water. Sheets of bilayers separated by bulk liquid are generally referred as lamellar phases (L). Some non-lamellar phases also exist, including the normal hexagonal liquid-crystalline phase (H_I) and the reverse hexagonal liquid-crystalline phase (H_{II}). However, Lipid bilayers have been found to be the universal basis for cell membrane structure, and therefore bilayers are commonly modelled in relevant studies.

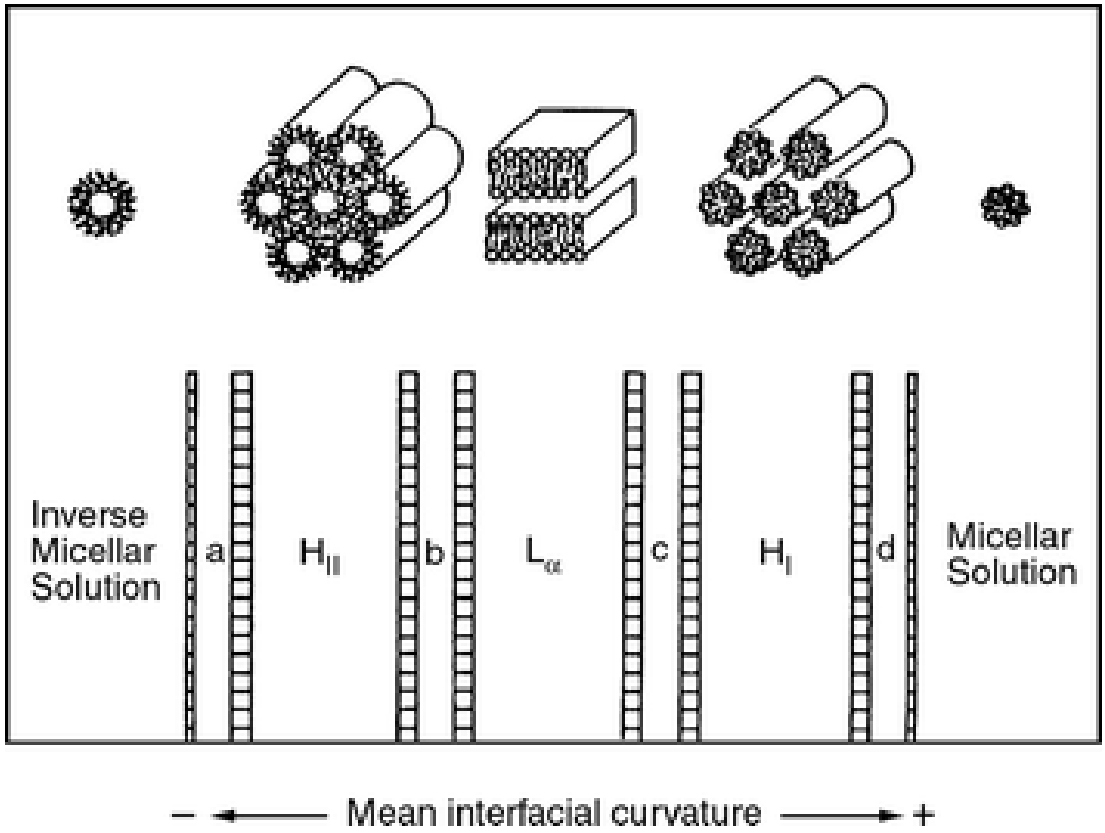

Figure 1.6: Dependence of phase transitions of lipid-water mixtures on hydration and temperature. L:lamellar phases, H_I:normal hexagonal liquid-crystalline phases, H_{II}:reverse hexagonal liquid-crystalline phases. Figure taken from reference [14]

The bilayer structure was not discovered until the 1920s [15]. Since then, the physics, chemistry and biological function of lipid bilayers have attracted interest, both from experimental and theoretical points of view. However, various features of biological membranes remain unclear. One of the main challenges is the description of the complex structure of real biological membranes, and another challenge is to relate the functioning of the membrane to its structure and dynamics. Therefore, simple membrane models are often chosen, both experimentally and with molecular simulations. Typical model membranes are lipid bilayers consisting of one to three types of lipids and possibly trans-membrane proteins (see Figure 1.2C). The experimental investigation of these thin and fragile structures is not always trivial. In the past decade, with the rapid development of

computational hardware, atomic-level simulations have been developed as a useful tool for lipid bilayer studies. Simulation models consisting of lipid, water, and solute atoms can be simulated to a high level of detail providing information on both the spatial organization and temporal dynamics of the system. The focus of my thesis is the modelling and simulation of bilayer systems consisting up to two non-water components.

Membranes are highly dynamic and characterized by distinct phases and internal fluctuating structures. Understanding the overall properties of membranes, especially its fluid characteristics is therefore a major task. Below melting temperature, lipid bilayers are classified to exist in "gel" or "S_o" (solid-ordered) phases. The ordered phase involves lipids forming a two-dimensional hexagonal lattice with the acyl chains in a fully extended conformation. Therefore, the movement of the lipids is restricted. For a membrane containing a single phospholipid type, the bilayer undergoes a transition to a liquid crystalline state after it is heated up to above the main transition temperature, "T_m". In this state, the lipids melt and rearrange themselves in a disordered form with both translational and orientational disordering, which is commonly referred as "L_d" (liquid-disordered) phase. Here, the lipid molecules are free to move around, rotate, exchange positions and may undergo flip-flop across the bilayer (at a rate of $\sim$ 0.01 s^{-1} [16]). Bilayers consisting of binary lipid mixtures are found to show a fluid-gel phase coexistence, whereas a new phase may be formed with the addition of non-phospholipid molecules.

Phases diagrams provide a complete understanding of the temperature and composition dependence of lipid phase behaviour (see figure 1.7 for an example of a phase diagram). Binary or ternary bilayer mixtures are commonly modelled in both experiments and simulation to characterise the lipid phase behaviour. The present understanding of membrane systems is largely based on experimental studies, such as atomic force microscopy, differential scanning calorimetry, fluorescence spectroscopy, nuclear magnetic resonance, and various scattering methods [4, 17, 18, 19, 20]. In this thesis, we aim to produce phase diagrams for the binary bilayer mixtures based on simulation observations.

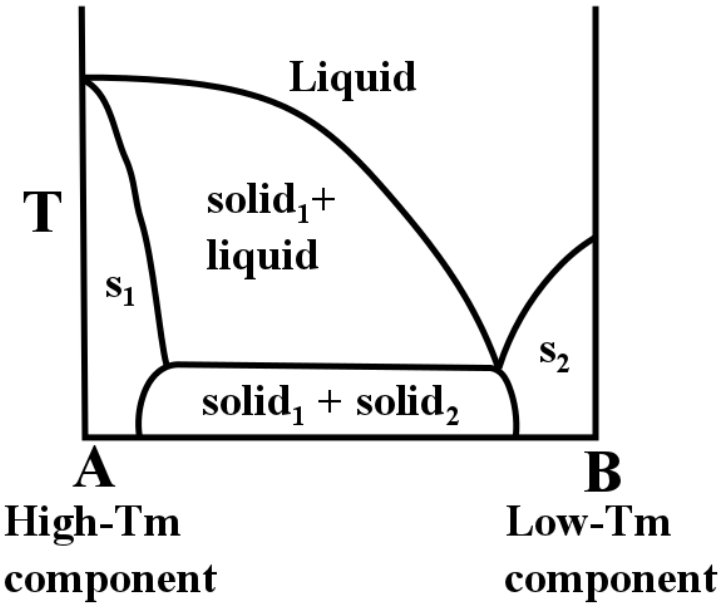

Figure 1.7: An example of a binary phase diagram, consisting a high T_m component A and a low T_m component B. At low temperature, phases coexist. At high temperature, components A and B mix completely in one uniform liquid phase. Figure adopted from reference [21]

It is well known that cholesterol affects the bilayer structure and therefore the bilayer phase behaviour [8, 22, 23, 24, 25]. Cholesterol molecules insert into bilayers with their hydroxyl groups oriented toward the aqueous phase. The hydrophobic ring system of cholesterol is located adjacent to the acyl tails of the phospholipids. Hydrogen bonds are formed between the hydroxyl group of cholesterol and the polar headgroups of phospholipids. A popular umbrella model was proposed to describe the mechanism of how cholesterol orients at the lipid bilayer. Since cholesterol consists of a small hydrophilic headgroup and a bulky rigid hydrophobic tetrameric ring system, the cholesterol body needs to be shielded by the large phospholipid polar group to avoid unfavourable interaction between water and the hydrophobic part of cholesterol. Hence, the phospholipids and cholesterols have to pack more tightly with increasing cholesterol content to share the limited space under the phospholipid headgroup. Such an effect of cholesterol

is named as a "condensing effect" [26]. The interaction between cholesterol and phospholipid decreases the mobility of the phospholipid tails in the fluid phase. However, the addition of cholesterol interferes with the close packing of fatty acid tails in the S_o phase, and thus "washes-out" the transition to the L_d phase. Phospholipid membranes with a high concentration of cholesterol have a fluidity intermediate between the S_o and L_d phases. Hence, a new phase is suggested, that is the liquid-ordered (L_o) phase. Phospholipids in the L_o phase have a liquid structure in the lattice plane together with conformationally ordered acyl chains. A distinctive L_o region in bilayer membranes which exists with a concentration of cholesterol generally 3 to 5 times higher than the surrounding bilayer, is named as a "lipid raft" [27]. The acyl chains of lipids within lipid rafts tend to be more extended and therefore more tightly packed. Generally, bilayers consisting of glycosphingolipids, cholesterol and saturated phospholipids are preferentially incorporated into the rafts.

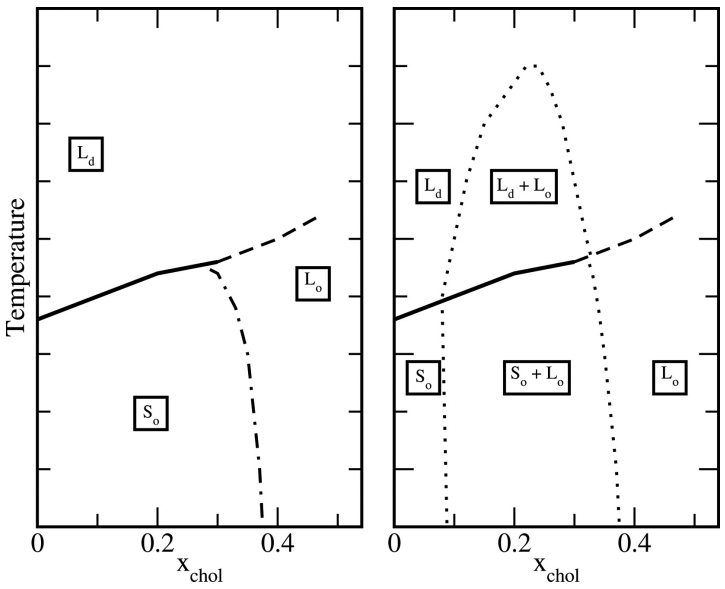

Figure 1.8: An example of a schematic phase diagram of a phospholipid/cholesterol bilayer. Figure taken from reference [28]

Quite a few studies have been reported on phase transitions. Consensus exists between experiments and simulations. Two possible phase diagrams supported

by various experimental and simulation studies are shown in figure 1.8. They are only different in the observation or not of the two-phase regions. A few experimental techniques have been employed to study the lipid-cholesterol mixture phase behaviour. Differential scanning calorimetry studies show that the main transitions of lipid-cholesterol mixtures broaden and the transition temperatures decrease gradually with the addition of cholesterol [29]. The structural properties of these mixtures have been probed using neutron scattering, x-ray diffraction and nuclear magnetic resonance [30, 31, 32]. The phase diagrams based on calorimetry and NMR spectra suggest the formation of cholesterol-rich and -poor domains (similar to the one on the right in figure 1.8) [33]. Instead, studies using fluorescence microscopy proposed that no domains formed in DPPC/cholesterol systems (similar to the one on the left in figure 1.8), but liquid-liquid coexistence occurs in three-component systems [34, 35]. A recent theoretical study present by Almeida suggested the lack of phase coexistence above the main phase transition, but the existence of a two-phase region below it [36]. Thus, the understanding of DPPC/cholesterol bilayer phase behaviour is not entirely clear.

Beside the influence on phase transition, the importance and the role of the structure of the cholesterol molecule on the bilayer structure has also been studied extensively using atomistic molecular dynamics simulation [37, 38, 39]. The two off-plane methyl groups (see figure 1.4) are modelled in atomistic simulations, so the cholesterol molecule has a smooth side and a rough side. The packing of saturated lipid chain atoms next to the smooth side of the cholesterol molecule is found to be tighter than that next to the rough side [40]. Therefore, the smoothness of the cholesterol molecule is important for its ordering capability [41]. The CG model of cholesterol employed in this thesis is highly coarse-grained and the asymmetric structure of cholesterol is not introduced explicitly, which may have a influence on the phospholipid-cholesterol interactions.

Apart from the saturated phospholipids, unsaturated phospholipids consisting of C=C bonds are also commonly found in real bilayers. The C-C bonds involved in the acyl chains of phospholipids can rotate freely. However, the existence of the *cis* double bond in unsaturated phospholipids, such as DOPC molecules, causes

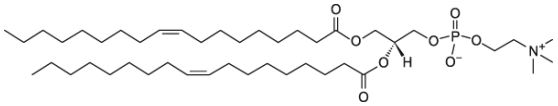

Figure 1.9: The chemical structure of the unsaturated phospholipid DOPC, with the unsaturated *cis* bonds shown in the lipid tails.

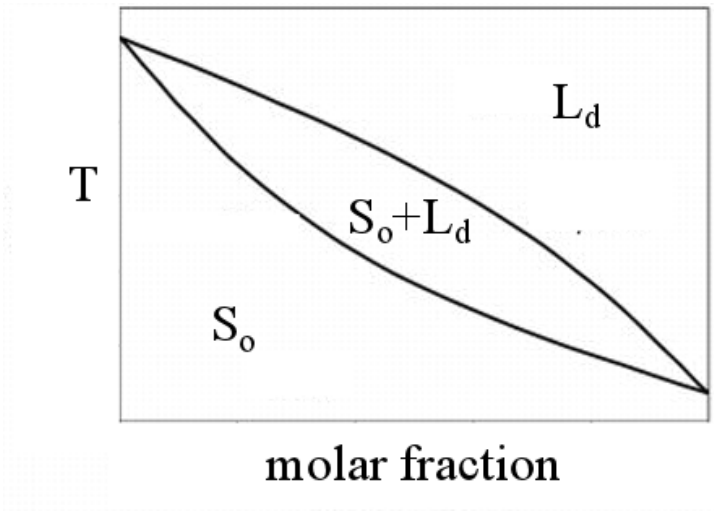

Figure 1.10: An example of a schematic phase diagram for a binary mixture lipid bilayer. "S_o": gel phase, "L_d": liquid phase, "S_o+L_d": gel/fluid phase coexistence.

a kink in the chain (see figure 1.9). The kink in DOPC lipid chains interferes with the packing of lipids in the crystalline state, and therefore lowers the phase transition temperature of DOPC with respect to that of DPPC, which is fully saturated. Unsaturated phospholipids are very important as they ensure that bilayer membranes exist in the fluid phase at body temperature. Therefore, particular attention has been paid to binary systems composed of saturated and unsaturated phospholipids. When DOPC molecules are added to a DPPC bilayer, they are considered as "impurities" and disrupt the tight gel phase structure of DPPC. Due to the mismatch in hydrophobic tails, DOPC is somewhat immiscible with DPPC. Experimentally, the separation of DPPC/DOPC mixtures into gel phase domains (DPPC rich) and fluid phase domains (DOPC rich) has been observed directly by fluorescence microscopy [42, 34]. The difference in partial concentrations in the two domains is expected to be large because of the presence of the *cis* double bond (see figure 1.10 for an example of a binary mixture phase diagram).

Several phase diagrams of DPPC/DOPC bilayers were reported theoretically [43] and experimentally (NMR [44], x-ray scattering[45, 46], fluorescence [47]. However, the phase separation of DPPC/DOPC bilayers is still lacking in information from a simulation perspective.

The purpose of this thesis is to apply molecular dynamics simulations to bilayers composed of DPPC with other surfactant components and use this model to investigate the properties of lipids in heterogeneous bilayers. The basic question is: how does the presence of a second component modify the phase transitions in lipid bilayers? To answer this question my work is structured in three steps. First we quantitatively study pure lipid bilayer phase behaviour. Secondly, we study the impact that cholesterol has on the properties of the bilayer. Finally, we studied the effect of other type of phospholipids on phase separation. A secondary object is to evaluate the application of the coarse-grained models to simulate phospholipids and cholesterol mixtures, as well as their associated phase and structural transitions.

The thesis is structured as follows:

In chapter 2, I discuss the theoretical framework of the classical molecular dynamics simulation method; the concept of the MARTINI Coarse-Grained force-field; the reasons why this force-field is selected; and the parameters used to investigate the bilayers reported in chapters 3, 4 and 5.

In chapter 3, the coarse-grained model of the DPPC/cholesterol bilayer is described in detail. This approach allows us to reach the time and length scales necessary to study structural and dynamic properties of the bilayer at various temperatures and cholesterol concentrations. The impact of cholesterol on the lipid bilayer structure and dynamics over a wide range of concentrations and temperatures is systemically analysed, and the simulation results are used to construct the phase diagram of the DPPC/CHOL mixture.

In chapter 4, lipid-cholesterol interactions are examined with the MARTINI

force-field and a modified coarse grained model of cholesterol. This chapter focuses on understanding the relationship between the CG cholesterol structure and the 'thread-like' structure seen with the CG model at high cholesterol content. We simulate the DPPC bilayer with enlarged and decreased size cholesterol-like isomorphs to explore the role of cholesterol size in the bilayer phase transition and cholesterol lateral organisation. Additionally, comparison of the modified cholesterol with naturally occurring sterols is provided.

In chapter 5, the gel-fluid phase transition of DPPC/DOPC phospholipid bilayers is examined. The effect of DOPC and the effect of the heterogeneity of the bilayers on the main phase transition is monitored by computing various structural parameters using asymmetric and symmetric DPPC/DOPC bilayer models. The phase separation is investigated and a complete phase diagram is constructed based on the simulation results.

Finally, in chapter 6, we summarise the major results obtained in this work and provide suggestions for future work on the subject of the present thesis.

References are included in each of these chapters and the page numbers where references are cited are given at the end of each reference.

References

[1] P. Mazzarello. A unifying concept: the history of cell theory. *Nature Cell Biology*, 1(1):E13 – E15, 1999. 19

[2] C. Nezelof. Henri dutrochet (1776 - 1847): an unheralded discoverer of the cell. *Annals of Diagnostic Pathology*, 7(4):264 – 272, 2003. 19

[3] D. Boal. *Mechanics of the cell*. Cambridge University Press, 2001. 19

[4] B. Alberts, A. Johnson, J. Lewis, M. Raff, K. Roberts, and P. Walter. *Molecular biology of the cell*. Garland, 4th edition, 2002. 20, 21, 25

[5] A. Lervik, F. Bresme, and S. Kjelstrup. Molecular dynamics simulations of the Ca^{2+}-pump: a structural analysis. *Phys. Chem. Chem. Phys.*, 14:3543–3553, 2012. 21

[6] S. R. Goodman. Chapter 2 - cell membranes. In *Medical Cell Biology (Third Edition)*, pages 27 – 57. Academic Press, San Diego, third edition edition, 2008. 20

[7] B. A. Holm, Z. Wang, E. A. Egan, and R. H. Notter. Content of dipalmitoyl phosphatidylcholine in lung surfactant: Ramifications for surface activityl. *Pediatr Res*, 39(5):805 – 811, 1996. 20

[8] R. A. Demel, L. L. M van Deenen, and B. A. Pethica. Monolayer interactions of phospholipids and cholesterol. *Biochimica et Biophysica Acta*, 135:11–19, 1967. 22, 26

[9] R. E. Olson. Discovery of the lipoproteins, their role in fat transport and their significance as risk factors. *American Society for Nutritional Services*, 128, 1998. 22

[10] S. Krimm. The hydrophobic effect: Formation of micelles and biological membranes. *Journal of Polymer Science: Polymer Letters Edition*, 18(10), 1980. 23

[11] D Chandler. Interfaces and the driving force of hydrophobic assembly. *Nature*, 436(7059):640–647, 2005. 23

[12] Emily E. Meyer, Kenneth J. Rosenberg, and Jacob Israelachvili. Recent progress in understanding hydrophobic interactions. *Proceedings of the National Academy of Sciences*, 103(43):15739–15746, 2006. 23

[13] C. Tanford. The hydrophobic effect and the organization of living matter. *Science*, 200(4345):1012–1018, 1978. 23

[14] J. M. Seddon. Structure of the inverted hexagonal (HII) phase, and non-lamellar phase transitions of lipids. *Biochimica et Biophysica Acta (BBA) - Reviews on Biomembranes*, 1031(1):1 – 69, 1990. 24

[15] M. Adams. Discovering the lipid bilayer. *Nature Education*, 3(9):20, 2010. 24

[16] E. Anibal Disalvo and S. A. Simon. *Permeability and Stability of Lipid Bilayers*. CRC Press, 1995. 25

[17] Z.V. Leonenko, E. Finot, H. Ma, T.E. S. Dahms, and D.T. Cramb. Investigation of temperature-induced phase transitions in DOPC and DPPC phospholipid bilayers using temperature-controlled scanning force microscopy. *Biophysical Journal*, 86(6):3783 – 3793, 2004. 25

[18] R. Lewis, D. Mannock, and R. McElhaney. Differential scanning calorimetry in the study of lipid phase transitions in model and biological membranes. In *Methods in Membrane Lipids*, volume 400 of *Methods in Molecular Biology*, pages 171–195. Humana Press, 2007. 25

[19] R. Lipowsky and E. Sackmann, editors. *Structure and Dynamics of Membranes I. From Cells to Vesicles*, volume 1A. Elsevier, 1995. 25

[20] J. Katsaras and T. Gutberlet. *Lipid Bilayers: Structure and Interactions*. Springer-Verlag, Berlin, 2001. 25

[21] S. L. Veatch and S. L. Keller. Seeing spots: Complex phase behavior in simple membranes. *Biochimica et Biophysica Acta (BBA) - Molecular Cell Research*, 1746(3):172 – 185, 2005. 26

[22] G. W. Feigenson. Phase diagrams and lipid domains in multicomponent lipid bilayer mixtures. *Biochmica et Biophysica Acta*, 1788:47–52, 2009. 26

[23] R.A. Demel and B. De Kruyff. The function of sterols in membranes. *Biochimica et Biophysica Acta (BBA) - Reviews on Biomembranes*, 457(2):109 – 132, 1976. 26

[24] T. McMullen, R. Lewis, and N. McElhaney. Cholesterolphospholipid interactions, the liquid-ordered phase and lipid rafts in model and biological membranes. *Current Opinion in Colloid & Interface Science*, 8(6):459 – 468, 2004. 26

[25] G. W. Stockton and I. C. Smith. A deuterium nuclear magnetic resonance study of the condensing effect of cholesterol on egg phosphatidylcholine bilayer membranes. i. perdeuterated fatty acid probes. *Chemistry and physics of lipids*, 17:251–63, 1976. 26

[26] H. M. McConnell and A. Radhakrishnan. Condensed complexes of cholesterol and phospholipids. *Biochimica et Biophysica Acta (BBA) - Biomembranes*, 1610(2):159 – 173, 2003. 27

[27] L. Anchisi, S. Dessi, A. Pani, and A. Mandas. Cholesterol homeostasis: A key to prevent or slow down neurodegeneration. *Frontiers in Physiology*, 3(486), 2013. 27

[28] Q. Waheed, R. Tjörnhammar, and O. Edholm. Phase transitions in coarse-grained lipid bilayers containing cholesterol by molecular dynamics simulations. *Biophysical Journal*, 103(10):2125 – 2133, 2012. 14, 27

[29] T. P. W. McMullen, R. N. A. H. Lewis, and R. N. McElhaney. Differential scanning calorimetric study of the effect of cholesterol on the thermotropic phase behavior of a homologous series of linear saturated phosphatidylcholines. *Biochemistry*, 32(2):516–522, 1993. PMID: 8422361. 28

[30] S. W. Hui and N. B. He. Molecular organization in cholesterol-lecithin bilayers by x-ray and electron diffraction measurements. *Biochemistry*, 22(5):1159–1164, 1983. 28

[31] S. Karmakar and V. A. Raghunathan. Cholesterol-induced modulated phase in phospholipid membranes. *Phys. Rev. Lett.*, 91:098102, Aug 2003. 28

[32] M. R. Vist and J. H. Davis. Phase equilibria of cholesterol/dipalmitoylphosphatidylcholine mixtures: deuterium nuclear magnetic resonance and differential scanning calorimetry. *Biochemistry*, 29(2):451–464, 1990. 28

[33] J. H. Davis, J. J. Clair, and J. Juhasz. Phase equilibria in DOPC/DPPC-d62/Cholesterol mixtures. *Biophysical Journal*, 96(2):521 – 539, 2009. 28

[34] S. L. Veatch and S. L. Keller. Separation of liquid phases in giant vesicles of ternary mixtures of phospholipids and cholesterol. *Biophysical Journal*, 85(5):3074 – 3083, 2003. 28, 29

[35] S.L. Veatch, I.V. Polozov, K. Gawrisch, and S.L. Keller. Liquid domains in vesicles investigated by NMR and fluorescence microscopy. *Biophysical Journal*, 86(5):2910 – 2922, 2004. 28

[36] P. F. Almeida. A simple thermodynamic model of the liquid-ordered state and the interactions between phospholipids and cholesterol. *Biophysical Journal*, 100(2):420 – 429, 2011. 28

[37] H. Martinez-Seara, T. Ròg, M. Kartunen, I. Vattulainen, and Ramon Reigada. Cholesterol induces specific spatial and orientational order in cholesterol/phospholipid membranes. *PLOS one*, 5:e11162, 2010. 28

[38] T. Ròg, M. Pasenkiewicz-Gierula, I. Vattulainen, and M. Karttunen. Ordering effects of cholesterol and its analogues. *Biochimica et Biophysica Acta (BBA) - Biomembranes*, 1788(1):97 – 121, 2009. 28

[39] S. A. Pandit and H. L. Scott. Multiscale simulations of heterogeneous model membranes. *Biochimica et Biophysica Acta (BBA) - Biomembranes*, 1788(1):136 – 148, 2009. 28

[40] T. Ròg and M. Pasenkiewicz-Gierula. Cholesterol effects on the phosphatidylcholine bilayer nonpolar region: A molecular simulation study. *Biophysical Journal*, 81(4):2190 – 2202, 2001. 28

[41] T. Róg and M. Pasenkiewicz-Gierula. Non-polar interactions between cholesterol and phospholipids: a molecular dynamics simulation study. *Biophysical Chemistry*, 107(2):151 – 164, 2004. 28

[42] L. Li and J. Cheng. Coexisting stripe and patch shaped domains in giant unilamellar vesicles. *Biochemistry*, 45(39):11819–11826, 2006. PMID: 17002282. 29

[43] R. Elliott, K. Katsov, M. Schick, and I. Szleifer. Phase separation of saturated and mono-unsaturated lipids as determined from a microscopic model. *The Journal of Chemical Physics*, 122(4):–, 2005. 30

[44] M. L. Schmidt, L. Ziani, M. Boudreau, and J. H. Davis. Phase equilibria in DOPC/DPPC: Conversion from gel to subgel in two component mixtures. *The Journal of Chemical Physics*, 131(17):–, 2009. 30

[45] T. T. Mills, J. Huang, G. W. Feigenson, and J. F Nagle. Effects of cholesterol and unsaturated DOPC lipid on chain packing of saturated gel-phase dppc bilayers. *General physiology and biophysics*, 28(2):126139, June 2009. 30

[46] K. Furuya and T. Mitsui. Phase transitions in bilayer membranes of dioleoylphosphatidylcholine/dipalmitoyl-phosphatidylcholine. *Journal of the Physical Society of Japan*, 46(2):611–616, 1979. 30

[47] B. R. Lentz, Y. Barenholz, and T. E. Thompson. Fluorescence depolarization studies of phase transitions and fluidity in phospholipid bilayers. 2. two-component phosphatidylcholine liposomes. *Biochemistry*, 15(20):4529–4537, 1976. 30

Chapter 2

Methodology

In this chapter, I discuss the techniques that I applied in my PhD study to simulate and investigate model membranes. I begin by describing the theory behind the molecular dynamics (MD) simulation approach and the coarse-grained (CG) force-field used to model the membrane. Finally, the chapter concludes with a section explaining the parameters employed to obtain the relevant membrane properties.

2.1 Molecular Dynamics (MD) simulation

The goal for this thesis is to use computational techniques to understand biological membranes. There are a range of techniques that can be applied in such studies. The choice of technique depends on the main target of the investigation and it is influenced by the need to obtain reliable results with the available computing power. Ideally, solving the time-dependent Schrödinger equation would provide all thermodynamic and dynamical properties of the system. However, the size and complexity of biological membranes makes such a solution impossible in practice. MD is a more computationally tractable technique whereby the solution of the classical equations of motion for a set of atoms is applied instead. The first MD simulations were performed in a system of hard core spheres by Alder and Wainwright in the late 1950's [1]. With the rapid development of computer hardware and software, MD simulations have been successfully used

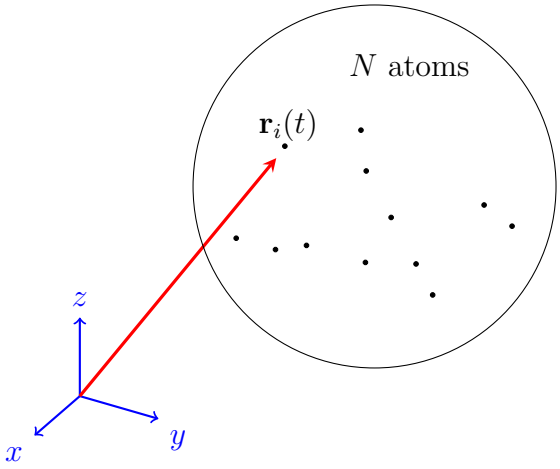

Figure 2.1: Illustration of the MD simulation approach.

to increase our understanding of phase transitions and the physical behaviour of interfaces [2, 3].

2.1.1 The idea

MD simulation generates the trajectory of every atom in a system containing N atoms that are assumed to behave classically interacting via a potential U, by numerical integration of Newton's equations of motion. The assumption based on Newton's laws has been proved to work reliably even for complex systems (see [4, 5] for general references).
Consider a system with N atoms (see figure 2.1). The internal energy is defined in terms of kinetic and potential energies,

$$E = K + U, \tag{2.1}$$

where K is the kinetic energy,

$$K \equiv \sum_{i=1}^{N} \frac{1}{2} m_i {v_i}^2, \tag{2.2}$$

m_i and $\mathbf{r}_i$ denote the atomic mass and coordinate of atom i, v_i is the velocity of particle i and t is time.
U is the potential energy which describes the intermolecular interactions. It is defined in terms of the coordinates of individual atoms, pairs, triplets etc. It is chosen by the simulator to reproduce the physics of the simulation system as accurately as possible.

$$\begin{aligned} U = &\sum_i U_1(\mathbf{r}_i) + \sum_i \sum_{j>i} U_2(\mathbf{r}_i, \mathbf{r}_j) + \\ &\sum_i \sum_{j>i} \sum_{k>j>i} U_3(\mathbf{r}_i, \mathbf{r}_j, \mathbf{r}_k) + \\ &\sum_i \sum_{j>i} \sum_{k>j>i} \sum_{l>k>j>i} U_4(\mathbf{r}_i, \mathbf{r}_j, \mathbf{r}_k, \mathbf{r}_l) + \cdots \end{aligned} \tag{2.3}$$

The first term, $\sum_i U_1(\mathbf{r}_i)$, involves only single particles, and represents the effects of any external fields which may be acting on the system. The remaining terms in equation 2.3 represent the effects of interparticle interactions. The second term, $\sum_i \sum_{j>i} U_2(\mathbf{r}_i, \mathbf{r}_j)$, which describes pair interactions is the most important one. The pair potential is defined in term of the relative positions of atoms ($r_{ij} =\mid \mathbf{r}_i - \mathbf{r}_j \mid$), the so called pair separation. The U_3 term involves triplets of molecules, i.e. the interaction between three atoms that e.g. appears in angular interactions. Careful choices of the first two terms have been found to be remarkably successful at reproducing liquid properties [5].
In MD simulations, the time evolution of the system is described by Newton's second law,

$$m_i \frac{\partial^2 \mathbf{r}_i}{\partial t^2} = \mathbf{F}_i \equiv -\frac{\partial U}{\partial \mathbf{r}_i} \tag{2.4}$$

where $\mathbf{F}_i$ is the force applied on the atom, and it is the negative derivative of the potential energy U. Equation 2.4 cannot be solved analytically for a system with more than two particles, so numerical methods must be applied. The equation is solved step-by-step, with a time step δt. The choice of δt depends on the method of solution, but it should be significantly smaller than the period of the highest vibrational frequency of the molecule so that the structure of the molecule can be

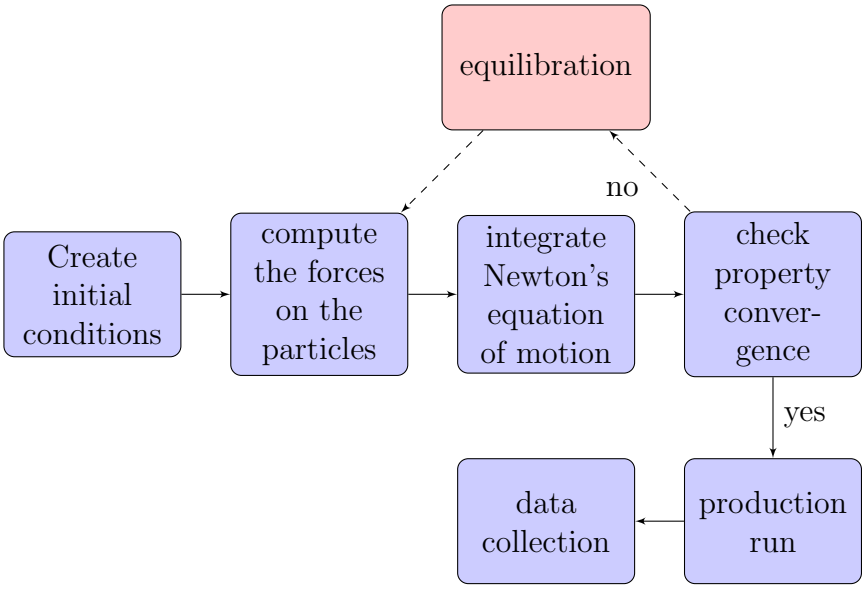

Figure 2.2: Schematic diagram showing an MD simulation stepwise

retained, and by extension also smaller than the time required for a molecule to diffuse its own length. To solve the equation of motion an integrator is applied, which given molecular positions and velocities at time t, estimates the same quantities at time $t + \delta t$:

$$\mathbf{r}_i(t) \rightarrow \mathbf{r}_i(t + \delta t) \rightarrow \mathbf{r}_i(t + 2\delta t) \rightarrow \cdots \rightarrow \mathbf{r}_i(t + N_s \delta t) \tag{2.5}$$

where N_s is the total number of time-steps in the simulation.
If we simulate the system until it reaches the desired state as described in the initial setting, the equilibration process of the simulation is finished and we can then calculate the physical properties using a time average. The general scheme of an MD simulation is shown in Figure 2.2. This simple, straightforward procedure describes the "experimental steps" of an MD simulation study.

2.1.2 Integrator

Accurate numerical solutions to Newton's equations are the key to perform computer simulations. Therefore, the accurate integration of the equations is essen-

tial, and this is achieved through the use of finite difference methods. A widely used integrator is the so-called leap-frog [6].
The system is initially set up with $\mathbf{r}_i(t=0)$ and $\dot{\mathbf{r}}_i(t=-\frac{1}{2}\delta t)$, so the leap-frog algorithm calculates the positions at time δt and velocities at $\frac{1}{2}\delta t$. It updates the positions and velocities as:

$$\dot{\mathbf{r}}_i(t+\frac{1}{2}\delta t) = \dot{\mathbf{r}}_i(t-\frac{1}{2}\delta t) + \frac{\delta t}{m_i}\mathbf{F}_i(t) \tag{2.6}$$

$$\mathbf{r}_i(t+\delta t) = \mathbf{r}_i(t) + \delta t\dot{\mathbf{r}}_i(t+\frac{1}{2}\delta t) \tag{2.7}$$

where $\mathbf{F}_i(t)$ is the force calculated at time t from the previous step. The time step used in all of my simulations is 0.02 ps, which has been found to be the optimum choice for the coarse-grained models [7]. It is a factor of 10 longer than the value of 0.002 ps used for typical all-atom models [8]. The much smoother interactions between coarse-grained molecules compared to atomistic ones make the use of large time step in coarse-grained models possible.
For an isolated system, the total energy E and the total momentum should be conserved. This principle is an indicator on the performance of the integrator. The leap-frog integrator is chosen for its accuracy and efficiency [9].

2.1.3 Initial conditions

As always when solving a differential equation, we require initial conditions. The nature of the numerical integrator requires us to have both $\mathbf{r}_i(t=0)$ and $\dot{\mathbf{r}}_i(t=-\frac{1}{2}\delta t)$. The initial positions are generated by adding molecules into the simulation box. Molecules can be added to the box in random positions or in a lattice. This can be done by using the *genbox* program from the GROMACS software package or other codes which can be found available on-line or home made. By using *genbox*, any solvent molecule will be removed from the simulation box where the distance between any atom of the solute molecules and any atom of the solvent molecule is less than the sum of the van der Waals radii of both atoms [10]. Therefore, the problem of overlapping with random positions

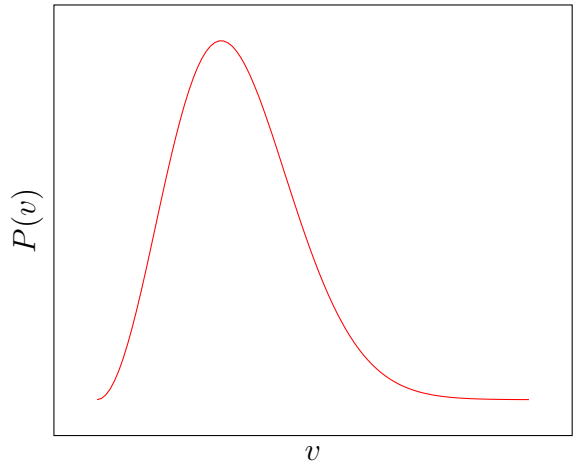

Figure 2.3: An example of the Maxwell-Boltzmann velocity distribution

can be avoided. One of the common reasons that MD simulations break down is a pathological initial condition, i.e. molecules are too close to each other, so that huge forces are present. In this study, pre-equilibrated bilayers (available from http://cgmartini.nl/cgmartini/) were used for the initial system set up. The bilayer is then solvated using a box of coarse-grained water molecules.
If the initial velocities of the molecules (v) are not available, initial velocities are typically chosen by drawing them randomly from a Maxwell-Boltzmann distribution (see Figure 2.3), v at the chosen reference temperature T:

$$p(v_x) = \sqrt{\frac{m}{2\pi kT}} \exp\left(\frac{m{v_x}^2}{2kT}\right) \tag{2.8}$$

where k is Boltzmann's constant, $1.381 \times 10^{-23} JK^{-1}$.
The centre-of-mass velocity of the simulation system is removed, in order to avoid the so-called 'flying ice cube effect'. This is a numerical integration artefact due to velocity rescaling, that almost all of the kinetic energy is converted into translation or rotation of the system resulting in a system with almost no kinetic energy associated with the intramolecular degrees of freedom [11].

2.1.4 Force calculation

As seen in Equation 2.4, the force acting on atom i is the negative derivative of U with respect to the position vector of atom i. The common functional forms of pair interactions between atoms can be further divided into bonded and non-bonded interactions, which are described in the following.

2.1.4.1 Non-bonded interactions

Non-bonded interactions are treated as pair-additive in our simulations. Both short-range and long-range interactions contribute, where long-ranged interactions fall off no faster than r_{ij}^{-d} where d is the dimensionality. The non-bonded interactions are computed on the basis of a neighbour list, which is set to only update every 10 steps using a grid with a distance r_{list} for potential energy calculation. The neighbour list contains a list of neighbours of a given atom i that are within the cut-off distance r_{list}. In our simulations r_{list} is set to 1.2 nm, the same as the cut-off distance of the non-bonded interactions (r_{cut}). The non-bonded interactions contains Lennard-Jones (LJ) and Coulomb terms, where the LJ interactions can be further divided into repulsion and dispersion terms:

$$\begin{aligned} V_{non-bonded}(r_{ij}) &= V_{LJ}(r_{ij}) + V_{coulomb}(r_{ij}) \\ &= 4\epsilon_{ij}\left[\left(\frac{\sigma_{ij}}{r_{ij}}\right)^{12} - \left(\frac{\sigma_{ij}}{r_{ij}}\right)^{6}\right] + \frac{1}{4\pi\varepsilon_0\varepsilon_r}\frac{q_i q_j}{r_{ij}} \end{aligned} \tag{2.9}$$

where ϵ_{ij} describes the depth of the potential well, and σ_{ij} represents the effective diameter at which the LJ interatomic potential is zero. q_i denotes the partial charge of particle i, ε_0 is the electrical permittivity of vacuum and ε_r represents the relative dielectric constant.

2.1.4.2 Bonded interactions

Bonded interactions are short-ranged. Not only pair interactions (bonds) are included, but also 3- (angle) and 4- (dihedral angle) body interactions:

$$V_{bonded}(r_{ij}) = V_{bond}(r_{ij}) + V_{angle}(r_{ij}) + V_{dihedrals}(r_{ij}) \tag{2.10}$$

The bond stretching between two covalently bonded atoms i and j is represented by a harmonic potential:

$$V_{bond}(r_{ij}) = \frac{1}{2} K_{bond}(r_{ij} - r_{bond})^2 \tag{2.11}$$

where K_{bond} represent the force constant and r_{bond} denotes the equilibrium distance where $V_{bond}(r_{ij})$ reaches its minimum value.
The angle vibration between a triplet of atoms ijk is also represented by a harmonic potential:

$$V_{angle}(\theta_{ijk}) = \frac{1}{2} K_{angle}(\theta_{ijk} - \theta^0_{ijk})^2 \tag{2.12}$$

where the force constant is represented by K_{angle} and θ^0_{ijk} is the equilibrium angle. The improper dihedral angle potential $V_{dihedral}$ is meant to keep the planar structures of planar groups, and is represented as a harmonic potential:

$$V_{im-d}(\xi_{ijkl}) = K_{im-d}(\xi_{ijkl} - \xi^0_{im-ijkl})^2 \tag{2.13}$$

where ξ_{ijkl} denotes the angle between the ijk and jkl planes, $\xi^0_{im-ijkl}$ represents the equilibrium angle and K_{im-d} is the force constant.

More details of the bonded and non-bonded intra-molecular interactions described by the MARTINI force-field will be given in the next section.

2.1.5 Ensembles

MD simulations generate the dynamic information, i.e. positions and velocities. Let us consider a system consisting of N atoms, we need to know all three components of the velocity of each atom and all three components of the position of each atom to characterise the system completely. However, in many MD studies, the macroscopic thermodynamic properties are the ones we are interested in, such as temperature, pressure, and heat capacity. These are average properties of the system and these properties do not depend on all the details of the system. Statistical mechanics is used to connect the microscopic simulations to the macroscopic properties.

The principle of statistical mechanics is that all possible states appear with an equal probability. For a system, we can imagine that we have many copies of the system and all the copies are characterised by the same set of constraints. The copies of the system is called an ensemble. If the ergodic hypothesis is fulfilled whereby the system can explore all possible states in phase space over a long period of time, either time or ensemble average can be used to characterise the system. Hence, the time averages of dynamic quantities can be connected to ensembles averages. Therefore, experimentally relevant information (macroscopic thermodynamic properties) may be calculated using the data obtained from a simulation.

Depending on the target of the MD simulation study, different thermodynamic ensembles can be applied in the simulations, such as the micro-canonical, canonical and isothermal-isobaric ensembles. A micro-canonical ensemble (NVE) is formed by systems isolated from surroundings, where internal energy (E), number of particles (N) and volume (V) are constant. A canonical ensemble (NVT) is used to represent the possible states of a system at constant temperature (T) in contact with a heat bath. There is exchange of heat between the heat bath and the system, so the temperature of the configurations in the trajectory fluctuates around the temperature of the heat bath. An isothermal-isobaric ensemble NPT describes systems in contact with a thermostat (T) and a barostat (P). The system exchanges heat with the heat bath, and the volume fluctuates whiles the system is coupled to a barostat. The total number of particles of the system is

constant, but the system energy and volume fluctuate at thermal equilibrium. Lipid bilayers are particularly sensitive to these constraint conditions, due to their complicated mixing behaviour at water-lipid interfaces. There is some debate about the best choice of ensemble to employ during simulations of lipid bilayers [12, 13]. Setting up MD bilayer simulations in the NVT ensemble is difficult since the correct box dimension is required. The NPT ensemble is a more suitable ensemble for lipid bilayer simulations and more convenient, since the area is unknown prior to simulation and the simulation is required to perform in the tensionless state. The simulation box fluctuates so that the internal pressure couples to the external pressure. All simulations studied in this work are conducted with the NPT ensemble. Here, the simulation box in direction z is coupled to the barostat independently from the lateral directions x and y. The surface tension (two interfaces in bilayer/water system) is derived from the tangential and normal pressures:

$$\gamma = L_z(P_n - P_t) \tag{2.14}$$

L_z denotes the box length in z direction, P_n is the normal pressure and P_t is the tangential pressure. Since real bilayers in solution often attain a tensionless state, the simulations performed here are in the tensionless state, which is achieved by setting the normal pressure P_n (P_{zz}) equal to the tangential pressure P_t ($P_{xx} + P_{yy}$)/2). P_{ij} is the ij component of the pressure tensor, where P_{xx} and P_{yy} are tangential to the bilayer, and P_{zz} is normal to the bilayer. More information of the thermostat and barostat parameters employed is given in the next subsection.

2.1.6 Berendsen thermostat and barostat

Conceptually, the Berendsen thermostat/barostat works by coupling the system to an external heat/pressure bath with a fixed reference temperature T_0/pressure P_0 [14]. The deviation of the system temperature/pressure is slowly corrected to

the reference value, as stated below:

$$\frac{dT}{dt} = \frac{T_0 - T}{\tau_T} \tag{2.15}$$

$$\frac{dP}{dt} = \frac{P_0 - P}{\tau_P} \tag{2.16}$$

where τ is the time constant for coupling. In all simulations described in this work, τ_T and τ_P are both set to 2.0 ps respectively. Thermostat and barostat are invoked once after every 10 integration steps. One of the advantages of the Berendsen algorithm is the flexibility of the strength of coupling, so the coupling time can vary depending on the purpose of simulation. But Berendsen pressure control algorithm does not yield the exact NPT ensemble.
The temperature is calculated from the total kinetic energy (K) of the system using the equipartition theorem,

$$K = \frac{1}{2}\sum_{i=1}^{N} m_i v_i^2(t) \tag{2.17}$$

$$\frac{1}{2} N_{df} kT = K \tag{2.18}$$

where k denotes the Boltzmann's constant and N_{df} denotes the degrees of freedom, defined as $N_{df} = 3N - 3 - N_c$. 3 degrees of freedom are removed as the three center-of-mass velocities are usually set to 0. N_c represents the number of intermolecular constraints imposed on the system. The heat flow into or out of the system needed to reach the desired temperature, T, can be controlled by rescaling the velocities of all particles with a time-dependent factor $[1 + \frac{n_{TC}\Delta t}{\tau_T}\{[T_0/T(t - \frac{1}{2\Delta t}) - 1\}]^{1/2}$ every n_{TC} steps (the derivation of the equations can be found in the GROMACS user manual [10]).
The pressure tensor $\mathbf{P}$ is calculated using the Clausius virial theorem:

$$\mathbf{P} = \frac{2}{V}(K - \Xi) \tag{2.19}$$

where V is the box volume, K is the kinetic energy, and the virial Ξ is defined as a cross product (the derivation of the equations can be found in the GROMACS user manual [10]):

$$\Xi = -\frac{1}{2}\sum_{i<j} \mathbf{r}_{ij} \otimes \mathbf{F}_{ij} \tag{2.20}$$

The scalar pressure P is computed from the trace of the pressure tensor:

$$P = trace(\mathbf{P})/3 \tag{2.21}$$

The barostat adjusts the coordinates of atoms and box vectors, and therefore rescales the volume to reach the desired pressure, P_0, according to equation 2.16. In all the simulations performed in this work, the pressure was maintained at 1 bar using the semi-isotropic Berendsen barostat. In the case of semi-isotropic scaling, the x and y directions are scaled isotropically, whereas the z direction is scaled independently. The compressibility in all three directions is set to 3.0×10^{-5} bar^{-1}.

2.1.7 Periodic Boundary Condition

The molecular dynamics approach is still limited in the size of the system, even with the power of high performance clusters. Periodic boundary conditions are introduced to allow us to neglect edge effects, which allows us to study the macroscopic properties with the limited number of atoms. The simulation box containing N atoms is replicated in all dimensions to form an infinite lattice. Consequently, as a molecule moves, its replica in each of the replicated boxes will move identically. If the molecule leaves the box, one of its images will enter through the opposite side. Therefore, the overall number of molecules in each box is conserved. There is no wall at the boundaries of the box, and no surface molecules. For standard simulation work, only the information on the molecules in the original box is recorded.

Figure 2.4 shows a periodic system in two-dimensions, containing four particles. As one particle, i, is moving out of the box, its images i_{1-8} would move in the

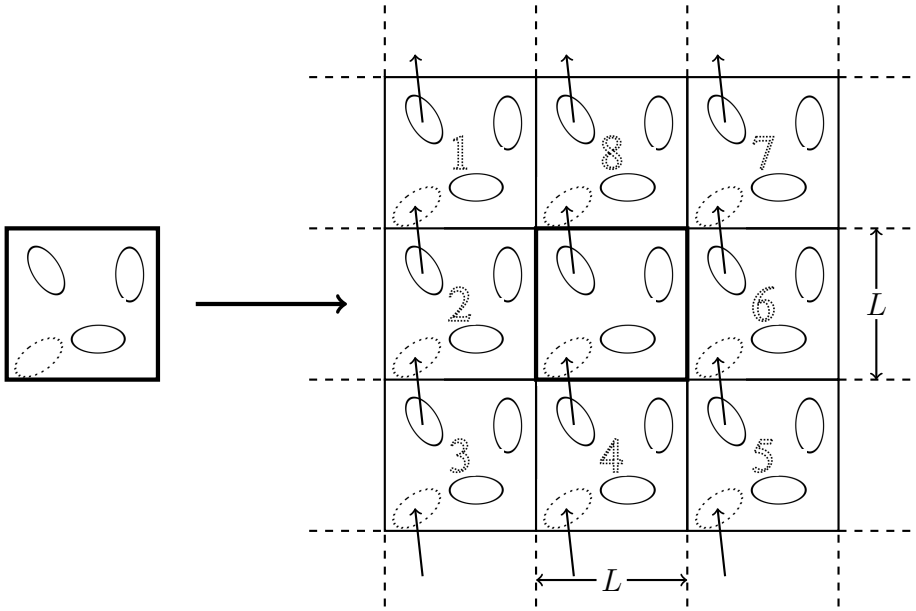

Figure 2.4: Periodic boundary conditions shown in two-dimensions. The square simulation cell at the centre is the simulation box which is replicated infinitely in all directions.

same way, and move across the corresponding boundaries.

It is important that the simulation box is big enough so that the particles cannot 'sense' the artificial symmetry of the periodic lattice. If this were not the case, a particle would interact with its own images in the neighbouring boxes. So the cut-off distance for force calculation is required to be less than half of the box length ($r_{cut} < L/2$). For all the simulations in this work, periodic boundary conditions are applied in all directions.

2.1.8 Modified non-bonded and bonded interactions

The calculation of the force on each particle is the most time-consuming step of an MD simulation. If we consider a system containing N atoms with pairwise additive interactions, we have to consider forces on each particle contributed by all its neighbours. The CPU time needed is proportional to N^2. Fortunately, several common techniques have been developed to speed up the simulations.

In MD simulations, forces are treated differently depending on their effective

range, including short- and long-range. The effect of atom j on the force sensed by a given atom i vanishes when the pair separation r_{ij} is greater than the cut-off distance for short-range interactions, i.e. Lennard-Jones pair interaction. The error incurred by ignoring the interactions at larger distance (greater than r_{cut}) can be made to be very small by choosing a relatively large r_{cut}. In many cases, long-range forces are crucial and must be considered, including Coulomb interaction between charged ions ($\sim r^{-1}$), dipole-dipole interactions between polar particles ($\sim r^{-3}$) and van der Waals attractions between atoms ($\sim r^{-6}$). Two other computational techniques are adopted to reduce the complexity of the calculation of short-range forces.

Minimum image convention: Combined with the usage of periodic boundary conditions, an atom will only interact with the nearest atom or image in the periodic array. For example, as shown in Figure 2.5, atom i interacts with l, $2j$ and $8k$.

Truncation: The Lennard-Jones potential is 'switched' to 0 when two atoms are separated further than r_{cut}. But this sudden truncation can cause large numerical errors in the integration step (discontinuity in the derivative). In GROMACS, a shift function is introduced to replace the standard non-bonded potentials, and much smaller error is produced.

After introducing a smooth function $S(r_{ij})$, the Lennard-Jones force function $F_\alpha(r_{ij})$ can be re-written:

$$\begin{aligned} F_s(r_{ij}) &= F_\alpha(r_{ij}) \quad r_{ij} < r_1 \\ &= F_\alpha(r_{ij}) + S(r_{ij}) \quad r_1 \leq r_{ij} < r_{cut} \\ &= 0 \quad r_{cut} \leq r_{ij} \end{aligned} \tag{2.22}$$

For all the simulations in this work, a standard shift function of GROMACS is applied to the Lennard-Jones potential function so that the forces decay smoothly to zero between 0.9 and 1.2 nm.

However, long-range forces cannot be treated in the same way. Simply applying a 'shifted' function can cause serious problems, as the long-range potential

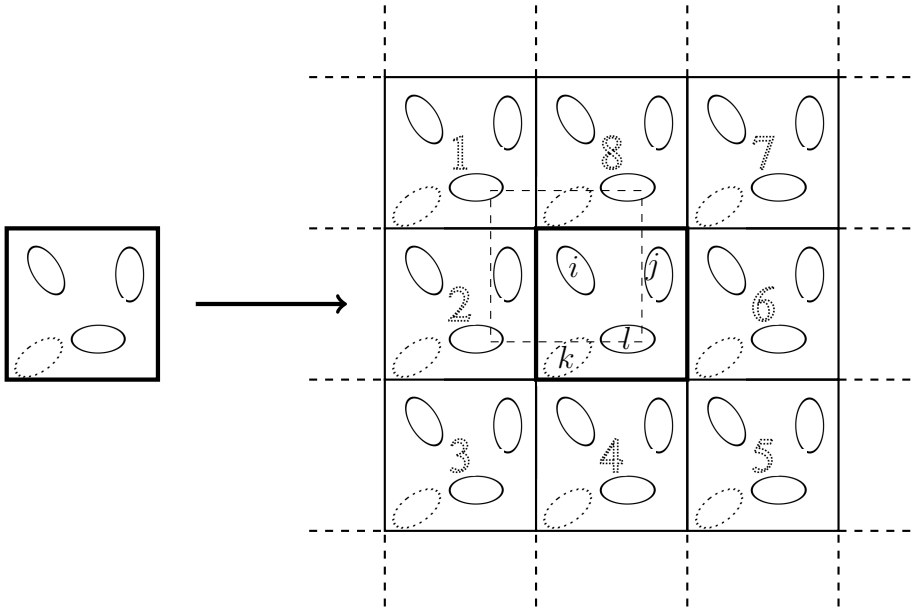

Figure 2.5: The minimum image convention shown in two-dimensions.

energy decays slower than r^{-3}. In MD simulations, long-range forces are split into two contributions: a short-ranged part and a smooth, field-like long-ranged part. There are two common methods which can be used to tackle the problem of the long-range forces, the Ewald sum and the reaction field method (see [2, 3] for details). The MARTINI force-field applied in this work has been parametrised with short range shifted electrostatic interactions. Here, the long range part of the coulombic interactions was eliminated in a similar way, by shifting the forces throughout the whole distance interval, 0 nm and 1.2 nm. Coulombic interaction are screened with a uniform relative dielectric constant $\varepsilon_r = 15$. Hence, the interaction between the charged particle i and other charged particles which are further than r_{cut}, is negligible. The electrostatic potential is shifted in this manner in order to mimic the effect of a distance-dependent screening.

2.2 MARTINI Coarse-Grained Force-field

Over the last few decades, several models of lipids have been developed at atomistic level that are able to reproduce experimental structural and dynamic data [15, 16, 17, 18, 19, 20]. Although atomistic models have been widely used to study a wide range of bilayer properties such as self-diffusion [21], impact of cholesterol [22, 23], lateral pressure profile [24, 25, 26] and transient ordered domain formation [27], the efficiency of atomistic level simulation is still limited by the computational cost (restricted to a few thousand lipid for up to a few hundred nanosecond). The study of large time- and size-scale phenomena (such as lipid domain formation and membrane-protein interactions), which is critical in many bilayer simulations, is not practical with atomistic models. A pre-assembled configuration is also compulsory for atomistic simulation studies. Otherwise, the bilayer cannot form spontaneously within the achievable time-scale by using atomistic models. A possible solution is the use of simpler, coarse-grained (CG) models. Instead of describing all the atoms within the molecules, atoms are grouped together and assigned to several pseudo-atoms in order to reduce the number of interactions that need to be calculated. Hence, the overall CPU time required can be lowered significantly (depending on the degree of coarse-graining), and large time/size scales are achievable (several thousands of lipids for several microseconds). Many coarse-grained force-fields have been developed ([28, 29, 30, 31, 32, 33, 34, 35]). The precise site-site interactions differ in every model, but in all cases there is a reduction from around 50 atomic sites to around 10 supersites for phospholipid molecules. In this study, we use a simple, efficient, and reliable CG model named MARTINI [31].

The MARTINI force-field is a commonly used force-field for biological systems available within the GROMACS package. The MARTINI force-field is currently able to model phospholipids, cholesterol, polymers, amino acids and some solvents (e.g. water, dodecane, octanol and benzene). Its performance has been tested extensively and provides good agreement compared with experimental results, including structural (liquid densities [31], area per lipid [31]), elastic (bending modulus [31]), dynamic properties (diffusion [31]) and thermodynamic phase transition temperature [36, 7]). In the following part of this section, I will de-

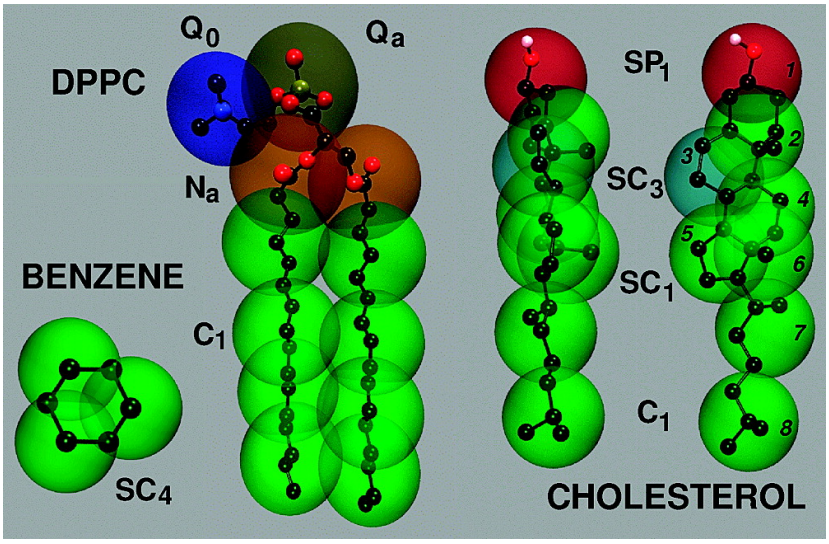

Figure 2.6: Figure taken from reference [31], shows the mapping between the real chemical structure and the CG sites for a few common molecules. The labels correspond to the types and subtypes the CG sites assigned to.

scribe the principles of the MARTINI CG force-field.

2.2.1 Atom type and interactions

The MARTINI model is based on a 4-to-1 mapping strategy. Every four atoms in the atomistic description are replaced by a single site in the MARTINI system. Exceptions are made with ring-like molecules, such as cholesterol, benzene and several amino acids, where the 4 to 1 mapping is found to be too coarse, and a 2 or 3 to 1 mapping strategy is employed instead. The CG sites are classified by their electrostatic nature, and are termed either: polar (P), non-polar (N), apolar (C), or charged (Q). For ring-like particles, a special pre-fix 'S' is applied to denote the ring nature. Each particle type is further divided with a number of subtypes to provide a more accurate description of the nature of the atomic structure. Subtypes are distinguished either by the hydrogen bonding capabilities (d=donor, a=acceptor, da=both, 0=none), or by the degree of polarity (from 1=low polarity, to 5=high polarity). Each CG site has a common mass of 72 amu (four water molecules), except for ring particles where $m = 45$ amu. Some typical

MARTINI CG models with assigned type and subtype are shown in Figure 2.6. For the molecules investigated in this work, DPPC is converted into 12 CG beads (phosphate group: Q_a, choline group: Q_o, glycerol ester: N_a, lipid tails: C_1), cholesterol is represented by 8 beads (polar -OH group: SP_1, sterol ring: SC, short tail: C_1), and each CG water (P4) site stands for four water molecules. Figure 2.7 shows a comparison of all-atom molecules and coarse-grained ones with the names of the CG beads, as well as an example of DPPC/CHOL mixture bilayer.

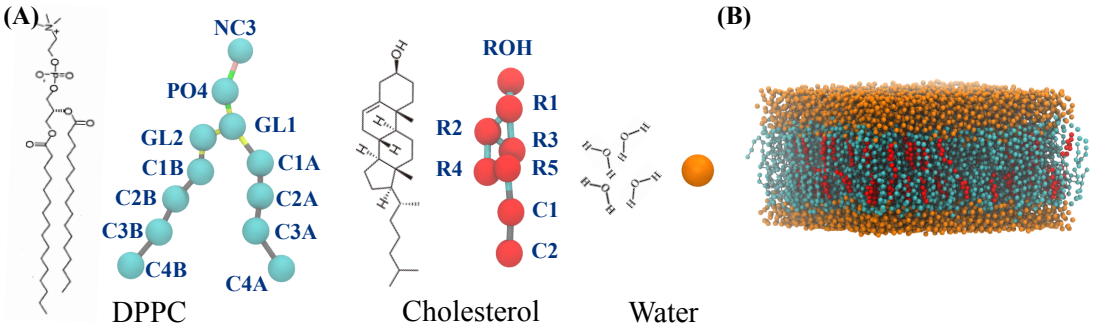

Figure 2.7: (A)Coarse grained molecular models employed on DPPC, Cholesterol and water molecules. Topologies of DPPC and cholesterol are given in table 2.2 and 2.1. (B)An example of a simulated bilayer

Interactions between CG sites still fall into two main categories: non-bonded and bonded interactions.

2.2.1.1 Non-bonded interactions

The truncated and shifted Lennard-Jones potential V_{LJ} is used here to describe the non-bonded interactions with reduced complexity of calculation. It consists of both repulsive and attractive terms. As shown in figure 2.8 as particles approach each other from infinite separation, the attractive forces initially dominate until the atom reaches the equilibrium distance (r_{eq}), where the Lennard-Jones potential attains its minimum value (equal to $-\varepsilon_{ij}$). The repulsive force become

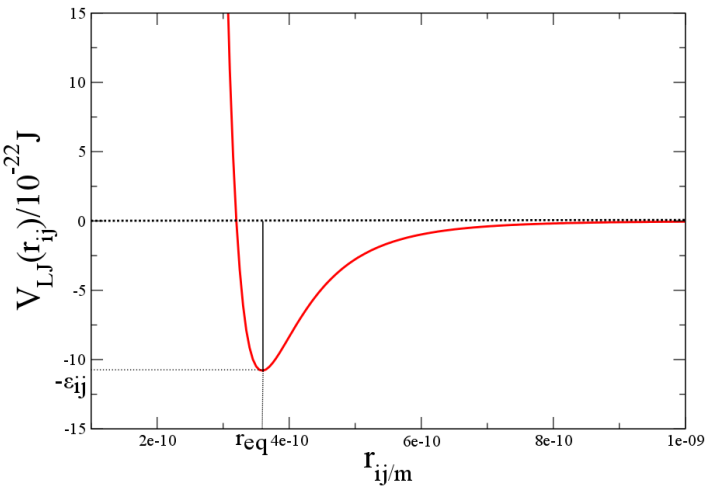

Figure 2.8: Plot of the Lennard-Jones potential for two H_2O molecules, with ε_{ij} = 1.08 $\times 10^{-21}$J and r_{eq} = 0.32 $\times 10^{-9}$m

more pronounced from this point, and the potential reaches zero at $r_{ij} = \sigma_{eff}$.

$$V_{LJ}(r_{ij}) = 4\varepsilon_{ij}\left[\left(\frac{\sigma_{ij}}{r_{ij}}\right)^{12} - \left(\frac{\sigma_{ij}}{r_{ij}}\right)^{6}\right] \tag{2.23}$$

The same effective size σ_{eff}=0.47 nm is used for all interaction pairs. The interaction strengths ϵ_{ij} are categorised into 10 levels according to the interaction sites, including: O, 5.6 kJ/mol; I, 5.0 kJ/mol; II, 4.5 kJ/mol; III, 4.0 kJ/mol; IV, 3.5 kJ/mol; V, 3.1 kJ/mol; VI, 2.7 kJ/mol; VII, 2.3 kJ/mol; VIII, 2.0 kJ/mol; and IX, 2.0 kJ/mol. Exceptions are made for three groups of particles.

1. **Ring particles**: the special particle set, 'S', is introduced to model ring structures (e.g. the cholesterol molecules investigated in this thesis). In this special set, a few modifications are made to reflect the structure as accurately as possible. σ_{eff} is reduced to 0.43 nm and the interactions between ring-ring particles are scaled to 75% of their original values, so that the ring particles can pack more closely without freezing. Within the ring systems, intermolecular LJ potentials are excluded. (for details of the information of the cholesterol CG model, see table 2.1).

2. **The antifreeze particles**: one particular problem for CG water is that it can transform to a solid state rapidly once a nucleation site is formed. The freezing temperature of CG water (280-300 K [31]) is usually higher than for explicit water. Therefore a group is introduced to prevent the unwanted freezing of water by disturbing the lattice packing of the CG water. The effective size of this group is increased to 0.57 nm from 0.47 nm. To avoid phase separation of the antifreeze particles (BP4) and normal CG water particles (P4), the interaction strength between BP4 and P4 is raised to 'O' level (5.6 kJ/mol) from 'I' level (5.0 kJ/mol). The rest of the interactions between the antifreeze particles and other particles remain the same as for the normal CG water particles. No freezing of water was observed in the simulations as low as 285 K, so no antifreeze particles were used for the simulations at and above 285 K. A small number of antifreeze particles ($n_{AF} = 0.05$) were involved in the systems below 285 K.
3. For the interactions between **charged** (Q-type) and the most **apolar types** (C1 and C2): σ_{eff} is scaled up to 0.62 nm. This ensures the charged particles keep their hydration shells in the apolar solvent.
Interactions between charged groups (Q-type) are described by a shifted Coulombic potential function (see Figure 2.9 for an example of a Coulombic potential function).

$$V_{el}(r_{ij}) = \frac{1}{4\pi\varepsilon_0\varepsilon_r}\frac{q_i q_j}{r_{ij}} \tag{2.24}$$

A relative dielectric constant of 15 was set in the MARTINI force-field, the role of dielectric constant in MARTINI force-field was discussed in the previous section 2.1.7.

2.2.1.2 Bonded interactions

The interactions between chemically connected CG sites are described by potential functions that depend on bond distance, bond angle, dihedral and improper dihedral angles.

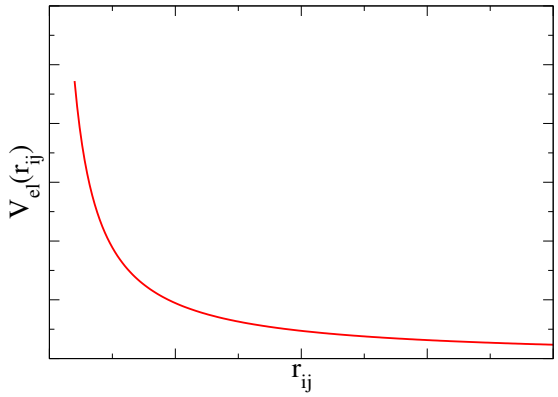

Figure 2.9: An example plot of Coulombic potential function for a pair of atoms with the same charge sign.

Bond stretching is represented by a harmonic potential:

$$V_{bond}(r_{ij}) = \frac{1}{2} K_{bond}(r_{ij} - r_{bond})^2 \tag{2.25}$$

The force constant, K_{bond}, is a constant with a value of 1250 kJ mol^{-1}nm^{-2}, and the equilibrium distance r_{bond} is set to 0.47 nm. Non bonded interactions are not calculated for bonded sites.
A weak harmonic potential is used to achieve chain stiffness:

$$V_{angle}(\theta_{ijk}) = \frac{1}{2} K_{angle}(cos(\theta_{ijk}) - cos(\theta^0_{ijk}))^2 \tag{2.26}$$

V_{angle} describes the chain stiffness. LJ interactions are included between particle i and its second nearest neighbours k. For aliphatic chains, the force constant K_{angle} is 25 kJ mol^{-1} with the equilibrium angle θ_{bond}= 180 °. The value of K_{angle} is increased to 45 kJ mol^{-1} and θ_{bond} is set to 120 ° for the description of cis-double bonds, whereas K_{angle} = 45 kJ mol^{-1} and θ_{bond}= 180 ° are used for trans-double bonds.
To preserve the rigidity of the ring structures, and to avoid fast oscillations due to the very high force constants, bonds and angles are partially replaced by an appropriate set of constraints using the LINCS algorithm. The LINCS is a Linear Constraint Solver for Molecular Simulations. It resets bonds to their correct

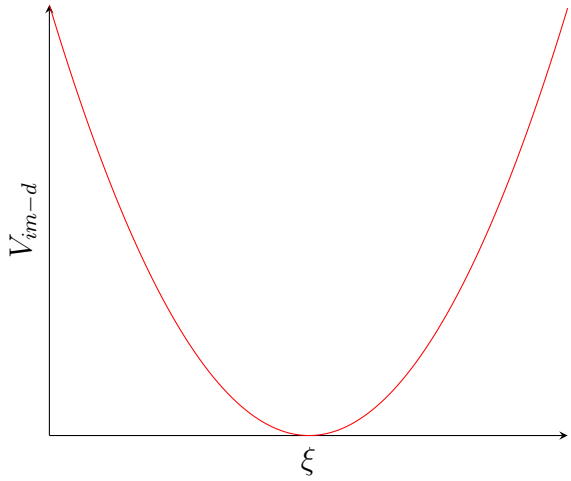

Figure 2.10: A example plot of improper dihedral potential

lengths after an unconstrained update [37].
The improper dihedral angle potential $V_{dihedral}$ is used to prevent out of plane distortions of planar groups (see Figure 2.10). In the case of the simulations of this work, only cholesterol molecules are described with the improper dihedral angle potential. It is represented as a harmonic potential:

$$V_{im-d}(\xi_{ijkl}) = K_{im-d}(\xi_{ijkl} - \xi^0_{im-ijkl})^2 \tag{2.27}$$

where ξ_{ijkl} denotes the angle between the ijk and jkl planes and $\xi^0_{im-ijkl}$ represents the equilibrium angle. K_{im-d} is the force constant, values of K_{im-d} for each improper dihedral angle with in CG cholesterol molecule are given in table 2.1.

2.2.2 Interpretation of Time Scale

The time scale of CG simulations cannot be compared with that of atomistic simulations directly. The dynamics of CG atoms are generally much faster due to the smoother underlying energy landscape, but a general scaling factor is investigated in various simulation systems. It has been found empirically that applying a scaling factor of 4 can reproduce experimental quantities well [31]. 4 is the speed up factor of CG water compared to real water in diffusional dynamics. But this empirical factor was not applied in calculating the data obtained in this thesis.

Table 2.1: CG topology of Cholesterol

atom			**bonds**			**constraints**	
id	bead type	atom	$i\ j$	length/nm	$K_{bond}/kJmol^{-1}nm^{-2}$	$i\ j$	length/nm
1	SP1	ROH	1 2	0.242	20000	1 3	0.493
2	SC1	R1	2 3	0.260	20000	1 4	0.604
3	SC3	R2	2 4	0.341	20000	3 4	0.272
4	SC1	R3	4 6	0.213	20000	3 5	0.346
5	SC1	R4	4 7	0.544	20000	4 5	0.294
6	SC1	R5	5 6	0.203	20000	5 7	0.406
7	SC1	C1	6 7	0.368	20000		
8	C1	C2	7 8	0.425	1250		
angles			**improper**				
$i\ j\ k$	θ_{ijk}/deg	$K_{angle}/kJmol^{-1}$	$i\ j\ k\ l$	ξ_{ijkl}/deg	$K_{im-d}/kJmol^{-1}rad{-}2$		
4 7 8	180.0	25	1 3 5 4	0	100		
			1 4 5 3	0	100		
			3 5 7 4	0	100		
			4 7 5 3	0	100		
			2 1 3 4	-45.0	300		
			2 4 3 1	45.0	300		
			6 4 5 7	-45.0	300		
			6 7 5 4	45.0	300		

Table 2.2: CG topology of DPPC

atom			**bonds**			**angles**		
id	bead type	atom	$i\ j$	length/nm	$K_{bond}/kJmol^{-1}nm^{-2}$	$i\ j\ k$	θ_{ijk}/deg	$K_{angle}/kJmol^{-1}$
1	Q0	NC3	1 2	0.470	1250	2 3 4	120.0	25.0
2	Qa	PO4	2 3	0.470	1250	2 3 5	180.0	25.0
3	Na	GL1	3 4	0.470	1250	3 5 6	180.0	25.0
4	Na	GL2	3 5	0.470	1250	5 6 7	180.0	25.0
5	C1	C1A	5 6	0.470	1250	6 7 8	180.0	25.0
6	C1	C2A	6 7	0.470	1250	4 9 10	180.0	25.0
7	C1	C3A	7 8	0.470	1250	9 10 11	180.0	25.0
8	C1	C4A	4 9	0.470	1250	10 11 12	180.0	25.0
9	C1	C1B	9 10	0.470	1250			
10	C1	C2B	10 11	0.470	1250			
11	C1	C3B	11 12	0.470	1250			
12	C1	C4B						

2.3 Analysis

Several order parameters are employed in this work in order to investigate the properties of the bilayers. I will describe below the general quantitative parameters used through the thesis; some more specific analysis for particular studies are given within the Results section.

2.3.1 Area per molecule

The area per molecule is one of the most common parameters used to monitor structural changes in bilayers. A clear, discontinuous change in area should be observed for a first-order phase transition. In single-component systems, it is a straightforward procedure to calculate the area per molecule, which can be defined as $A = (L_x \times L_y)/N$ (N is the total number of molecules per monolayer and $L_x \times L_y$ is the cross sectional area of the simulation box). However, things are more complicated with multi-component systems, e.g. with the cholesterol containing bilayers in this thesis. The commonly reported area per molecule is calculated by dividing the cross-sectional area over the total number of lipids, regardless of type. The resulting area would be the average area per lipid, but not the specific area for every species. Here the Voronoi tessellation method [38] is employed which allows us to compute the specific area for each type of molecule. The voronoi tessellation method is a powerful approach to resolve the structural organization of the bilayer. It has been used extensively to interpret various biological systems, such as the bilayer structure around proteins [39] and in ionic solutions at low concentrations [40]. Given a set of n points, the space is subdivided into n polygons for each point after applying the Voronoi algorithm. Hence, the specific area per molecule can be obtained by calculating the area of the polygon occupied by each molecule. There are a few steps to construct a Voronoi diagram (see Figure 2.11):

1. Start with two points that next to each other.
2. Draw the perpendicular bisector of the segment that joins these two points,

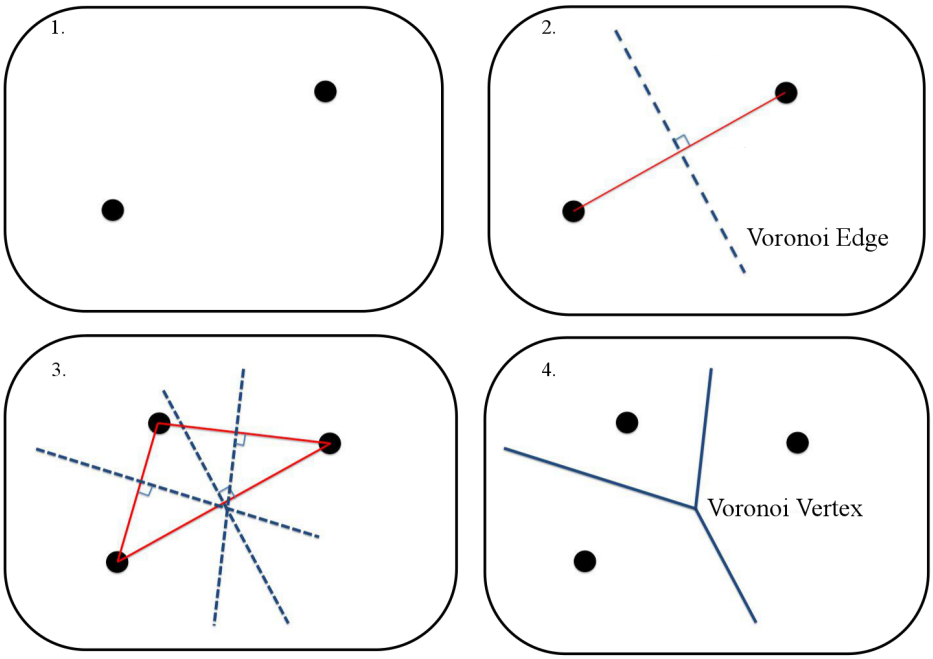

Figure 2.11: Illustration of how Voronoi diagram is constructed step-by-step.

which is a Voronoi edge.
3. Add a third point and repeat previous step for every two points.
4. Remove each section of the Voronoi edges that violate the equidistant rule. The Voronoi vertex is the point equidistant to three points. For every extra point added, the same method described above is repeated.

In this work, the phospholipids DPPC and DOPC, and cholesterol molecules are involved in the bilayers that needed to be analysed. The bilayers are first split into the upper and lower monolayers according to the sign of the vector between head and tail groups (phospholipid: PO4 and C2A; Cholesterol: ROH and C2). The head groups of the phospholipids and the cholesterol are projected onto the xy plane (see Figure 2.12A). A two dimensional Voronoi construction for each monolayer is then performed to determine, for each head group, that region of the monolayer that is nearer to that head group than any other (see Figure 2.12B). The area of each molecule is then taken to be the area of its enclosing polygon. The resulting area per phospholipid/cholesterol is taken as

an average through all polygons in both monolayers. The code employed in this work is based on the open source code Qhull (http://www.qhull.org) and it was kindly provided by Dr Anders Lervik.

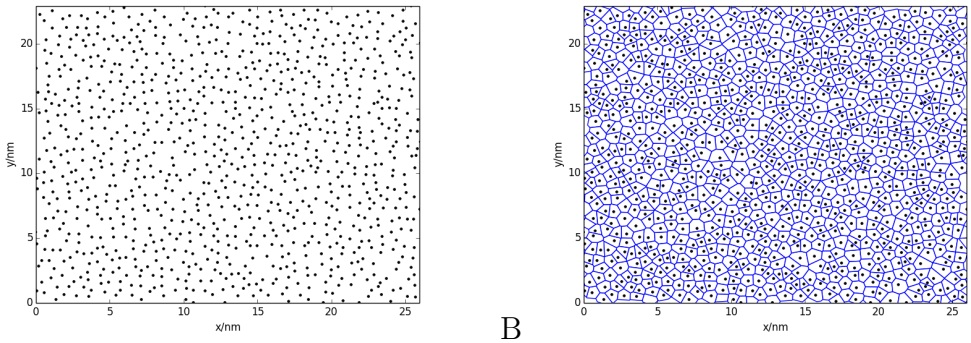

Figure 2.12: (A)The head group beads of phospholipid (PO4) from a single leaflet are projected onto a 2D plane as black dots, (B) The Voronoi diagram of the same head groups and the corresponding polygon is defined with blue lines.

2.3.2 Chain order parameter

Phospholipids contain long carbon chains, the orientation of which can vary with the thermodynamic state. These aliphatic chains are much less well-ordered above the melting temperature of the lipids. The presence of cholesterol is a further influence on the structure of the chain. Cholesterol induces conformational changes in the lipid chains. Such a change in chain ordering can be monitored by computing a chain order parameter, S_{chain}. It measures the orientation of each consecutive bond with respect to the bilayer normal (S_{bond}). By averaging the S_{bond} values of all the bonds vectors within the lipid tails, the chain order parameter S_{chain} is obtained:

$$S_{\text{bond}} = \frac{1}{2}(3\langle\cos^2\theta\rangle - 1) \tag{2.28}$$

$$S_{\text{chain}} = \langle S_{\text{bond}}\rangle \tag{2.29}$$

where θ is the angle between the bond vector and bilayer normal ($z - axis$ here, see Figure 2.13 for the visual representation). The angular brackets denote a time

average used for calculation (S_{chain} values reported in this thesis were averaged over 100 configurations taken from the last 100 ns of the microsecond long simulation trajectories) and also over all CG sites in tails. S_{chain} is 1 when there is perfect alignment of the bonds with the bilayer normal. A value of zero indicates a completely random bond orientation and a lipid tail that is perpendicular to the bilayer normal results in a value of -0.5 [41]. In experiments, the chain ordering is usually measured using deuterium NMR which measures the angle between the bilayer normal and the carbon-deuterium bond and gives the order parameter S_{CD}. Therefore, the order parameters S achieved from simulations and experiments cannot be compared directly. However, the order parameters are related as $S_{\text{chain}} = -2S_{CD}$ to a good approximation that makes the comparison with deuterium NMR results possible.

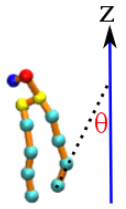

Figure 2.13: Representation of the observation of order parameter S_{chain}. The observed bond vector is tilted at an angle α with respect to the bilayer normal (z-axis).

2.3.3 Radial distribution function

2-dimensional radial distribution functions (RDF) are used to quantify the long range correlations in the bilayer plane. For the correlation between group A and B, the RDF is described as:

$$g_{AB}(r) = \frac{\langle \rho_B(r) \rangle}{\langle \rho_B \rangle} = \frac{1}{\langle \rho_B \rangle} \frac{1}{N_A} \sum_{i \in A}^{N_A} \sum_{i \in B}^{N_B} \frac{\delta(r_{ij} - r)}{4\pi r^2} \tag{2.30}$$

where $\langle \rho_B(r) \rangle$ denotes the particle density of group B particles at a distance r from A; $\langle \rho_B \rangle$ is the average number density of B particles; r_{ij} is the distance

between individual A-B pairs. RDFs are a convenient tool to show the difference in translational ordering between gel (longer and stronger correlations) and fluid (weak correlations at long range) phases. The middle CG sites of the phospholipid chains, C2A and C2B, were selected to compute the RDFs [42], which provide a clearer view of the packing structure of the phospholipids on the bilayer plane.

2.3.4 Lateral diffusion coefficient

Apart from the structural parameters, dynamic properties are also of interest in understanding the bilayers. The lateral diffusion coefficients, D, of each type of lipid are computed using the Einstein relation.

$$\langle \Delta r(t)^2 \rangle = \frac{1}{N} \sum_{i=1}^{N} \{ \mathbf{r}_i(t) - \mathbf{r}_i(0) \}^2 \tag{2.31}$$

$$\langle \Delta r(t)^2 \rangle = 4Dt^{\alpha} \tag{2.32}$$

$$D = \lim_{t \to \infty} \frac{1}{4t} \langle \Delta r(t)^2 \rangle \tag{2.33}$$

where the brackets $\langle\rangle$ represents an ensemble average over molecules and time-origins; $\langle \Delta r(t)^2 \rangle$ is the average mean squared displacement of the lipids at time t. The value of α indicates whether the normal diffusion is observed. In normal diffusion processes, the mean squared displacement is found to be a linear function of time i.e. $\alpha = 1$ (see equation 2.33). Super-diffusion and sub-diffusion are defined as diffusion processes with non-linear relationship to time, with $\alpha > 1$ and < 1 respectively. For a large system such as the bilayers in this study, the movement of the system's center of mass has to be subtracted to avoid overestimation in the mean square displacement and misinterpreting in the resulting diffusion coefficient [43].

In this work, all lateral diffusion coefficients reported were computed from the regime with normal diffusion behaviour (see Figure 2.14A as an example). In this work, 5000 configurations across 500 ns simulation time were employed to perform the calculation over all lipid molecules.

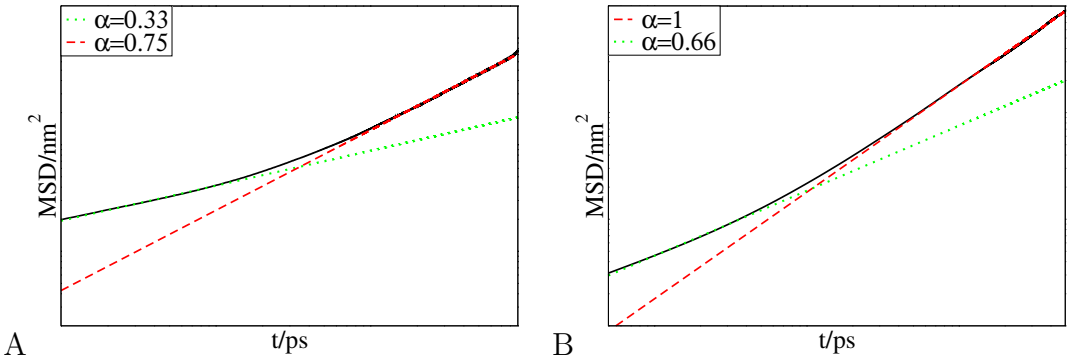

Figure 2.14: Example plots of MSD vs. time showing the diffusion of DPPC lipids within a fully hydrated pure DPPC bilayer in gel phase at 285 K (A) and fluid phase at 315 K (B). The dashed and dotted lines are the fittings corresponding to different diffusion behaviours with different α values. In gel phase, only sub-diffusion behaviour is achieved within the time-scale, while normal diffusion is seen in fluid phase.

References

[1] B. J. Alder and T. E. Wainwright. Phase transition for a hard sphere system. *The Journal of Chemical Physics*, 27(5):1208–1209, 1957. 38

[2] G. A. Chapela, G. Saville, S. M. Thompson, and J. S. Rowlinson. Computer simulation of a gas-liquid surface. part 1. *J. Chem. Soc., Faraday Trans. 2*, 73:1133–1144, 1977. 39, 52

[3] D. Frenkel and J. P. McTague. Computer simulations of freezing and supercooled liquids. *Annual Review of Physical Chemistry*, 31(1):491–521, 1980. 39, 52

[4] D. Frenkel and B. Smit. In *Understanding Molecular Simulation (Second Edition)*, pages 63 – 107. Academic Press, San Diego, second edition edition, 2002. 39

[5] M.P. Allen and D.J Tildesley. In *Computer Simulation of Liquids*. Oxford University Press, New York, 1987. 39, 40

[6] R.W Hockney, S.P Goel, and J.W Eastwood. Quiet high-resolution computer models of a plasma. *Journal of Computational Physics*, 14(2):148 – 158, 1974. 42

[7] S. J. Marrink, J. Risselada, and A. E. Mark. Simulation of gel phase formation and melting in lipid bilayers using a coarse grained model. *Chemistry and Physics of Lipids*, 135(2):223 – 244, 2005. 42, 53

[8] M. Winger, D. Trzesniak, R. Baron, and W. F. van Gunsteren. On using a too large integration time step in molecular dynamics simulations of coarse-

grained molecular models. *Phys. Chem. Chem. Phys.*, 11:1934–1941, 2009. 42

[9] H.J.C. Berendsen and W.F. van Gunsteren. Practical algorithms for dynamic simulations. In *Molecular-dynamics simulation of statistical-mechanical systems. Proceedings of the International School of Physics Enrico Fermi*, pages 43–65. North-Holland, Amsterdam, 1986. 42

[10] D. van der Spoel, E. Lindahl, B. Hess, A. R. van Buuren, E. Apol, P. J. Meulenhoff, P. D. Tieleman, A. L. T. M. Sijbers, A. K. Feenstra, R. van Drunen, and H. J. C. Berendsen. *GROMACS User Manual version 4.5.6*, 2013. 42, 48, 49

[11] S. C. Harvey, R. K.-Z. Tan, and T. E. Cheatham. The flying ice cube: Velocity rescaling in molecular dynamics leads to violation of energy equipartition. *Journal of Computational Chemistry*, 19(7):726–740, 1998. 43

[12] D. P. Tieleman and H. J. C. Berendsen. Molecular dynamics simulations of a fully hydrated dipalmitoylphosphatidylcholine bilayer with different macroscopic boundary conditions and parameters. *The Journal of Chemical Physics*, 105(11):4871–4880, 1996. 47

[13] RichardW. Pastor and ScottE. Feller. Time scales of lipid dynamics and molecular dynamics. In Jr. Merz, K. and B. Roux, editors, *Biological Membranes*, pages 3–29. Birkhäuser Boston, 1996. 47

[14] H. J. C. Berendsen, J. P. M. Postma, W. F. van Gunsteren, A. DiNola, and J. R. Haak. Molecular dynamics with coupling to an external bath. *The Journal of Chemical Physics*, 81(8):3684–3690, 1984. 47

[15] K. M Merz Jr. Molecular dynamics simulations of lipid bilayers. *Current Opinion in Structural Biology*, 7(4):511 – 517, 1997. 53

[16] D.P Tieleman, S.J Marrink, and H.J.C Berendsen. A computer perspective of membranes: molecular dynamics studies of lipid bilayer systems. *Biochimica et Biophysica Acta (BBA) - Reviews on Biomembranes*, 1331(3):235 – 270, 1997. 53

[17] J. W. Essex, M. M. Hann, and W. G. Richards. Molecular dynamics simulation of a hydrated phospholipid bilayer. *Philosophical Transactions of the Royal Society of London. Series B: Biological Sciences*, 344(1309):239–260, 1994. 53

[18] E. Egberts, S. Marrink, and H. Berendsen. Molecular dynamics simulation of a phospholipid membrane. *European Biophysics Journal*, 22(6):423–436, 1994. 53

[19] P. van der Ploeg and H.J.C. Berendsen. Molecular dynamics of a bilayer membrane. *Molecular Physics*, 49(1):233–248, 1983. 53

[20] P. van der Ploeg and H. J. C. Berendsen. Molecular dynamics simulation of a bilayer membrane. *The Journal of Chemical Physics*, 76(6):3271–3276, 1982. 53

[21] E. Lindahl and O. Edholm. Molecular dynamics simulation of NMR relaxation rates and slow dynamics in lipid bilayers. *The Journal of Chemical Physics*, 115(10):4938–4950, 2001. 53

[22] E Falck, M Patra, M Karttunen, MT Hyvnen, and I Vattulainen. Lessons of slicing membranes: interplay of packing, free area, and lateral diffusion in phospholipid/cholesterol bilayers. *Biophysical journal*, 87(2):10761091, August 2004. 53

[23] M. Patra. Lateral pressure profiles in cholesterol/DPPC bilayers. *European Biophysics Journal*, 35(1):79–88, 2005. 53

[24] J Gullingsrud and K Schulten. Lipid bilayer pressure profiles and mechanosensitive channel gating. *Biophysical journal*, 86(6):34963509, 2004. 53

[25] M. Carrillo-Tripp and S. E. Feller. Evidence for a mechanism by which -3 polyunsaturated lipids may affect membrane protein function. *Biochemistry*, 44(30):10164–10169, 2005. PMID: 16042393. 53

[26] J. Gullingsrud, A. Babakhani, and J. A. McCammon. Computational investigation of pressure profiles in lipid bilayers with embedded proteins. *Molecular Simulation*, 32(10-11):831–838, 2006. 53

[27] T. Murtola, T. Ròg, E. Falck, M. Karttunen, and I. Vattulainen. Transient ordered domains in single-component phospholipid bilayers. *Phys. Rev. Lett.*, 97:238102, Dec 2006. 53

[28] B. Smit, P. A. J. Hilbers, K. Esselink, L. A. M. Rupert, N. M. Van Os, and A. G. Schlijper. Structure of a water/oil interface in the presence of micelles: a computer simulation study. *The Journal of Physical Chemistry*, 95(16):6361–6368, 1991. 53

[29] J. C. Shelley, M. Y. Shelley, R. C. Reeder, S. Bandyopadhyay, and M. L. Klein. A coarse grain model for phospholipid simulations. *The Journal of Physical Chemistry B*, 105(19):4464–4470, 2001. 53

[30] S. Izvekov and G. A. Voth. A multiscale coarse-graining method for biomolecular systems. *The Journal of Physical Chemistry B*, 109(7):2469–2473, 2005. 53

[31] S. J. Marrink, A. H. de Vries, and A. E. Mark. Coarse grained model for semiquantitative lipid simulations. *The Journal of Physical Chemistry B*, 108(2):750–760, 2004. 53, 54, 57, 59

[32] R. Goetz and R. Lipowsky. Computer simulations of bilayer membranes: Self-assembly and interfacial tension. *The Journal of Chemical Physics*, 108(17):7397–7409, 1998. 53

[33] C. Loison, M. Mareschal, K. Kremer, and F. Schmid. Thermal fluctuations in a lamellar phase of a binary amphiphilesolvent mixture: A molecular-dynamics study. *The Journal of Chemical Physics*, 119(24):13138–13148, 2003. 53

[34] M. J. Stevens. Coarse-grained simulations of lipid bilayers. *The Journal of Chemical Physics*, 121(23):11942–11948, 2004. 53

[35] O. Lenz and F. Schmid. A simple computer model for liquid lipid bilayers. *Journal of Molecular Liquids*, 117(13):147 – 152, 2005. 53

[36] SJ Marrink and AE Mark. Molecular view of hexagonal phase formation in phospholipid membranes. *Biophysical Journal*, 87(5):3894–900, 2004-12-01 00:00:00.0. 53

[37] B. Hess, H. Bekker, H. J. C. Berendsen, and J. G. E. M. Fraaije. LINCS: A linear constraint solver for molecular simulations. *Journal of Computational Chemistry*, 18(12):1463–1472, 1997. 59

[38] W. Brostow, M. Chybicki, R. Laskowski, and J. Rybicki. Voronoi polyhedra and delaunay simplexes in the structural analysis of molecular-dynamics-simulated materials. *Phys. Rev. B*, 57:13448–13458, Jun 1998. 62

[39] A. Lervik, F. Bresme, and S. Kjelstrup. Molecular dynamics of the ca^{2+}-pump: a structural analysis. *Phys. Chem. Chem. Phys.*, 14:3543–3553, 2012. 62

[40] J.C.G Montoro, F. Bresme, and J.L.F. Abascal. Ionic association in electrolyte solutions - a voronoi polyhedra analysis. *J. Chem. Phys.*, 101:10892–10896, 1994. 62

[41] LV Schäfer, DH de Jong, A Holt, AJ Rzepiela, AH de Vries, B Poolman, JA Killian, and SJ Marrink. Lipid packing drives the segregation of transmembrane helices into disordered lipid domains in model membranes. *Proc. Natl. Acad. Sci.*, 108:1343–1348, 2011. 65

[42] D. Mohammad-Aghaie, E. Mace, C. A. Sennoga, J. M. Seddon, and F. Bresme. Molecular dynamics simulation of liquid condensed to liquid expanded transitions in DPPC monolayers. *J. Phys. Chem. B*, 114:1325–1335, 2010. 66

[43] E. Lindahl and O. Edholm. Molecular dynamics simulation of NMR relaxation rates and slow dynamics in lipid bilayers. *The Journal of Chemical Physics*, 115(10):4938–4950, 2001. 66

Chapter 3

Phase behavior of DPPC/Cholesterol mixtures

In this chapter we present a CG-MD simulation study of a saturated DPPC phospholipid bilayer containing cholesterol. The properties studied are the area per lipid, chain order parameters, radial distribution function, lateral packing and diffusion coefficient. Most of the experimental effects of cholesterol on these properties and the phase diagrams are reproduced qualitatively in this work. Based on the results of structural and dynamics properties we propose a DPPC/cholesterol temperature-composition phase diagram, which we compare with the experimental and computational phase diagrams. The work detailed in this chapter has been published as [1]:

Y. Zhang, A. Lervik, J. Seddon and F. Bresme, "A coarse-grained molecular dynamics investigation of the phase behavior of DPPC/cholesterol mixtures", *Chemistry and Physics of Lipids*, 2014, in press
doi: 10.1016/j.chemphyslip.2014.07.011

3.1 Introduction

Cell membranes are primarily composed of a phospholipid bilayer. A large array of other components including proteins, carbohydrates and sterols can be embedded within cell membranes. In animal cells, cholesterol is one of the major

non-lipidic constituents. It plays a predominant role in membrane functions, and can make up almost half of the membrane. Despite being discovered in 1769 by François Poulletier de la Salle [2], efforts to understand cholesterol at the atomic level have only taken place in the last few decades. Recent experimental and simulation studies have shown the strong influence on membrane properties the addition of cholesterol has. Nevertheless, recent investigations on bending modulus of cholesterol containing lipid bilayers reveals the fact that lipid composition is another factor in such a perturbation [3]. The conclusion has been made that cholesterol perturbs the lipid membrane non-universally. Cholesterol has been shown to influence the bulk biophysical properties of phospholipid membranes [4, 5, 6], such as the membrane fluidity and permeability [7, 8]. With an increased amount of cholesterol present in lipid membrane, a cholesterol-rich domain, named a 'lipid raft' (discussed in chapter 1), is suggested [9, 10, 11].

In this work, we are interested in the phase behaviour of bilayers mainly constructed with DPPC (1,2-dipalmitoyl-sn-glycero-3-phosphocholine) phospholipids. DPPC has a relatively high transition temperature of 41.2 °C[12, 13] and undergoes a well-defined gel-fluid phase transition. The general features of different phases have been discussed in chapter 1 and will be used to distinguish the phase transition. When cholesterol is introduced, the phase behaviour of the lipid membrane becomes much more complex. Cholesterol intercalates between the DPPC molecules and restrains the flexibility of surrounding phospholipids. As a consequence, a new thermodynamically stable state between the 'S_o' (solid-ordered) and 'L_d' (liquid-disordered) is formed, named the 'L_o' (liquid-ordered) phase proposed by Ipsen et al. in 1987 [14]. The new phase is characterized by an intermediate translational and conformational order between that of the gel phase and fluid phase.

The effect of cholesterol on membrane properties, including structural and dynamic properties, has been studied extensively experimentally in the past decades [15]. The phase behaviour of the phospholipid/cholesterol bilayer has been investigated using different approaches; calorimetry (DSC) [16], NMR [17] and X-ray scattering [13]. DSC can be used to investigate the phase transition by reporting the sudden enthalpy change within the system. NMR on the other hand is a very useful technique to probe the conformational properties of the lipid chains, while

the bilayer thickness, area per lipid and density profiles can be easily extracted from X-ray scattering studies. These techniques focus on different parameters and it is not straightforward to compare the phase diagrams obtained from different techniques, especially between experimental and simulation studies. A strong modification of the phase transition has been observed upon addition of 25 mol% cholesterol [18, 19, 20], with the formation of the 'L_o' phase at high concentrations of cholesterol. With the rapid development of computational techniques, simulation provides another powerful approach to gain a microscopic insight on the nature of lipid bilayer phase transitions with the possibility of extending these studies to extreme conditions, i.e. very high pressure and temperature. There is a good agreement between simulation and experiment for bilayers with either very low or high contents of cholesterol [18, 19, 20, 21, 22, 23, 24]. It has been found that the bilayer remains in the gel phase with the addition of a small amount of cholesterol, whereas a pure L_o phase is observed in cholesterol rich ($x_{chol} \geq 0.4$) lipid bilayers [18]. Contradictory conclusions in bilayers with intermediate concentrations of cholesterol have been reported, and so this topic is still the focus of great debate.

Some simulation work using coarse-grained models have revealed phase coexistence both below (S_o/L_o) and above (L_d/L_o) the main transition temperature of the DPPC [21], whereas some other studies based on fully atomistic models report only single phases [20]. The situation with experiments remains unclear as well. Veatch et al. [25, 26] indicated the formation of phase coexistence in ternary mixtures, but not with binary mixtures. In contrast, studies based on calorimetric, NMR and electron double resonance techniques found the existence of cholesterol-rich and cholesterol-free domains, which is consistent with some simulation studies [27, 4, 28].

It is clear that it is not fully understood how DPPC/Cholesterol bilayers respond to temperature and addition of cholesterol. Neither the nature of transitions nor the roles of cholesterol are entirely obvious. Because the phase diagram provides information on the properties of bilayers, an understanding of the phase behaviour is important for those interested in membrane functions.

Historically, atomistic simulation studies on lipid phase transitions have been full of difficulties due to the large length and time scales required to probe such phe-

nomena, usually several thousand of lipids and tens of microseconds. Here, the work on DPPC/CHOL mixtures in this chapter is based on the MARTINI [29] coarse-grained (CG) forcefield, which was developed to allow simulations of larger length and time scales. In this chapter, a systematic analysis of the impact of cholesterol on lipid bilayer structural and dynamical properties over a wide range of temperatures is presented. This work demonstrates the success of application of the MARTINI force field, with the construction of the DPPC/CHOL temperature-composition phase diagram.
We begin this chapter by describing the Methods applied and the Results obtained to identify different phases. A complete DPPC/CHOL phase diagram is then proposed and discussed.

3.2 Simulation Methods

3.2.1 Force-field and simulation details

As mentioned in the Introduction section, classical all-atom/united-atom molecular simulations are not ideal for the study of lipid membrane phase behaviour. Instead, the standard MARTINI CG model with MARTINI 2.0 force field is used in all the simulations reported in this chapter, including DPPC, cholesterol and water molecules. The initial configurations of DPPC (T = $325K$) and DPPC/CHOL (T = $300K$, $x_{chol} = 0.3$) bilayers were taken from the simulation work of Marrink and co-workers [29] (available on-line at: http://md.chem.rug.nl/cgmartini/), which contain about 100 lipids only. We then replicated the pure DPPC bilayer in the xy dimensions and achieved a configuration with 2048 DPPC molecules and 32000 water pseudo-molecules, corresponding to 62.5 water molecules per lipid for full hydration (30.1/12.6 water molecules/lipid at 325K/293K are required for fully hydration) [30]. The DPPC/CHOL ($x_{chol} = 0.3$) bilayer was replicated to obtain a large bilayer consisting of 2032 DPPC and 1024 cholesterols. The bilayer was solvated with over 30000 water pseudo-molecules. Configurations with different concentrations of cholesterol ($x_{chol} = 0.2 - 0.5$) were achieved by randomly removing the appropriate number of DPPC or cholesterol

molecules from both monolayers. The resulting two monolayers were constructed with the same composition and given a typical simulation box in dimensions of $\{L_x, L_y, L_z\} = \{25, 25, 10\}$ nm with 4×10^4 particles including $\approx$ 2000 DPPC molecules.

All the simulations were performed at constant temperature. The temperatures of the lipids (including DPPC and cholesterol) and water were maintained separately by Berendsen thermostats [31] with a 2.0 ps time constant. For the investigation of membrane phase behaviour, systems were simulated at a range of temperatures from 283 K to 323 K (285 K - 325 K for the pure DPPC bilayer) with 10 K intervals. The Berendsen barostat [31] was used for pressure coupling with a time constant of 2.0 ps. Compressibility was set to 3.0×10^{-5} bar^{-1} in the x/y and z directions, whereas pressure was maintained at 1 bar semi-isotropically in all directions. Therefore, all the simulations are at the physically relevant tensionless state. The equations of motion were integrated using the leap-frog algorithm, with a time step of 20 fs. Periodic boundary conditions were applied in all directions. All the simulations were performed using the GROMACS software package (version 4.5) [32].

Standard interaction parameters for particle diameter, interaction strength and charges were applied, which have been optimized for the MARTINI CG model [29]. Details of the description of these parameters can be found in Chapter 2).

After the energy minimization of the initial configuration, bilayers were equilibrated and simulated for up to 10 μs at low temperature (285 K/283 K). The final configurations at low temperature were used as the starting configurations for higher temperature runs. To monitor the liquid-gel phase transition ($x_{chol} = 0, 0.2$), the final configurations of the highest temperature runs (325 K/323 K) were cooled down back to low temperature (285 K/283 K) in 10 K increments. The trajectories were saved every 5000 steps (0.1 ns). The first few μs in the trajectory was discarded and used as a pre-equilibration phase.

3.2.2 Analysis

In order to investigate the lipid coordination number and define the gel phase, a Voronoi analysis was performed on two of the central beads in the acyl chains of

DPPC (C2A/C2B). The neighbours of these C2 beads can be then identified. In typical solid phase, lipids should be hexagonally packed (six neighbours). In the case of lattice defects, five and seven-fold coordination would be observed. The following criterion developed by Marrink [33] was employed: A tail is considered to be in an ordered phase if the C2A/C2B site of the tail has exactly six neighbours and at least five of these six neighbours lie within a distance smaller than 0.75 nm. The cut off distance 0.75 nm is the distance of the first minimum of the radial distribution function of the C2A/C2B beads in the solid phase. For bilayers containing cholesterol, the R3 site was instead used as it lies in approximately the same xy plane as C2A/C2B (see figure 3.1, full description of the CG DPPC and cholesterol molecular models is given in chapter 2 section 2.2.1). We used this criterion to calculate the percentage of hexagonal packing at each state and to monitor the gel/liquid phase formation process.

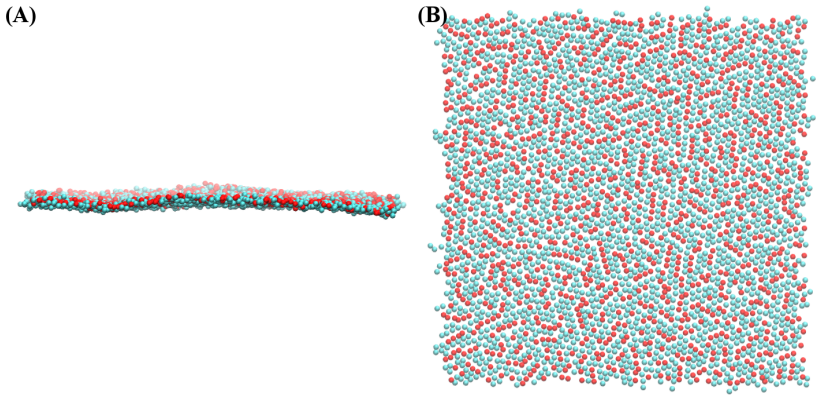

Figure 3.1: Snapshots showing the vertical positions C2A/C2B and R3 sites. C2A/C2B sites and R3 sites are found to lie in the same xy plane, as seen from a side view (A) and a top view (B). C2A/C2B site: cyan, R3: red.

3.3 Results and discussion

3.3.1 Phase transition in pure DPPC bilayers

The gel-fluid phase transition of pure DPPC bilayers has been studied extensively using both experiments and simulations. The main phase transition temperature

has been reported at 41.2 °C [12, 13]. A sharp transition should be observed as the solid phase (S_o) melts and gives a disordered liquid structure (L_d). Simulations with the MARTINI force field have also been proven to reproduce the $S_o \rightarrow L_d$ transition in previous studies [33].

3.3.1.1 Gel formation

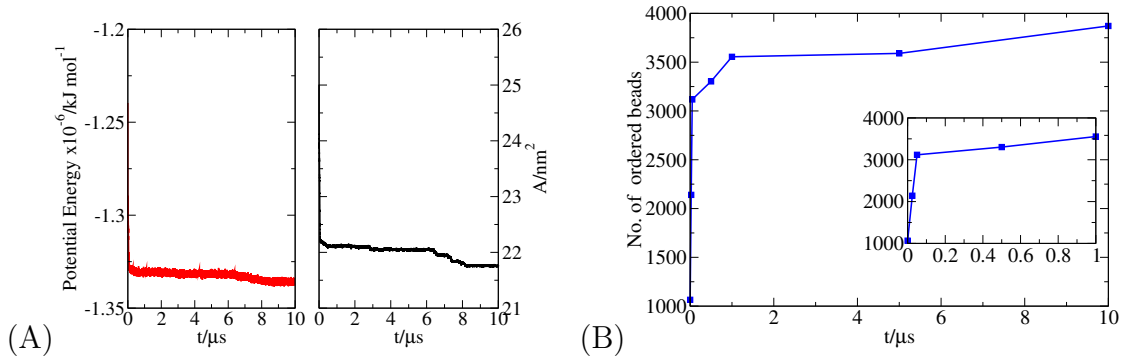

Figure 3.2: (A)Evolution of the cross-sectional area of the simulation box (black) and potential energy (red) at 285 K. (B)Number of ordered C2 beads defined using the criterion discussed in section 3.2.2 is plotted as a function of time.

We started the analysis by checking the equilibration state of the low temperature DPPC bilayer (S_o). Figure 3.2A shows the time evolution of the cross-sectional area of the simulation box and the potential energy for DPPC bilayer at 285 K. At this temperature, the system reaches its thermodynamically stable state after $\approx$ 8 μs. However, the bilayer is not still fully ordered at the end of our simulation time (see in Figure 3.3). We can still see some defects after 10 μs simulation time. Figure 3.3 shows the time evolution of the pure DPPC bilayer simulation quenched from 325 K to 285 K. Within the first 100 ns, C2 beads quickly rearrange and give six-fold coordination (see Figure 3.3). The rapid gel domain growth slows down afterwards (see Figure 3.2B), whereas a few small fluid domains persist for the duration of the simulation. These small fluid domains merge into a single domain minimizing the line tension through diffusive motion. A small fluid domain is still found even after 10 μs ($\approx$ 5% of total DPPC lipids). Reorganisation of lipids may help to eliminate the final fluid domain, as

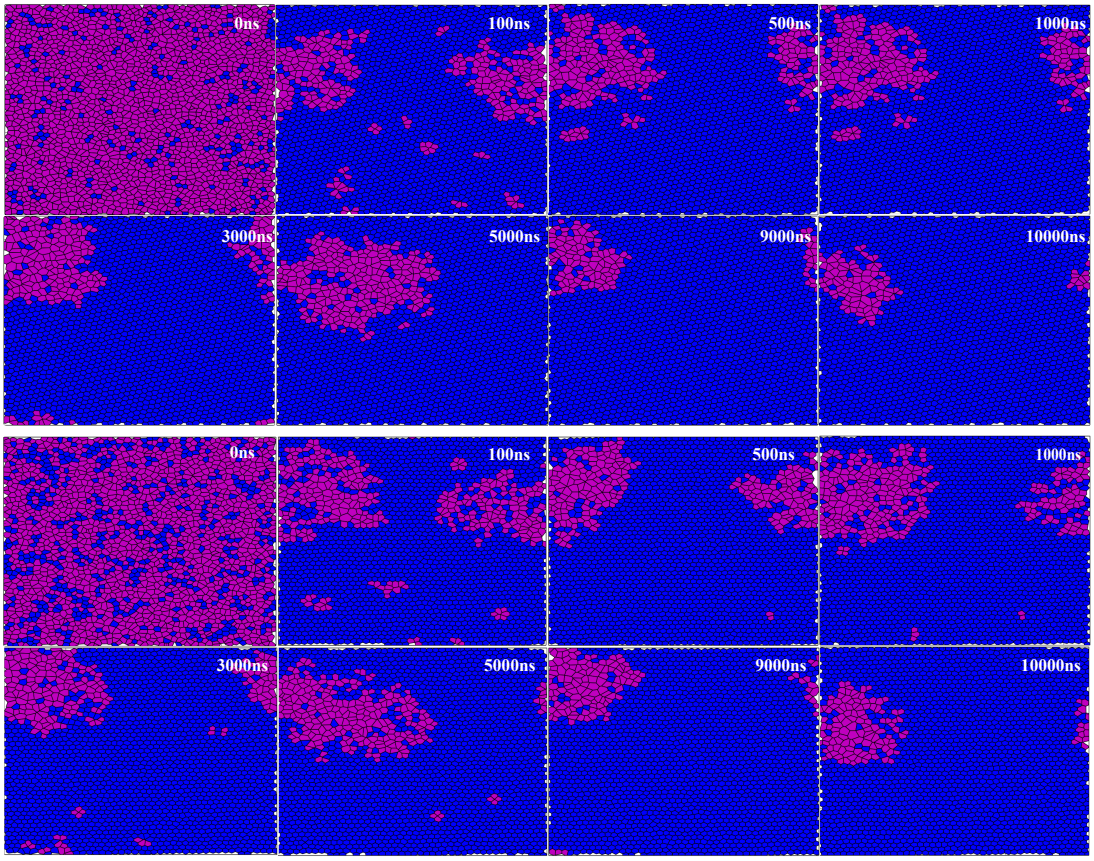

Figure 3.3: Time resolution of the top (top figure) and bottom (bottom figure) monolayers showing the liquid-gel phase transformation represented by C2 beads (ordered: blue, disordered: magenta)

the remaining fluid phase is trapped at this stage. Previous simulation studies have shown that for smaller systems it is possible to achieve a fully homogeneous gel phase, however this is clearly a finite size artefact [33]. The Voronoi analysis showed that the corresponding areas of ordered and disordered DPPC are 0.4629 and 0.6676 nm^2/molecule respectively, which agree well with the experimental values [30].

By comparing the ordering in the top and bottom monolayers, a strong coupling can be seen between the gel domain formation in the two monolayers. Whenever lipids from one monolayer are triggered to form the ordered state, the lipids

Table 3.1: Parameters obtained from Voronoi analysis show the growth of the gel domain. Number of ordered/disordered C2 beads: N_o/N_d; area of ordered/disordered DPPC molecule: A_o/A_d; percentage of gel/fluid domain area: ordered%/disordered%

time/μs	N_o	N_d	A_o/nm^2	A_d/nm^2	ordered%	disordered%
0	1065	3031	0.5653	0.6455	26.22	73.78
0.5	3303	493	0.4639	0.6467	87.11	12.89
1	3555	541	0.4668	0.6424	87.55	12.45
5	3590	506	0.4626	0.6460	87.79	12.21
10	3871	225	0.4629	0.6676	95.31	4.69

at roughly the same xy coordinates follow simultaneously. The final configuration from this simulation was then taken to use as the initial configuration of higher temperature simulations.

3.3.1.2 Solid-liquid phase transition

Results shown in Figure 3.4A provide clear evidence of the $S_o \rightarrow L_d$ transition in pure DPPC bilayer. The distinctive jumps in area per lipid and chain order parameter are characteristic of the structural change upon heating from 285 K to 325 K. The area per lipid increased from 0.491 nm^2 to 0.637 nm^2, which indicates the change in lateral packing and the disappearance of translational ordering. During the heating process, a discontinuity is observed between 305 K and 315 K. The behaviour of the area per lipid obtained in our work is in good agreement with previous simulation results and experimental observations [34, 35, 36]. The clear discontinuity is also found in the plot of the chain order parameter (S_{chain}). The value of S_{chain} is almost halved at 325 K (≈ 0.4, corresponding to L_d, see figure 3.5) compared with 285 K (≈ 0.8, corresponding to S_o). This dramatic decrease reveals the loss of orientational ordering in the lipid acyl chains.

The RDFs for various temperatures are reported in Figure 3.4B, which give great insight into the structural properties of the membrane. The radial distribution function (RDF) is constructed from the middle beads C2A/C2B of the DPPC acyl chains. We use the RDFs here to monitor the lateral packing of the

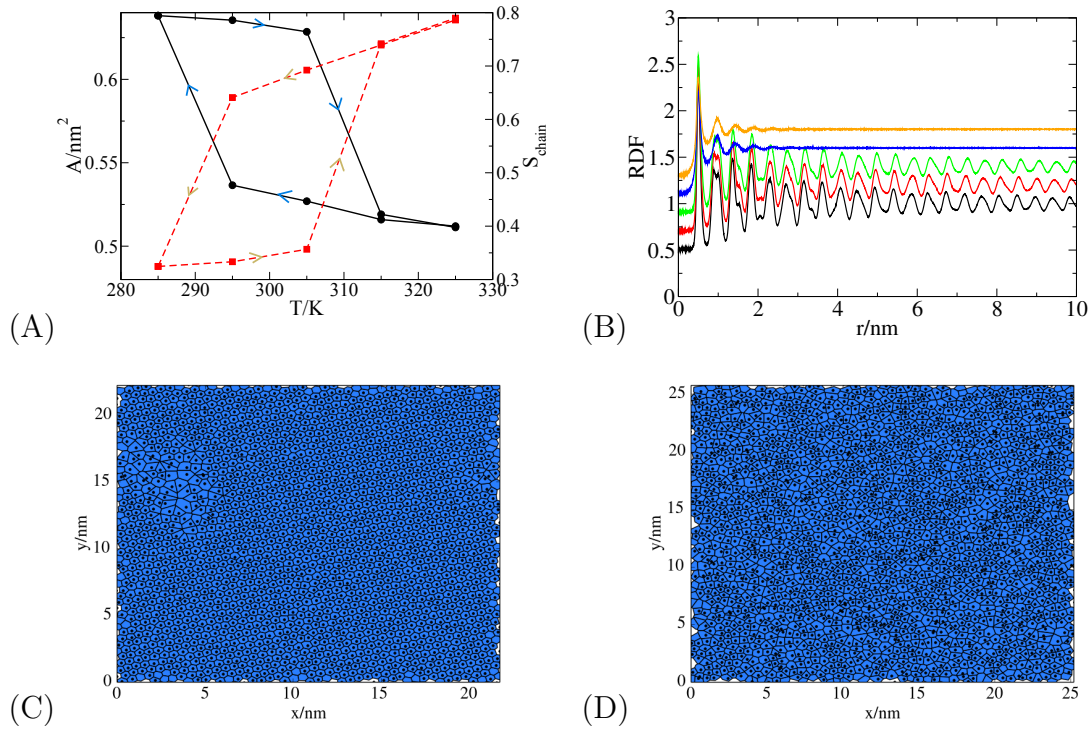

Figure 3.4: Simulation results for a pure DPPC bilayer at various temperatures. (A) Average chain order parameter (solid black lines), area per DPPC molecule (dashed red lines). The arrows indicate the direction of heating and cooling cycles. (B) RDFs computed using the C2A and C2B beads in the middle of each acyl chain. From bottom to top, 285 K, 295 K, 305 K, 315 K and 325 K. RDFs have been shifted vertically by 0.3 units for better clarity. Voronoi construction of one monolayer at 285 K (C) and 325 K (D). The beads employed for the Voronoi construction C2A and C2B are represented by black dots and the corresponding area is colored blue.

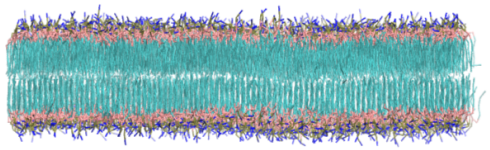

Figure 3.5: Snapshot of pure DPPC bilayer (side view) showing the straightened lipid acyl chains at 285 K.

lipid chains. The strong long range oscillations found at low temperatures (285 K to 305 K) show evidence for a regular packing of DPPC lipids. The distance at

which the RDF displays its successive minima correspond to the various coordination shells. The first minimum is found at 0.75 nm, which agrees with the criteria suggested by Marrink for the identification of ordered lipid tails [33]. The peaks found in low temperature systems (285 K to 305 K) at 0.5, 0.88, 1.0, ..., nm correspond to the distance of inter-lipids expected for a hexagonal close packing structure. In hexagonal packed bilayers (gel phase), the maxima are expected at $d, d\sqrt{3}, 2d, \cdots$, where d is the shortest lipid-lipid distance. In our case, bilayers at 285 K, 295 K and 305 K fit this hexagonal structure well. We can also see from the RDFs that the long range ordering is lost at high temperatures (315 K and 325 K) due to the large amplitude out of plane fluctuations. The clear change in RDFs is compatible with the $S_o \rightarrow L_d$ transition and the transition point is found between 305 K and 315 K.

Snapshots of bilayers analysed using Voronoi construction based on C2A and C2B beads give information on the translational ordering straight from visualisation. It is seen in Figure 3.4C that lipids form a hexagonal packing within the xy plane, although some defects can be seen. At 325K (see Figure 3.4D), the lipid chains melt as can be seen by the heterogeneous distribution of Voronoi polygon areas and shapes. The same criterion used to monitor the gel formation process is applied here to monitor the gel-fluid transformation. When the system is heated from 305 K to 315 K, lipids melt and eventually form the fluid phase (see Figure 3.6). The metastable state of gel phase remains for the first 10 ns. Small fluid domains grow rapidly and only one large gel patch is surrounded by fluid lipid after 20ns. As was seen for the freezing process, fluid state lipids can still appear metastable for a very long simulation time after the "quick growth" stage. In this case, fluid phase lipids are still observed after microseconds.

The pure DPPC bilayer was simulated with a heating→cooling loop. A large hysteresis loop was observed (see Figure 3.4A). Both under cooling and overheating can lead to a persistence of domains and hence the presence of a Van der Waals loop [37]. Thus, some fluid lipids can remain disordered, while some gel lipids can be restrained to an ordered state beyond the transition temperature. The observation of hysteresis is attributed to kinetic trapping. Reduction of the heating or cooling rate (quasi-static) should reduce the width of the hysteresis loop. Larger system size and longer simulation time can also contribute to con-

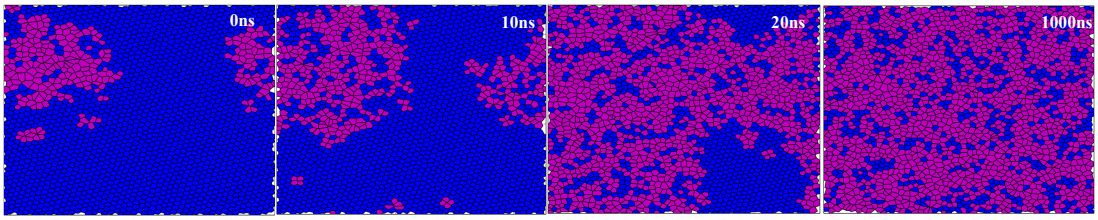

Figure 3.6: Time resolution of the half bilayer showing the gel-liquid phase transformation represented by C2 beads (ordered: blue, disordered: magenta)

vergence towards the transition temperature closer to experimental results [33]. By combining all these results we can conclude that there is a sharp melting transition between 305 K and 315 K for DPPC bilayer. This observation is consistent with previous experimental measurements and simulation estimates using the same force-field [13, 36, 38].

3.3.2 Impact of cholesterol on phase transition

3.3.2.1 $S_o \rightarrow L_d$ transition and formation of L_o phase

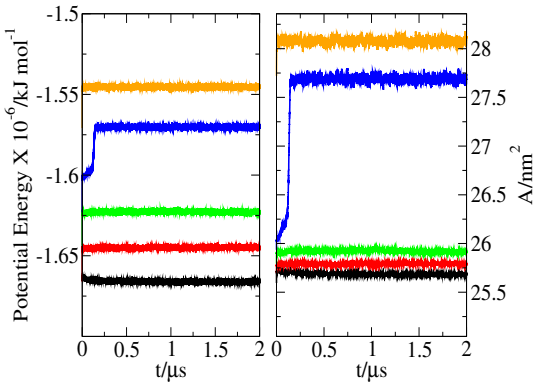

Figure 3.7: (A)Evolution of potential energy (left) and the cross-sectional area of the simulation box (right). From top to bottom: 283 K, 293 K,303 K, 313 K and 323 K

To study the impact of cholesterol on the phase behaviour of the DPPC membrane, bilayers with a wide range of cholesterol compositions were simulated.

Cholesterol molecules were embedded in both monolayers with equal number initially. The composition remained relatively stable, nevertheless cholesterol molecules were found to flip-flop across the two monolayers.

The original DPPC/CHOL bilayer ($x_{chol} = 0.3$) was quenched to 283 K and then heated to 323 K in intervals of 10 K. The rest of the bilayers were obtained by removing the appropriate number of DPPC or cholesterol molecules. Figure 3.7 shows the equilibration process of the DPPC/CHOL bilayer ($x_{chol} = 0.2$). As was the case for the pure DPPC bilayer, the structural properties are reported. In Figure 3.8A and B, the area per DPPC and per cholesterol are reported separately as obtained form the Voronoi tessellation method. The variation of $a_{DPPC}(x_{chol})$ and $a_{chol}(x_{chol})$ across temperature with different degrees of x_{chol} is shown. Resulting values of $a_{DPPC}(x_{chol})$ and $a_{chol}(x_{chol})$ were obtained from an ensemble average over the simulation trajectories. We note that both $a_{DPPC}(x_{chol})$ and $a_{chol}(x_{chol})$ vary with composition x_{chol}. The area per DPPC $a_{DPPC}(x_{chol})$ increases with increasing temperature when $x_{chol} \leq 0.3$. A clear discontinuity is observed between 303 K and 313 K which can be attributed to the $S_o \rightarrow L_d$ transition. Hysteresis behaviour is also observed in the DPPC/CHOL mixture bilayer (see Figure 3.8A, $x_{chol} = 0.2$), but with a much smaller hysteresis loop with respect to the pure DPPC bilayer, suggesting the reduced $S_o \rightarrow L_d$ activation energy due to the addition of cholesterol. Above $x_{chol} = 0.4$ we see no temperature dependence of the area per DPPC lipid, however it is interesting to note that upon decreasing x_{chol} we observe an increase of a_{DPPC}. No phase transition can be concluded for $x_{chol} \geq 0.4$. This observation is in disagreement with the recent CG simulation work on the same systems [20], where a phase transition was still observed with $x_{chol} = 0.5$.

The same trend is seen in $a_{chol}(x_{chol})$ (see Figure 3.8B), where little change is observed with molar fraction greater than 30 mol%. The difference between $a_{DPPC}(x_{chol})$ and $a_{chol}(x_{chol})$ decreases with increasing cholesterol content. The partial area of DPPC and cholesterol calculated through the Voronoi algorithm can also be used to provide a route to estimate the average area per molecule.

$$a(x_{chol}) = \frac{A}{N_{DPPC} + N_{chol}} = a_{DPPC}(x_{chol})(1 - x_{chol}) + a_{chol}(x_{chol})x_{chol} \quad (3.1)$$

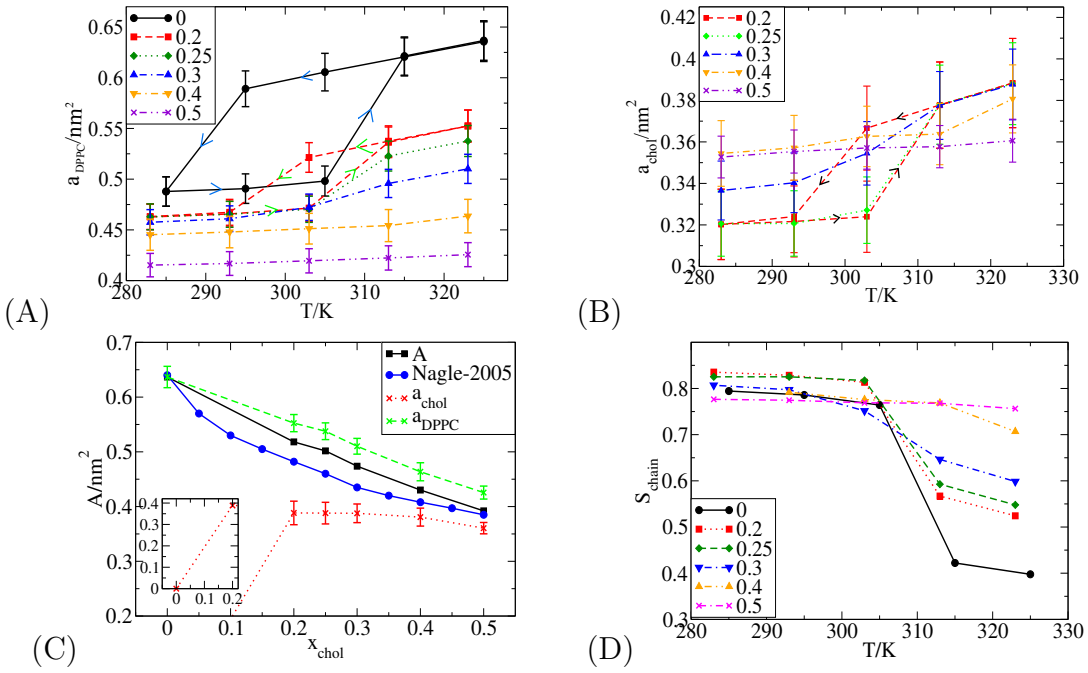

Figure 3.8: Area per DPPC (A) and cholesterol (B) across temperature with different compositions of cholesterol. (C) The partial area of DPPC (cross, dashed line) and cholesterol (cross, dotted line) at 323 K obtained in this work in shown. We also compared average area per molecule $A(x_{chol})$ calculated for the same bilayer (square, solid line) and values reported by previous publication (diamond, solid line) [35]. (D) average chain order parameter versus temperature for different concentrations of cholesterol

The value of $a(x_{chol})$ is commonly reported in experiments and simulations, and is a critical parameter to identify the 'condensing effect' of cholesterol. In Figure 3.8C, we compared the average area $a(x_{chol})$ with the experimental value reported by Nagle et al. [35] for the same mixture in the fluid phase. In this work, they derived the partial area of DPPC and cholesterol by numerically fitting the existing atomistic simulation results of $a(x_{chol})$ to the equation above. However, the area of cholesterol was obtained with a negative value at low x_{chol}. They explained the observation as follows : the local perturbation around cholesterol is believed to remain unaltered by an added DPPC molecule, since DPPC just joins its fully fluid companions in a region where has no cholesterol at low x_{chol}.

Therefore, the local perturbation on the DPPC molecules that are neighbour to the cholesterol contributes to $a_{chol}(x_{chol})$, not to $a_{DPPC}(x_{chol})$.

The average chain order parameter, S_{chain} (see Figure 3.8D), shows he orientational ordering effect introduced by cholesterol. With low concentrations of cholesterol ($x_{chol} \leq 0.3$), sharp slopes can be noticed when the system temperature raises from 303 K to 313 K. The value of S_{chain} shows a significant drop thus showing the acyl chains have melted ($S_o \rightarrow L_d$). The features of S_{chain} ($x_{chol} \geq 0.4$) mirrors what we have seen for the area per molecule in Figure 3.8 A and B. The clear first order transition from S_o to L_d is absent.

The same phase behaviour of DPPC/CHOL mixtures is also confirmed by the 2D radial distribution functions (see Figure 3.9A) and snapshots of the systems (see Figure 3.9B and C). The loss of long range oscillations indicates the absence of translational order. As seen in Figure 3.9A, we observe an abrupt loss of long range order behaviour between 303 K and 313 K, which is compatible with an $S_o \rightarrow L_d$ phase transition. At $x_{chol} = 0.4$, the transition temperature interval increased by to the range of 313 K-323 K, whereas no change in the RDFs can be seen when $x_{chol} = 0.5$. Interestingly, bilayers with high cholesterol content ($x_{chol} \geq 0.4$) feature longer ranged order than the ones in the L_d phase, but lack the characteristic long range and peak intensity expected for a solid phase. This combined with the fact that we observe a high degree of order along the aliphatic chain, allows us to conclude the formation of an L_o phase, which is also consistent with the strong conformational order imposed by the cholesterol on the phospholipids. Snapshots of monolayer from the Voronoi construction provide clear insight into the lateral packing of DPPC tails and cholesterol molecules, which gives similar conclusions. At low cholesterol content membranes, ($x_{chol} \leq 0.3$), hexagonal order is seen at low temperatures but absent at high temperature (see Figure 3.9B and C). In contrast, lateral packing order at high temperature does not differ from low temperature for $x_{chol} = 0.4, 0.5$. As seen in Figure 3.9 B5 and C5, cholesterol packs well within the ordered phase, and does not perturb the surrounding DPPC lipids. Another interesting fact we can conclude from the analysis of these snapshots is the regular lateral organisation of cholesterol molecules. They tend to form "thread-like" clusters (see Figure 3.9 B5 and C5).

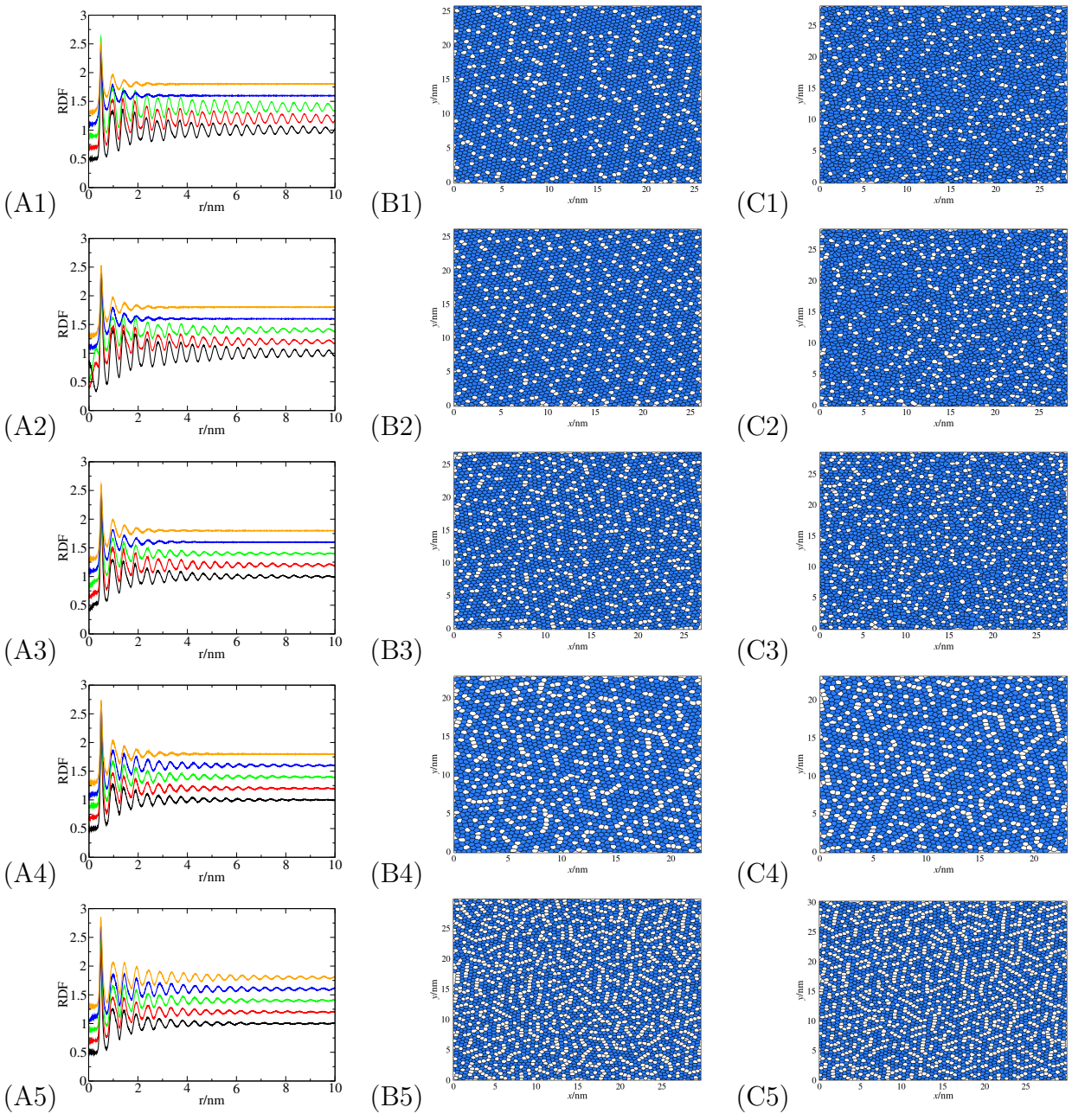

Figure 3.9: 2D RDFs calculated of the middle beads (C2A and C2B) from DPPC acyl chains is given for x_{chol} = 0.2 (A1), x_{chol} = 0.25 (A2), x_{chol} = 0.3 (A3), x_{chol} = 0.4 (A4) and x_{chol} = 0.5 (A5). From bottom to top: 283 K, 293 K, 303 K, 313 K, 323 K. RDFs have been shifted vertically by 0.3 units for better clarity. Snapshots with the same number denotation represent the corresponding Voronoi construction plots for half of bilayer at 283K (B1-5) and 323K (C1-5). Cholesterol molecules are coloured in white, C2 beads from DPPC are shown in blue.

Details of this behaviour will be discussed in the next chapter.
From the results reported above, we conclude that addition of cholesterol tends to smooth out the first order $S_o \rightarrow L_d$ melting transition and the transition temperature lies between 303 K and 313 K. No clear evidence is found for a phase transition at high composition of cholesterol. Instead, a new phase, L_o, is identified across the temperature range 283 to 313 K for high cholesterol content membranes, which is in agreement with experiments and recent simulation works [20, 27].

3.3.2.2 Phase transition across x_{chol}

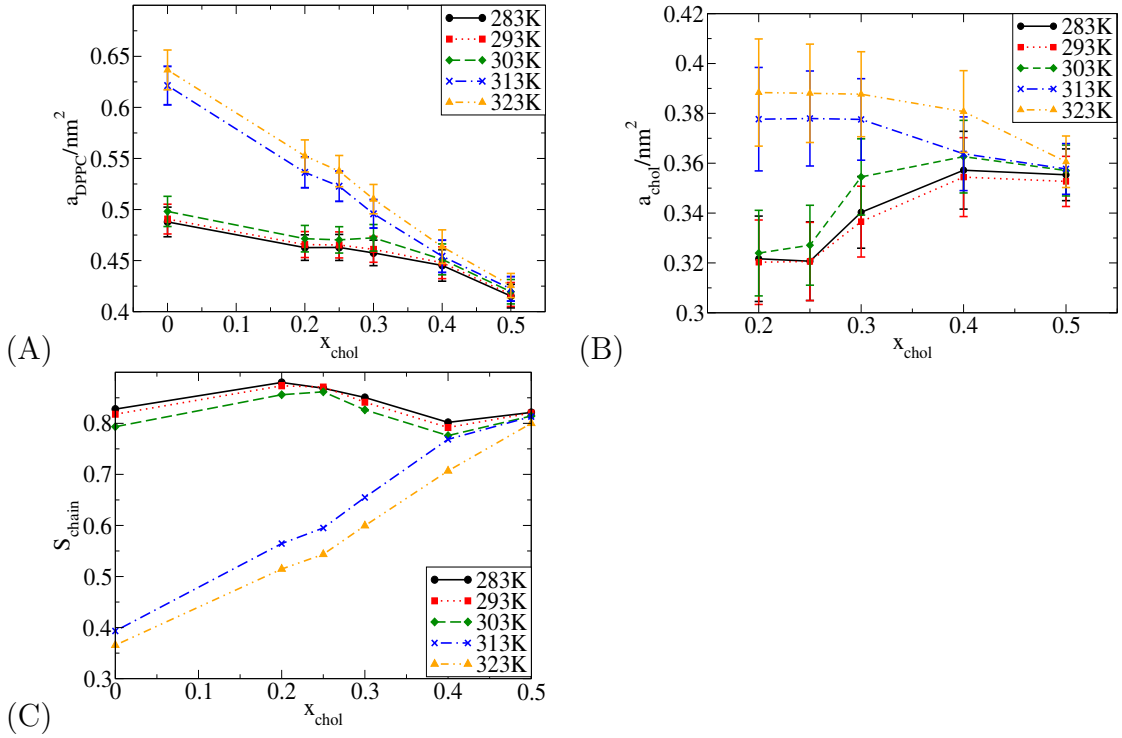

Figure 3.10: Area per DPPC(A)/cholesterol(B) versus concentration of cholesterol for different temperatures. (B) Average chain order parameter as a function of cholesterol molar fraction and temperature.

From the investigation with varying temperature at different cholesterol contents, we have gained insight onto how the $S_d \rightarrow L_d$ transition behaves. We now

perform additional analyses to understand the possible $L_d \rightarrow L_o$ and $S_o \rightarrow L_o$ transition by monitoring the variation of the order parameters as a function of cholesterol molar fraction. In this section, results are reported at constant temperature and the impact of varying cholesterol concentration at different thermal states will be identified.
As was performed above, the area per DPPC/CHOL is examined first as this is one of the most important structural parameters. We have shown in Figure 3.10 A that the area per DPPC decreases with addition of cholesterol at all temperatures. Such an observation is in agreement with a recent simulation study on the same system [39]. The condensing effect of cholesterol is confirmed again by this observation. However, the difference seen at high temperature ($\geq$ 313 K) is remarkable and results from the different densities of the L_d ($\geq$ 313 K) and S_o ($\leq$ 303 K) phases, whereas only minor changes are observed at low temperature ($\leq$ 303 K). With the highest cholesterol content ($x_{chol} = 0.5$, $a_{DPPC}(x_{chol})$) converges to ≈ 0.42 nm^2. In Figure 3.10B, $a_{chol}(x_{chol})$ increases at low temperature ($\leq$ 303 K) with increasing amount of cholesterol present in the bilayer. Local perturbation introduced by cholesterol is more and more pronounced, so that the lateral organisation of the original solid phase is perturbed. Another piece of evidence of the cholesterol condensing effect is noticed at high temperatures, where $a_{chol}(x_{chol})$ decreases instead.

Important changes are also observed in the chain order parameter (see Figure 3.10 C). S_{chain} shows its insensitivity to x_{chol} at low temperature ($\leq$ 303 K), reflecting the remaining high degree of order in the lipid aliphatic chains. The dramatic increase of S_{chain} with increasing amount of cholesterol ($\geq$ 313 K), is an indication of the straightened hydrocarbon chains of the DPPC molecules in the immediate vicinity of the cholesterol.
Unlike the clear first order $S_o \rightarrow L_d$ transition as we observed from Figure 3.4, a gradual change of translational order with the addition of cholesterol is seen in Figure 3.11. One essential characteristic of the different phases used to identify S_o, L_d and L_o is the degree of translational order. At high temperatures of 313 K (see Figure 3.11D) and 323 K (see Figure 3.10E), a distinctive liquid-like long-range oscillation that differs from the typical fluid phase is observed in going

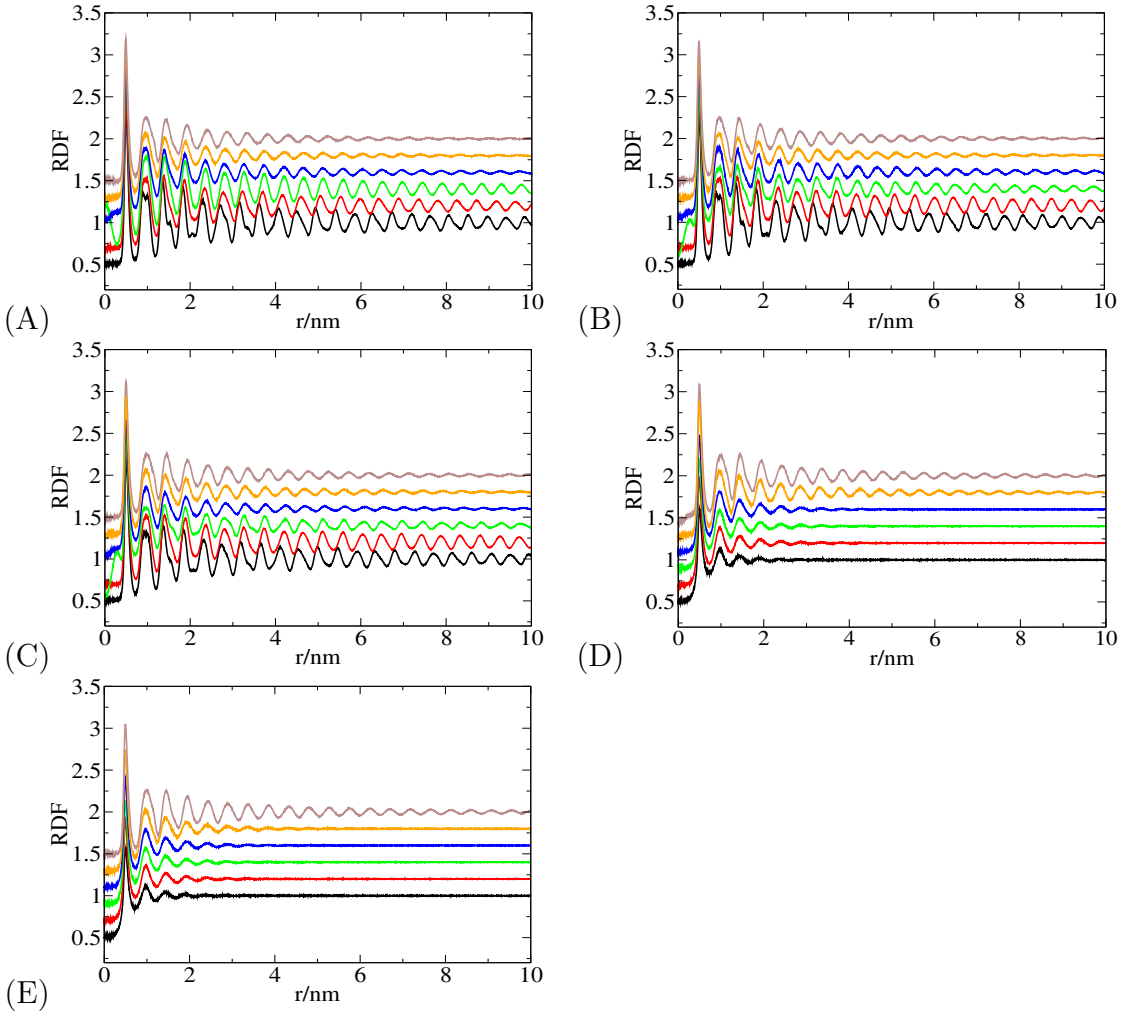

Figure 3.11: RDFs represented using the central beads (C2A and C2B) in the phospholipid chains at (A) 283 K, (B) 293 K, (C) 303 K, (D) 313 K and (E) 323 K. From bottom to top, $x_{chol} = 0, 0.2, 0.25, 0.3, 0.4$ and 0.5 The RDFs have been shifted by 0.3 units vertically for better clarity.

from $x_{chol} = 0.3$ to 0.4 or from $x_{chol} = 0.4$ to 0.5 respectively. Our results would indicate the $L_d \rightarrow L_o$ transition with $x_{chol} = 0.35$ and $T \approx 308$ K, also $x_{chol} = 0.45$ and $T \approx 308$ K. The lack of discontinuities or abrupt changes in the order parameter indicates that the transition between these phases is weak, possibly second order.
However, the gradual change seen in the results cannot provide clear information on possible phase coexistence in the T/x_{chol} domain. A new system will be introduced and discussed later to give us an insight into the existence of phase coexistence, so that a reliable DPPC/CHOL phase diagram can be constructed based on more evidence.

3.3.3 Lipid dynamics

Membrane fluidity is strongly affected by cholesterol, as well as the structural properties. The lateral diffusion coefficient is a dynamic parameter to characterise the bilayer fluidity. In this section, we report the Mean Square Displacement (MSD) upon varying the temperature (see Figure 3.12C) and cholesterol concentration (see Figure 3.12A-B). Results are obtained from the final 500 ns trajectories of each system, and clearly some did not reach diffusive behaviour within the time scale. In the case of 323 K (see Figure 3.12A), the MSDs features a diffusive regime after 300 ns, whereas only the bilayer of $x_{chol} = 0.4$ is found with diffusive behaviour at 293 K and the rest are characterised by sub-diffusive behaviour.

Our diffusion coefficients (see Table 4.1) are compatible with those reported in experiments for lipids in the L_d phase [40], of the order of $10^{-7}\text{cm}^2\text{s}^{-1}$. Filippov and co-workers [40] also concluded that the lipid diffusion coefficient decreases slightly with increasing cholesterol content, but remains of the same order of magnitude. From the results given at 323K, a monotonic reduction in the DPPC diffusion coefficient is also observed with the addition of cholesterol. Such sub-diffusive behavior has also been reported in computer simulations of proteins in lipid membranes, where it was found that crowding had a large impact on the lipid

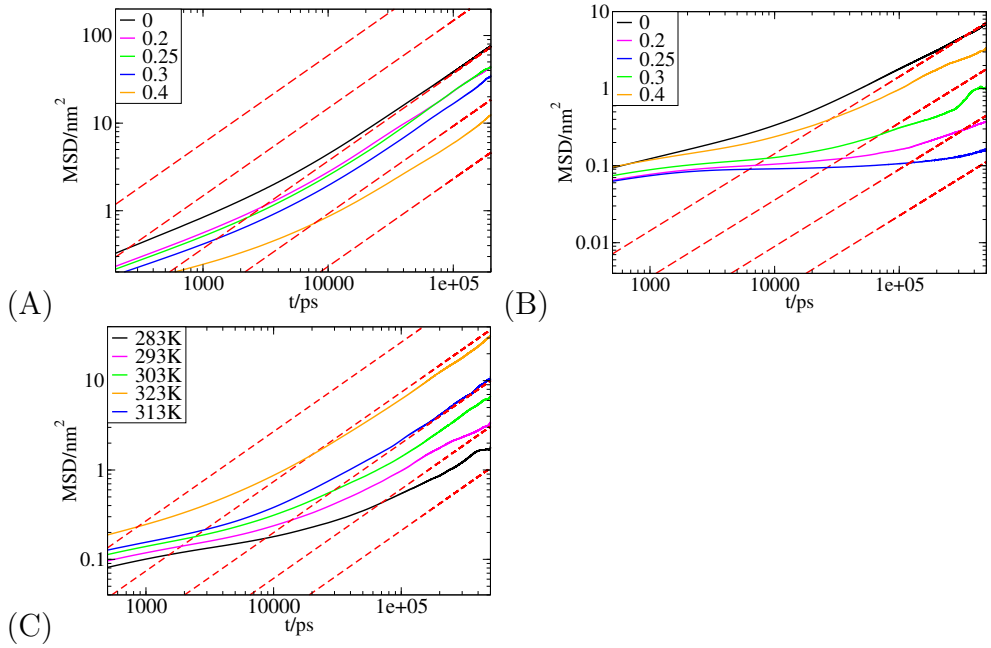

Figure 3.12: Mean square displacement (MSD) of DPPC/CHOL bilayers as a function of cholesterol content at $T = 323$ K (A) and $T = 293$ K (B). (C) Temperature dependence of the MSD of bilayers at $x_{chol} = 0.4$. Dashed lines represent the expected behavior of the MSDs in the diffusive regime.

Table 3.2: Lateral diffusion coefficient of DPPC, $D_{DPPC}/10^{-7}\mathrm{cm}^2\mathrm{s}^{-1}$. The hyphen "–" represents a system for which diffusive behaviour was not reached in our simulation time scale. t_D is the threshold time needed for the lipids to reach normal diffusive behaviour.

x_{chol}	303K	313K	323K	t_D/ns(323 K)
0	–	7.81	9.28	75
0.20	–	4.47	5.63	100
0.25	–	3.72	5.68	120
0.30	–	2.71	4.23	150
0.40	0.34	0.53	1.53	200

molecules lateral diffusion [41]. We have estimated the threshold time needed for the lipid molecules to reach the diffusive regime. This time was estimated from a fitting of the equation $\langle \Delta r(t)^2 \rangle = 4Dt^{\alpha}$ to independent 500 ps segments of the mean square displacement. At times smaller than t_D the exponent is close to 0.5 hence indicating sub-diffusive behaviour. As the time approaches t_D, the exponent converges towards 1 as expected for normal diffusion. Our results (see Table 3.2) show that the threshold time increases with the concentration of CHOL. This result is consistent with previous simulation studies [42] and shows that addition of CHOL molecules increases the characteristic time-scale for the lipid molecules sub-diffusive behaviour.

We also note that the diffusion coefficient obtained for $x_{chol} = 0.4$ is about one order of magnitude smaller (of the order of $10^{-8}\text{cm}^2\text{s}^{-1}$), compared with a typical L_d phase. Good agreement is found with the diffusion coefficient observed for L_o phase DOPC by pulse field gradient NMR experiments [40], which was reported values around $1 \times 10^{-8}\text{cm}^2$ in the temperature range of 303-333 K. This is consistent with the conclusion made from structural parameters, where L_o formation is investigated at high cholesterol concentration ($x_{chol} \geq 0.4$). The activation energy, E_a, can also be estimated by fitting our data to the Arrhenius equation, resulting a value of 57 kJ/mol for the L_o phase at $x_{chol} = 0.4$. Previous experiments have reported similar results for comparable bilayers in the L_o phase, including DOPC/CHOL/water and POPC/CHOL/water, with values which lie between $55 - 65$ kJ/mol.

3.3.4 Investigation of possible S_o/L_o and L_o/L_d coexistences

As concluded in the previous section, addition of cholesterol clearly leads to the formation of an L_o phase, but phase coexistence remains unclear from the normal approach of simulation. Various previous studies have drawn different conclusions, however there seems to be a common consensus that an S_o/L_o coexistence region exists which involves CHOL-rich and CHOL-poor phases. Exploring S_o/L_o and L_o/L_d coexistence by simulation is limited by timescale and system size. The slow dynamics of lipids means the phase separation may be restricted within the timescales normally employed in simulation studies. For a bilayer similar to the

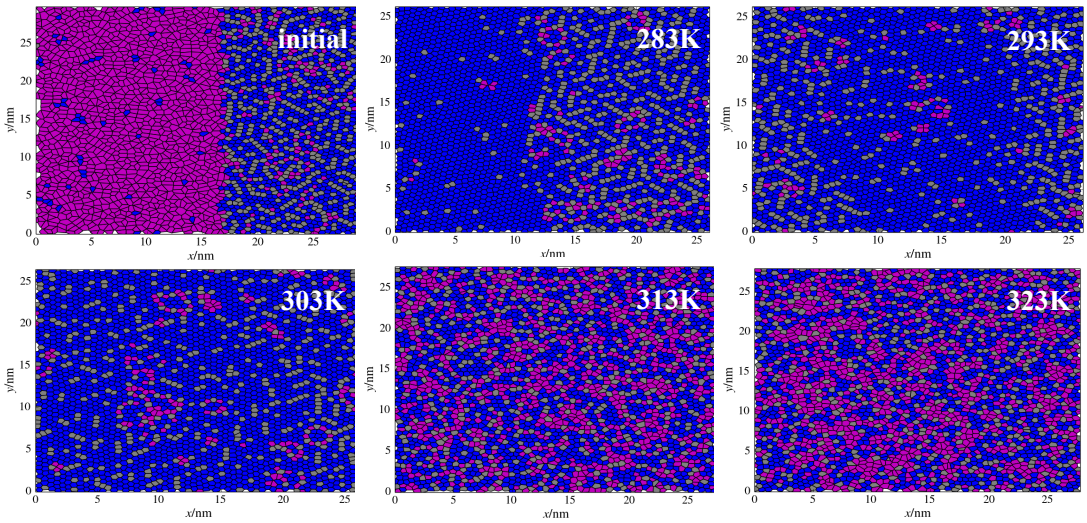

Figure 3.13: Voronoi construction of the initial configuration (top-left) and configurations obtained after 10 μs at different temperatures. Grey polygons represent cholesterol, and blue and magenta DPPC in the ordered (gel or L_o) or disordered (L_d) phases as defined in the text.

size of the ones we simulated here, hundreds of μs are needed to observe significant demixing. A large system size is also essential, so that different phase regions can separate.

To explore the possible CHOL-rich/CHOL-poor coexistence, a more practical simulation approach was introduced. A new DPPC/CHOL system ($x_{chol} = 0.3$), was generated by removing 60% of the cholesterol molecules on one side of the box from an L_o phase bilayer. The resulting bilayer consists of two parts, approximately half of it remains in the L_o phase and the other half now is cholesterol-free. The two monolayers are kept identical in composition. Hence, we can monitor the demixing process and the change of cholesterol-free/cholesterol-rich interface. The initial configuration was simulated for 10 μs at a range of temperatures from 283 K to 323 K. The same criteria as applied in the analysis of DPPC gel formation [33] was used here to identify the ordered (gel or L_o) or disordered (L_d) phases. Snapshots of the bilayer obtained after each run are represented in Figure 3.13. The initial configuration shows the clear boundary between CHOL-rich and CHOL-free regions. When the bilayer is heated up to 303 K, the existence of CHOL-rich and CHOL-poor regions is no longer easy

to identify by direct visualisation. A more quantitative method is used here to explore the local molar fraction of cholesterol at different temperatures; the preferred cholesterol concentration(s) in the bilayer plane can then be obtained from the histogram of local x_{chol}. A typical Gaussian distribution is expected for a uniformly distributed DPPC/CHOL bilayer, where the peak is located at the average concentration(x_{chol}, 0.3). In contrast a double peak distribution will be observed if phase coexistence is present, where the peaks correspond to different compositions.

A 5×5 grid is applied on the xy plane of the bilayer, resulting in 25 sub-bilayers

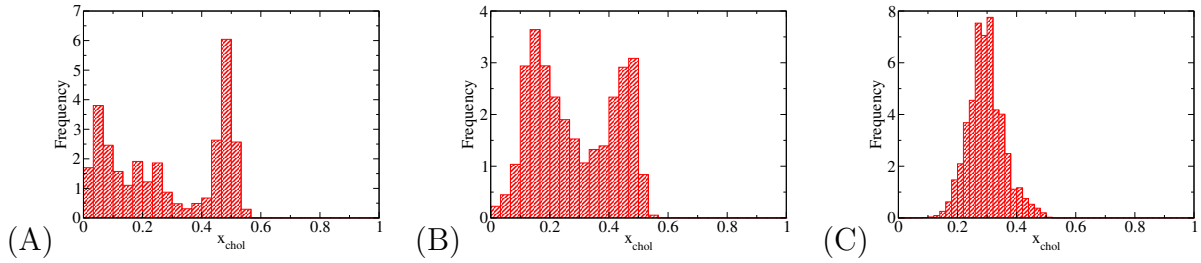

Figure 3.14: Histogram of cholesterol concentration at 283 K (A) and 293 K (B) and 303 K (C).

and around 60 lipids in each grid to allow sufficient statistics. The molar fraction of cholesterol is calculated for each sub-bilayer. The data used to generate the histograms represented in Figure 3.14A-C are taken from an ensemble average over 9 μs with approximately 2000 configurations. At 283 K, two distinctive peaks at $x_{chol} \approx 0.1$ and ≈ 0.5 are present, corresponding to the S_o and L_o phases respectively. The non-normal distribution shown in figure 3.14A results from the extremely slow dynamics of lipids at this temperature. With the consequent speeding up of dynamics at higher temperature, the histogram at 293 K is much better defined than the one at 283 K (see figure 3.14B). A bi-normal distribution with two distinctive maxima at $x_{chol} \approx 0.15$ and ≈ 0.45 is found, illustrating the existence of S_o/L_o coexistence. These results will be used to define the tie-lines in our phase diagram.

The boundaries of large domains quickly vanish with increasing temperature. At 303 K (see Figure 3.14C), an almost homogeneous distribution of cholesterol molar fraction with only one main peak centred at $x_{chol} \approx 0.25$ is present. It

shows the absence of phase coexistence, or the two CHOL-rich and CHOL-poor phases are close in cholesterol concentration that they are not resolved with our approach. A single peak with normal distribution indicates no phase coexistence exists. To summarize, only S_o/L_o phase coexistence below 303 K is confirmed and the lack of L_o/L_d concluded from our approach agrees with previous computer simulation investigations [43, 22]. Together with the observations and data reported in previous sections, we hence constructed a DPPC/CHOL temperature-composition phase diagram based on bilayer structural and dynamic properties. However, we are aware of the limitations of current simulation models and methods which restrict very large time/size scales. As a consequence, the precision of the simulation estimates are also limited and we plot the phase diagram with estimated uncertainties in the coexistence lines.

In figure 3.15, our proposed phase diagram shows the existence of L_o at high

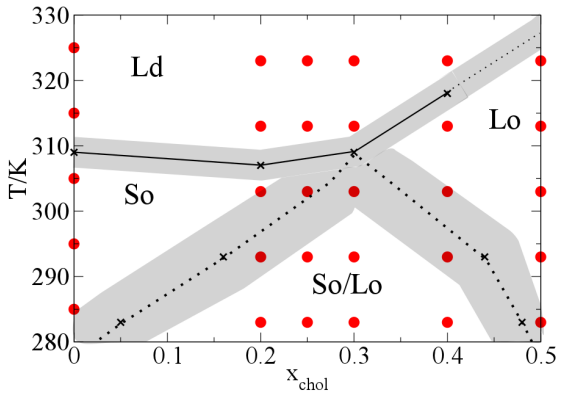

Figure 3.15: DPPC/CHOL phase diagram proposed in this work. The S_o/L_o coexistence lines were estimated from the analysis of the cholesterol histograms, while the S_o/L_o transition is based on the analysis of the area per DPPC and mean chain order parameter. The L_d/L_o line was inferred from the analysis of the radial distribution functions. The grey areas give an indication of the estimated uncertainties in the coexistence lines.

cholesterol concentration. S_o exists with low cholesterol content, whereas S_o and L_o coexist with intermediate concentration of cholesterol below the melting temperature of pure DPPC bilayer. The disordered L_d phase is transformed from S_o with the increase of temperature. Our results did not show any evidence for

L_d/L_o coexistence. A slight increase in the melting temperature of 10 K for x_{chol} =0.5 is observed in some similar studies [20] which was not seen in our present simulation.

3.4 Conclusion

We have investigated the phase behaviour of fully hydrated DPPC/Cholesterol bilayer mixtures by utilizing the MARTINI force-field and coarse-grained molecular dynamics simulations. Our analysis suggests that the addition of cholesterol fluidise the DPPC gel phase and stabilises the liquid ordered phase. The $S_o \rightarrow L_d$ phase transition can still be observed with $T_m \approx 308$ K for bilayers that $x_{chol} \leq 0.3$. At high cholesterol concentration, $x_{chol} = 0.5$ the L_o phase dominates the phase diagram as the single phase in the wide range of temperatures investigated, $283\ K < T < 323\ K$. The lipid has highly ordered lipid acyl chains similar to those in S_o phase, but also with severely disrupted translational order similar to a dense fluid. The lateral diffusion coefficient is of the order of that of the L_d phase, but about 2-10 times smaller than that of the L_d phase which is in a good agreement with experiments. The calculated activation energy, of the order of 57 kJ/mol, also highlights the sluggish dynamics of L_o phase lipids.
The contentious issue raised in identifying possible L_o coexistence with L_d or S_o phases was also examined. Our results suggest the formation of S_o/L_o, but not L_d/L_o coexistence. With the continuity in behaviour observed with $L_o \rightarrow L_d$ transformation, a second order transition scenario seems to be the most likely for the MARTINI force-field. Overall, the proposed phase diagram provides a general idea of the DPPC-cholesterol phase behaviour and provides insight into the molecular organization of the molecules in the different phases. These results illustrate that coarse-grained molecular dynamics simulation is a powerful tool for making qualitative observations of the dynamic phase behaviour of lipid bilayers on time and length scales that are not accessible to atomistic simulation.
Summary:

- Investigated the phase behaviour of fully hydrated DPPC/Cholesterol bi-

layer mixtures using MARTINI force-field CG-MD simulations.

- Understood the structural and dynamic properties of DPPC/cholesterol bilayers quantitatively.
- Confirmed the formation of L_o at high cholesterol concentrations.
- Found that the addition of cholesterol fluidise the S_o phase and stabilises the L_o phase.
- Proposed a temperature-composition DPPC/Cholesterol phase diagram based on the novel study of phase coexistence exploration.

Future work:

- A reparametrization of the MARTINI model (e.g., targeting the properties of the S_o phase).
- Longer stimulations of investigating S_o/L_o and L_d/L_o coexistences to eliminate the uncertainties in proposed phase diagram.

References

[1] Y. Zhang, A. Lervik, J. Seddon, and F. Bresme. A coarse-grained molecular dynamics investigation of the phase behavior of DPPC/cholesterol mixtures. *Chemistry and Physics of Lipids*, 2014. DOI: 10.1016/j.chemphyslip.2014.07.011. 73

[2] R. E. Olson. Discovery of the lipoproteins, their role in fat transport and their significance as risk factors. *American Society for Nutritional Services*, 128, 1998. 74

[3] J. Pan, T. T. Mills, S. Tristram-Nagle, and J. F. Nagle. Cholesterol perturbs lipid bilayers nonuniversally. *Physical Review Letters*, 100:198103, 2008. 74

[4] G. W. Feigenson. Phase diagrams and lipid domains in multicomponent lipid bilayer mixtures. *Biochmica et Biophysica Acta*, 1788:47–52, 2009. 74, 75

[5] R.A. Demel and B. De Kruyff. The function of sterols in membranes. *Biochimica et Biophysica Acta (BBA) - Reviews on Biomembranes*, 457(2):109 – 132, 1976. 74

[6] T. P.W. McMullen, R. N.A.H. Lewis, and R. N. McElhaney. Cholesterolphospholipid interactions, the liquid-ordered phase and lipid rafts in model and biological membranes. *Current Opinion in Colloid & Interface Science*, 8(6):459 – 468, 2004. 74

[7] L. Bagatolli and S. Kumar. Phase behavior of multicomponent membranes: Experimental and computational techniques. *Soft Matter*, 5:3234–3248, 2009. 74

[8] T. Xiang and B. D. Anderson. Phase structures of binary lipid bilayers as revealed by permeability of small molecules. *Biochimica et Biophysica Acta*, 1370:64–76, 1998. 74

[9] H. Jelger Risselada and S. J. Marrink. The molecular face of lipid rafst in model membranes. *PNAS*, 105:17367–17372, 2008. 74

[10] C. L. Armstrong, D. Marquardt, H. Dies, N. Kucerka, Z. Yamani, T. A. Harroun, J. Katsaras, A. Shi, and M. C. Rheinstadter. The observation of highly ordered domains in membranes with cholesterol. *PLOS one*, 8:e66162, 2013. 74

[11] M. C. Rheinstadter and O. G. Mouritsen. Small-scale structure in fluids cholesterol-lipid bilayers. *Current Opinion in fluid cholesterol-lipid bilayers*, 18:440–447, 2013. 74

[12] T. Schubert, E. Schneck, and M. Tanaka. First order melting transitions of highly ordered dipalmitoyl phosphatidylcholine gel phase membranes in molecular dynamics simulations with atomistic detail. *The Journal of Chemical Physics*, 135(5):055105, 2011. 74, 79

[13] S. Tristram-Nagle and J. F. Nagle. Lipid bilayers: thermodynamics, structure, fluctuations, and interactions. *Chemistry and Physics of Lipids*, 127(1):3 – 14, 2004. 74, 79, 84

[14] J. Hjort Ipsen, G. Karlström, O.G. Mourtisen, H. Wennerström, and M.J. Zuckermann. Phase equilibria in the phosphatidylcholine-cholesterol system. *Biochimica et Biophysica Acta (BBA) - Biomembranes*, 905(1):162 – 172, 1987. 74

[15] L. X. Finegold. *Cholesterol in Membrane Models*. CRC Press: Boca Barton, FL, 1985. 74

[16] A. Dopico, R. A. H. Lewis, D. Mannock, and R. McElhaney. *Methods in Molecular Biology*, volume 400, pages 171–195. Humana Press, 2007. 74

[17] T. H. Huang, C.W.B. Lee, S.K. Das Gupta, A. Blume, and R.G. Griffin. A ^{13}C and ^{2}H nuclear magnetic resonance study of phosphatidylcholine/cholesterol interactions: Characterization of liquid-gel phases. *Biochemistry*, 32:13277–13287, 1993. 74

[18] T. T. Mills, G. E.S. Toombes, S. Tristram-Nagle, D. Smilgies, G. W. Feigenson, and J. F. Nagle. Order parameters and areas in fluid-phase oriented lipid membranes using wide angle x-ray scattering. *Biophysical Journal*, 95(2):669 – 681, 2008. 75

[19] H. McConnell and A. Radhakrishnan. Theory of the deuterium NMR of sterolphospholipid membranes. *Proceedings of the National Academy of Sciences of the United States of America*, 103(5):1184–1189, 2006. 75

[20] Q. Waheed, R. Tjörnhammar, and O. Edholm. Phase transitions in coarse-grained lipid bilayers containing cholesterol by molecular dynamics simulations. *Biophysical Journal*, 103(10):2125 – 2133, 2012. 75, 85, 89, 98

[21] T. Murtola, E. Falck, M. Patra, M. Karttunen, and I. Vattulainen. Coarse-grained model for phospholipid/cholesterol bilayer. *The Journal of Chemical Physics*, 121(18):9156–9165, 2004. 75

[22] P. F. Almeida. A simple thermodynamic model of the liquid-ordered state and the interactions between phospholipids and cholesterol. *Biophysical Journal*, 100(2):420 – 429, 2011. 75, 97

[23] S. L. Veatch and S. L. Keller. Seeing spots: Complex phase behavior in simple membranes. *Biochimica et Biophysica Acta (BBA) - Molecular Cell Research*, 1746(3):172 – 185, 2005. 75

[24] F. Meyer and B. Smith. Effect of cholesterol on the structure of a phospholipid bilayer. *PNAS*, 106:3654–3658, 2009. 75

[25] S. L. Veatch and S. L. Keller. Separation of liquid phases in giant vesicles of ternary mixtures of phospholipids and cholesterol. *Biophysical Journal*, 85:3074 – 3083, 2003. 75

[26] S. L. Veatch, I.V. Polozov, K. Gawrisch, and S. L. Keller. Liquid domains in vesicles investigated by NMR and fluorescence microscopy. *Biophysical Journal*, 86:2910 – 2922, 2004. 75

[27] M. R. Vist and J. H. Davis. Phase equilibria of cholesterol/dipalmitoylphosphatidylcholine mixtures: deuterium nuclear magnetic resonance and differential scanning calorimetry. *Biochemistry*, 29(2):451–464, 1990. 75, 89

[28] Y. Chiang, A. J. Costa-Filho, and J. H. Freed. Dynamic molecular structure and phase diagram of DPPC-cholesterol binary mixtures: A 2D-ELDOR study. *J. Phys. Chem. B*, 1370:11260–11270, 1998. 75

[29] S. J. Marrink, H. J. Risselada, S. Yefimov, D. P. Tieleman, and A. H. de Vries. The MARTINI force field: coarse grained model for biomolecular simulations. *The Journal of Physical Chemistry B*, 111(27):7812–7824, 2007. PMID: 17569554. 76, 77

[30] J. F. Nagle and S. Tristram-Nagle. Structure of lipid bilayers. *Biochimica et Biophysica Acta (BBA) - Reviews on Biomembranes*, 1469(3):159 – 195, 2000. 76, 80

[31] H. J. C. Berendsen, J. P. M. Postma, W. F. van Gunsteren, A. DiNola, and J. R. Haak. Molecular dynamics with coupling to an external bath. *The Journal of Chemical Physics*, 81(8):3684–3690, 1984. 77

[32] B. Hess, C. Kutzner, D. van der Spoel, and E. Lindahl. GROMACS 4: Algorithms for highly efficient, load-balanced, and scalable molecular simulation. *Journal of Chemical Theory and Computation*, 4:435–447, 2008. 77

[33] S. J. Marrink, J. Risselada, and A. E. Mark. Simulation of gel phase formation and melting in lipid bilayers using a coarse grained model. *Chemistry and Physics of Lipids*, 135:223–244, 2005. 78, 79, 80, 83, 84, 95

[34] C. Hofsäß, E. Lindahl, and O. Edholm. Molecular dynamics simulations of phospholipid bilayers with cholesterol. *Biophysical Journal*, 84(4):2192 – 2206, 2003. 81

[35] O. Edholm and J. F. Nagle. Areas of molecules in membranes consisting of mixtures. *Biophysical Journal*, 89(3):1827 – 1832, 2005. 81, 86

[36] S. J. Marrink, A. H. de Vries, and A. E. Mark. Coarse grained model for semiquantitative lipid simulations. *The Journal of Physical Chemistry B*, 108(2):750–760, 2004. 81, 84

[37] K. Esselink, P. A. J. Hilbers, and B. W. H. van Beest. Molecular dynamics study of nucleation and melting of nalkanes. *The Journal of Chemical Physics*, 101(10):9033–9041, 1994. 83

[38] M. Patra, M. Karttunen, M.T. Hyvönen, E. Falck, P. Lindqvist, and I. Vattulainen. Molecular dynamics simulations of lipid bilayers: Major artifacts due to truncating electrostatic interactions. *Biophysical Journal*, 84(6):3636 – 3645, 2003. 84

[39] E. Falck, M. Patra, M. Karttunen, M. T. Hyvönen, and I. Vattulainen. Lessons of slicing membranes: Interplay of packing, free area, and lateral diffusion in phospholipid/cholesterol bilayers. *Biophysical Journal*, 87(2):1076 – 1091, 2004. 90

[40] A. Filippov, G. Oradd, and G. Lindblom. Lipid lateral diffusion in ordered and disordered phases in raft mixtures. *Biophys. J.*, 86:891–896, 2004. 92, 94

[41] M. Javanainen, H. Hammaren, L. Monticelli, J. Jeon, M. S. Miettinen, H. Martinez-Seara, R. Metzler, and I. Vattulainen. Anomalous and normal diffusion of proteins and lipids in crowded lipid membranes. *Faraday Discuss*, 161:397–417, 2012. 94

[42] J. Jeon, H. Martinez-Seara, M. Javanainen, and R. Metzler. Anomalous diffusion of phospholipids and cholesterols in a lipid bilayer and its origins. *Phys. Rev. Lett.*, 109:188103, 2012. 94

[43] S. L. Veatch, K. Gawrisch, and S. L. Keller. Closed-loop miscibility gap and quantitative tie-lines in ternary membranes containing diphytanoyl PC. *Biophysical Journal*, 90(12):4428 – 4436, 2006. 97

Chapter 4

Effect of cholesterol modification on DPPC/Cholesterol bilayers

The observation of 'thread-like' cholesterol clusters has been reported before in analogs of cholesterol with atomistic models [1], and was rationalised as the result of a fine balance between cholesterol/cholesterol weak interactions and the stronger interactions of cholesterol with the lipid molecules in the ordered phase. Such linear structures have also been reported in atomistic computer simulations of 'smoother' cholesterol-bilayer membranes in the liquid-ordered phase [2]. We consider that the geometry of the MARTINI cholesterol model could play an equally important role in determining the bilayer structural organization. The MD simulations with standard and modified models of cholesterol confirm the validity of this conjecture, showing the effect on lipid bilayer lateral organisation and phase transition upon varying the size of the CG model cholesterol. This empirical observation relates to a prediction of naturally occurring sterols in similar studies using MARTINI force-field which are currently available.

4.1 Introduction

To understand the lateral structure of cholesterol where it forms regular distributions, both experimental and theoretical approaches [3, 4] have been reported. Despite the rapid development of techniques, the actual atomistic level molecular

organisation and detailed nature of lipid-cholesterol interactions corresponding to such organisation still remains a challenging problem. Three conceptual models are commonly used to explain the lipid-cholesterol interaction. The Condensed Complex Model was proposed from a study on lipid monolayers at the vapor-water interface by McConnell and Radhakrishnan [5], and based on low free-energy stoichiometric lipid-cholesterol complexes with smaller cross-sectional areas. The Superlattice Model suggests that a long-range repulsive force is created by the difference in molecular lateral area between cholesterol and the phospholipid. A regular distribution of cholesterol molecules is predicted when the molar fraction of cholesterol brings the mixture to a critical point [6, 7]. The Umbrella Model was proposed based on the distinct structure of cholesterol which consists of a small hydrophilic headgroup and a bulky rigid hydrophobic tetrameric ring system. The mismatch in size between head and body favours the existence of phospholipid molecules adjacent to the cholesterol, so that the unfavourable interaction between water and the non-polar cholesterol body can be minimised by shielding of the large phospholipid polar headgroup. To minimize the free energy in a membrane, cholesterol will therefore avoid cluster formation or at least large cluster formation at high concentrations [8].

Some earlier simulation studies showed that the ordering induced by cholesterol is strongly related to its chemical structure [9, 10]. There are three main structural elements, a small hydrophilic domain with a single -OH group, a large rigid planar body with several fused rings, and a short branched alkyl chain. The large rigid group forms an asymmetric planar structure with two off-plane methyl groups on one side. The unfavourable interaction between saturated acyl chains and off-plane methyl groups decreases the chain ordering and packing of lipids facing the rough side, whereas the chain order is found to increase when interacting with the smooth side. Atomistic molecular dynamics simulations reported by Martinez-Seara et al. [2] showed how the two off-plane methyl groups impact on the lipid lateral distribution. When planar cholesterol molecules are introduced without the off-plane methyl groups, they are found to form linear arrays instead of exhibiting triangular ordering as seen with regular cholesterol.

The cholesterol molecule has a cross-sectional area (0.27 nm^2) [11] which lies between that of a single acyl chain (0.21 nm^2) [11] and two acyl chains (0.42 nm^2) [11]

in the gel phase. This implies a strong mismatch in packing, whereby cholesterol will be unable to insert into the 2D hexagonal lattice, but rather will disrupt it. We have set out to test this idea by varying the size of the cholesterol molecule using coarse-grained modelling. The work on MARTINI [12] DPPC and cholesterol bilayers discussed in chapter 3 clearly shows the formation of linear cholesterol clusters in L_o phase lipid membranes. In this chapter, we address how the cholesterol molecular structure influences the lateral distribution of lipids and can disrupt the lipid phase transitions. A series of coarse-grained molecular dynamics simulations was performed with the original MARTINI cholesterol, and with enlarged/decreased size cholesterol-like sterols.

4.2 Methods

4.2.1 Force-field and simulation details

Coarse-grained molecular dynamics simulations were performed on bilayer membranes of fully saturated 1,2-dipalmitoyl-sn-glycero-3-phophocholine (DPPC) with 20 and 50 mol% of cholesterol(CHOL) using the MARTINI 2.0 force field. Both lipids are fully described in chapter 2. Differently from the full-atom/united-atom model of cholesterol, the detailed molecular structure is not apparent in this coarse-grained model, e.g. the two off-plane methyl groups. Instead, CG cholesterol exists with smooth surfaces on both sides (see figure 4.1). For comparison, enlarged (CHO1) and decreased (CHO2) size cholesterol molecules are introduced, and we have performed simulations with the same compositions and temperatures as for CHOL. The details of constructing CHO1 and CHO2 will be explained later in the section.

Each membrane system consists of either 2432 or 2304 DPPC molecules and a corresponding number of sterol molecules, 640 (20% of cholesterol) or 2304 (50% of cholesterol). These bilayers were obtained from the simulation work of Marrink and co-workers [12] (available on-line at: http://md.chem.rug.nl/cgmartini/) with certain modifications. An appropriate number of DPPC or CHOL molecules from both leaflets were removed from the given configuration, where x_{CHOL}=0.3 (N_{DPPC}=38 and N_{chol}=16). The resulting two monolayers were constructed so

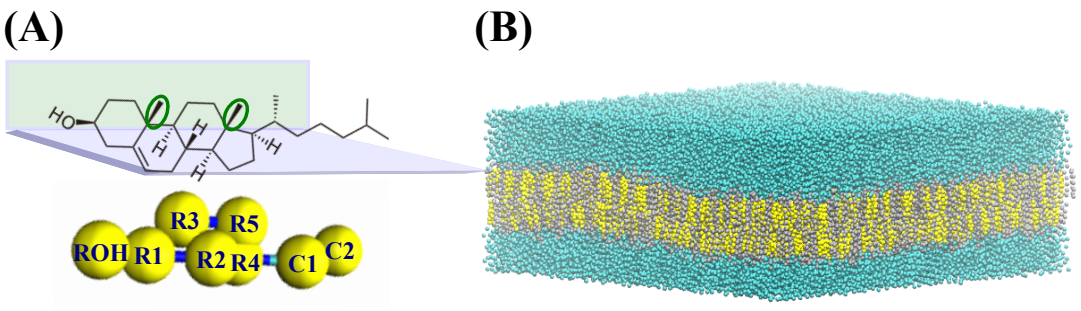

Figure 4.1: (A) Comparison of the coarse-grained cholesterol (including CHOL, CHO1 and CHO2) model applied in this work with assigned beads and its three-dimensional chemical structure. Two off-plane methyl groups are highlighted. (B) Example of a DPPC/50%CHOL bilayer.

they have equal composition and the whole "patch" was replicated in the xy plane to generate the bilayer systems used in this work. To achieve a fully hydrated bilayer, either 38000 or 50000 CG water particles were added to the system, which are equivalent to 50 real water molecules per lipid.
The simulations were performed using the GROMACS software package (version 4.5) [13] in the NPT ensemble. Standard simulation conditions were applied here as described in chapter 3. In total, each system was simulated for 2 μs. The first μs was considered as equilibration time and it was discarded when computing ensemble averages.

$$U_{LJ}(r) = 4\epsilon_{ij}\left[\left(\frac{f\sigma_{ij}}{r}\right)^{12} - \left(\frac{f\sigma_{ij}}{r}\right)^{6}\right] \tag{4.1}$$

The change in size of cholesterol was achieved by adjusting the Lennard-Jones potential. In the standard MARTINI 2.0 force field, σ and ϵ are fixed to certain values according to the particle type and interaction level [12]. To construct the new cholesterol models with enlarged (CHO1) and decreased (CHO2) sizes, we applied a scale factor on the original values of σ to change the effective size (see equation 4.1). All other parameters remain unchanged within the standard MARTINI force field.

4.2.2 Analysis

A number of quantitative parameters are reported in this chapter. Apart from the theory of the standard structural and dynamic properties described in chapter 2, some extra analysis was performed for this work.

A cholesterol cluster is defined here based on the Voronoi construction, where we project R3 beads from cholesterol and C2 beads from DPPC onto the xy plane separately for both leaflets. If one R3 bead is found to be one of the nearest neighbours of another R3 bead, these two R3 beads are considered to be connected. When n R3 beads are found to be connected in the way described above ($n \geq 4$), a cluster consisting of n cholesterol molecules is assigned. The shape properties of the spatial conformation of the cluster can be described in terms of the gyration tensor $\mathbf{S}$ [14]

$$\mathbf{S} = \frac{1}{N}\sum_{n=1}^{N}(x_n^i - x_{COM}^i)(x_n^j - x_{COM}^j), \qquad i,j = 1,...,d, \tag{4.2}$$

where $x_{COM}^i = \sum_{n=1}^{N} x_n^i/N$ are the coordinates of the centre of mass position of cholesterol; N denotes the total number of monomers within the cluster; d is the dimensionality of the space, and $d = 2$ in this case to account for the two dimensional character of the membrane. The asphericity, A_d, of the cluster embedded in d dimensions of space is defined as [15]:

$$A_d = \frac{1}{d(d-1)}\sum_{i=1}^{d}\frac{(\lambda_i - \bar{\lambda})^2}{\bar{\lambda}^2} = \frac{1}{d(d-1)}\frac{Tr(\Delta)^2}{\bar{\lambda}^2} \tag{4.3}$$

where λ_i denotes the eigenvalues of the gyration tensor describing the distribution of monomers inside the cluster, $\bar{\lambda}$ represents the arithmetic mean of the radius of gyration and $\Delta = \mathbf{S} - \bar{\lambda}\mathbf{I}$ ($\mathbf{I}$ is the unity matrix). To characterize the cholesterol clusters in this work, we calculated the asphericity in 2-dimensions and reported as ensemble averages. The average asphericity of given conformations

in 2D spaces, $\langle A_2 \rangle$, is further defined as:

$$\langle A_2 \rangle = \left\langle \frac{(\lambda_2 - \lambda_1)^2}{(\lambda_2 + \lambda_1)^2} \right\rangle \tag{4.4}$$

with λ_i being the eigenvalue of the gyration tensor. A perfectly linear cluster would give a value of $\langle A_2 \rangle$ of 1, whereas $\langle A_2 \rangle$ approaches 0 for a spherical shape.

4.3 Results and discussion

4.3.1 Cholesterol cluster formation at $x_{CHOL} = 0.5$

The work reported in chapter 3 on DPPC/CHOL bilayers shows the clear formation of cholesterol clusters at $x_{CHOL} = 0.5$. We now discuss the properties of cholesterol clusters quantitatively. To investigate the influence of temperature, bilayers were simulated at 283 K and 313 K, and analyses were performed by monitoring the variation of the structural parameters as functions of cholesterol size and temperature. As seen in figure 4.2A, the enlarged CHO1 and decreased size CHO2 cholesterol molecules are generated as described in the Methods section with expected enlarged and decreased cross-sectional area values respectively. The area per cholesterol varies linearly with the scale factor applied within the LJ potential. The van der Waals volume of a coarse-grained cholesterol molecule, $V_{chol} = 0.38$ nm^3, is calculated as the average volume of one cholesterol molecule from a simulation of pure cholesterol. The volumes of CHO2 and CHO1 were obtained in the same way, as 0.28 and 0.53 nm^3, respectively. The volume ratio for CHO2/CHOL/CHO1 is calculated to be 0.74:1:1.4. Likewise, A_{DPPC} also changes upon changing the scale factor but with a weaker response in DPPC/CHO1 bilayers. By applying a scale factor of 1.15, A_{DPPC}(CHO1) is almost the same as A_{DPPC}(CHOL), whereas the ratio of A_{DPPC}(CHO2):A_{DPPC}(CHOL) is found to be equal the scale factor applied on CHO2 (f=0.85). Furthermore, the cross sectional area for both DPPC and cholesterol is independent of temperature. The clear increase in the area per lipid in going from CHO2 to CHO1 suggests a possible phase change (see figure 4.2). Another approach to examine the translational

ordering is to monitor the two dimensional radial distribution function, 2D RDF, (figure 4.2B). The behaviour of the RDFs with temperature mirrors the trend observed in the molecular area. RDFs of the DPPC/CHOL bilayer feature a weak, liquid-like ordering which decays with a long correlation length. This form of decay indicates the appearance of the L_o phase, as do other parameters from chapter 3. With the smaller CHO2 molecules, the RDFs show much stronger longer range oscillations, which correspond the typical behaviour of a gel phase. In contrast, the longer range correlation disappears quickly by around 4 nm in DPPC/CHO1 bilayers, which indicates a loss of translational order similar to the fluid phase. For the data of the average acyl chain order parameter, $S_{chain} \approx 0.8$ is obtained in all bilayers, regardless of temperature and of the cholesterol model employed. Therefore, an L_o phase can be confirmed for DPPC/CHO1 and DPPC/CHOL bilayers at both temperatures.

Following the typical structural parameters, we carried out a quantitative anal-

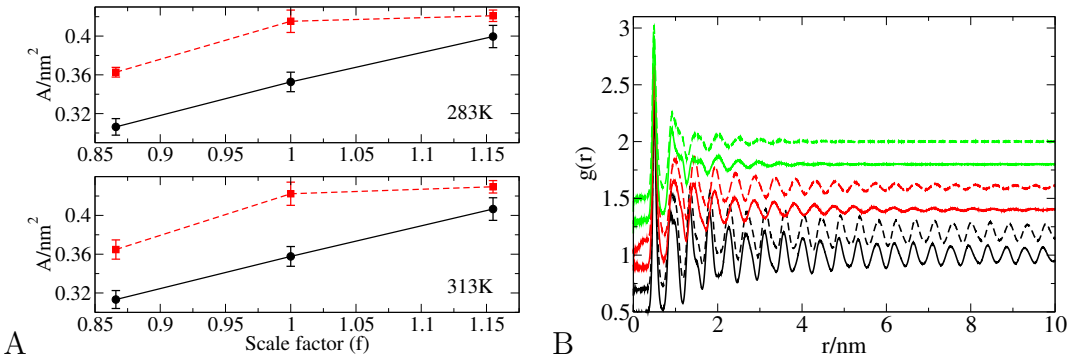

Figure 4.2: (A) Variation of area per DPPC (red solid square) and cholesterol (black solid circle) responding to the scale factor(f, as stated in equation 4.1) on LJ potential at 283K and 313K. (B) 2D RDF of the central beads (C2A and C2B)of each phospholipid chain at 283K (solid lines) and 313K (dashed lines) in DPPC/CHOL (middle two), DPPC/CHO2 (bottom two) and DPPC/CHO1 (top two) bilayers.

ysis of cholesterol clusters and found a strong influence of cholesterol size on the bilayer structure. In Table 4.1, the 2D asphericity $\langle A_2 \rangle$ provides direct information on the cluster shape. CHOL clusters appear to have the greatest asphericity at both 283 K and 313 K, the value increasing slightly from 0.696 to 0.741 with increasing temperature. At both temperatures, the $\langle A_2 \rangle$ of CHO2 is similar but

slightly smaller than the CHOL one. In contrast, CHO1 obtained by enlarging the CHOL gives values of cluster asphericities as low as 0.482 at 283 K and 0.468 at 313K. These findings reveal that CHOL and CHO2 favour linear clusters, whereas CHO1 tends to form circular ones. Whilst the cholesterol molecule size alters the overall shape of the clusters, the temperature exerts only a very small influence on the asphericity. Statistical results (see figure 4.3 A - B) also show that some large clusters are formed containing as many as 30 CHO1 molecules. This leads to a greater average cluster size (≈ 7 molecules in each defined cluster) compared with CHOL and CHO2. $\cos\theta$ is computed to understand the cluster linearity, where θ is the angle formed by every 3 consecutive beads within a single cluster (see figure 4.3 C - D). A clear loss of linearity in both CHO1 and CHO2 is observed, but with no evidence of other preferred shapes. These results are compatible with the conclusions made from the asphericity calculation. Same as the area per lipid and the RDFs, the results observed from the cluster analysis also show as temperature-independent.

Table 4.1: Total number of clusters within the bilayer and average cluster size

283K	No. of Clusters	cluster size	$\langle A_2 \rangle$
CHOL	220	5.5864	0.6963
CHO2	181	5.5414	0.6304
CHO1	196	6.8061	0.4823
313K	No. of Clusters	cluster size	$\langle A_2 \rangle$
CHOL	246	5.6220	0.7414
CHO2	180	5.4389	0.6482
CHO1	202	7.0347	0.4681

The change of cluster shape can be also monitored from the snapshots of the leaflets obtained from the Voronoi tessellation method. In figure 4.4, cholesterol clusters in each monolayer are plotted and highlighted according to their asphericity. Most of the CHOL clusters were coloured in red (see figure 4.4B and E), reflecting the tendency for being linear. More bulk (blue, see figure 4.4 C and F) clusters are populated in the CHO2/DPPC system. CHO1 clusters tend to consist of a mixture of both linear and spherical ones. These snapshots

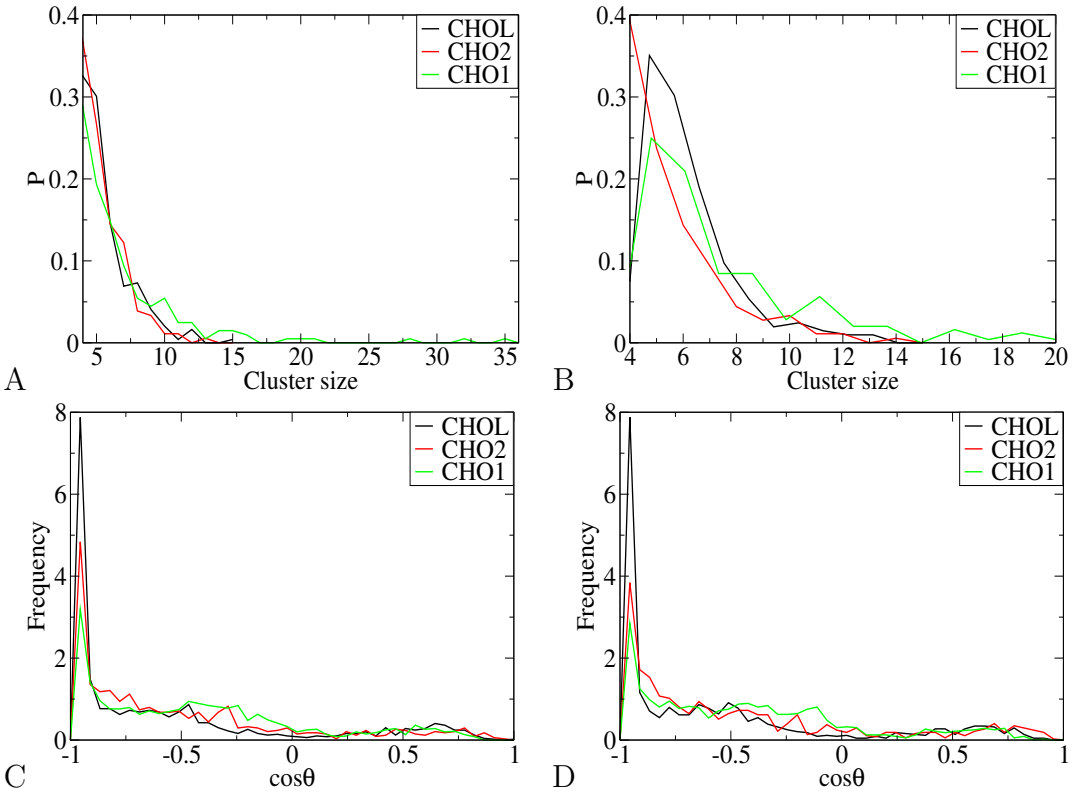

Figure 4.3: Probability distribution of cluster size found in lipid bilayers at 313K (A) and 283K(B). Frequency calculated for each three of consecutive cholesterol beads from the same cluster at 313K (C) and 283K (D).

obtained from the Voronoi construction also give us an idea of the lateral packing from visualization. Regular hexagonal packing with six nearest neighbours is expected for ordered gel phase bilayers, which can been seen in the system of DPPC/CHO2 and DPPC/CHOL(see figure 4.4 A-B and D-E). Interestingly, DPPC/CHO1 bilayers have lost this regular packing. Nearest neighbour around cholesterol molecules is analysed using Delaunay triangulation [16]. Such information can be used to provide quantitative information on the spatial order in DPPC/cholesterol membranes. C2A and C2B beads from the middle of the lipid chains were selected to perform the analysis. In figure 4.5, both CHOL and CHO2 give the same lipid coordination number of six. However, CHO1 is more likely to have a greater number of DPPC neighbours, with an overall number of seven nearest neighbours. Seven-fold disinclinations identify lattice defects with CHO1

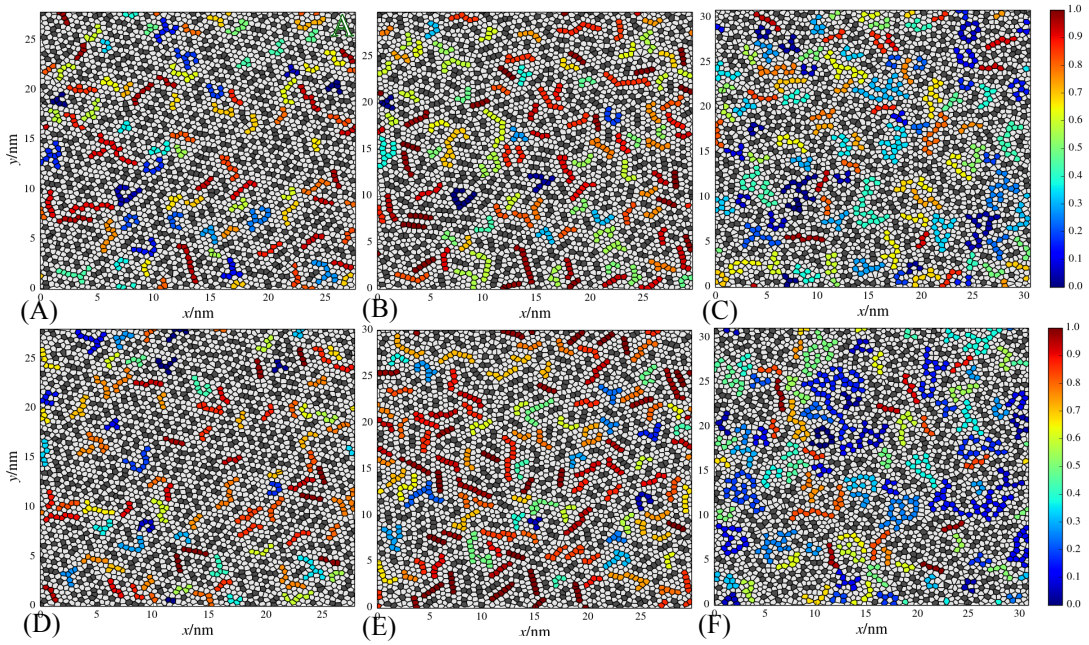

Figure 4.4: Snapshots of half bilayers show the asphericity of cholesterol clusters at 283K ((A)CHO2 (B) CHOL (C) CHO1) and 313K ((D)CHO2, (E)CHOL, (F)CHO1). C2 beads of DPPC are shown in light grey, cholesterol beads not considered as clusters are shown in dark grey.

molecules. Similar to the RDFs, the nearest neighbour coordination number indicates that the enlarged cholesterol molecule type CHO1 has less ability to pack laterally with DPPC.

The importance of the cholesterol model size for the lateral packing is also confirmed by computing the pair correlation function for cholesterol/DPPC bilayers, which is helpful to investigate what types of molecule are favoured in adjacent positions to cholesterol molecules (see figure 4.6). The RDFs were computed using the middle beads C2A and C2B in the acyl chains for DPPC, and site R3 at the same z position were selected to represent cholesterol. For the original CHOL, the main peak for CHOL-CHOL pair correlation is found at a distance of 0.5 nm, corresponding to the first coordination shell. The first peak for CHOL-DPPC is also located at 0.5 nm. Therefore, there is no preference for locating either CHOL or DPPC adjacent to CHOL, as the bilayer is crowded

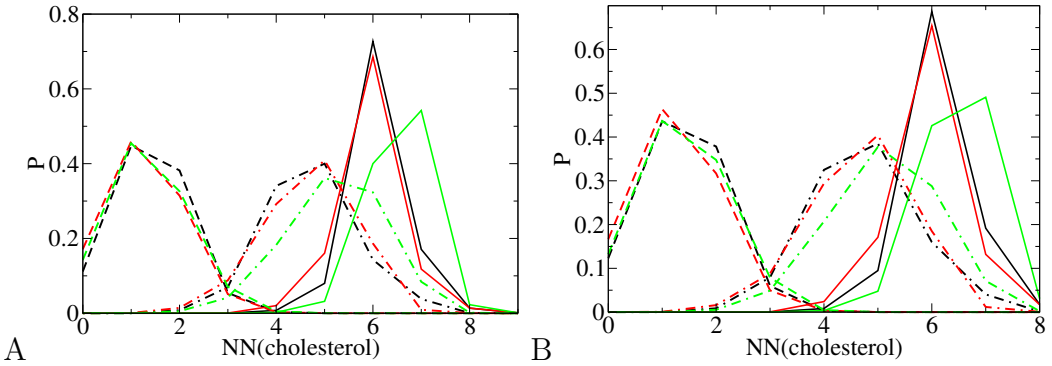

Figure 4.5: Probablity of finding N nearest neighbour cholesterol (dashed lines), DPPC (dash-dotted lines) and any (solid line) molecules around a given cholesterol molecule at 313K (A) and 283K (B).

by cholesterol molecules at this high concentration. On the other hand, CHO2 is preferentially located adjacent to CHO2, whereas CHO1 tends to avoid being located adjacent to CHO1.

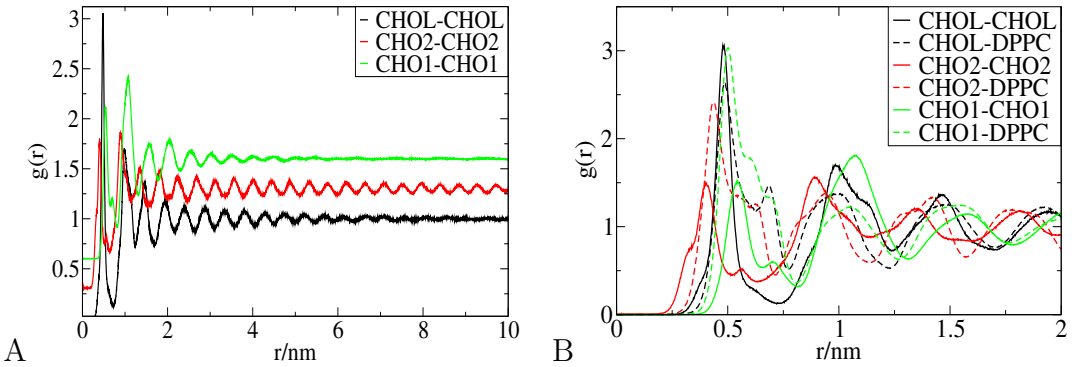

Figure 4.6: 2D RDF of cholesterol-cholesterol at 283K (A). Comparison of 2D RDFs showing corrleation between cholesterol-cholesterol and cholesterol-DPPC (B).

Information on the average structure of the lipid bilayer can be obtained from the number density profile of a selected group along the bilayer normal. The thickness and structure of the bilayer can also be obtained from the density profile. In figure 4.7 A, the number density profiles of DPPC and cholesterol obtained from simulations at 313 K are shown. Because the total number of particles is the same

Table 4.2: Thickness of DPPC/cholesterol monolayers, h/nm, and the difference between the thicknesses of DPPC and cholesterol molecules.

	h_{DPPC}	$h_{cholesterol}$	Δh
DPPC/CHOL	1.999 ± 0.052	1.446 ± 0.031	0.552
DPPC/CHO2	2.016 ± 0.052	1.460 ± 0.036	0.556
DPPC/CHO1	1.999 ± 0.053	1.438 ± 0.033	0.561

in all cholesterol-containing bilayers, and the beads of CHO1 have larger var der Waal radii, the resulting number per volume is expected to be lower, as seen in figure 4.7 A. The average structure of the lipid bilayer in figure 4.7 A, unambiguously demonstrates that cholesterol is shielded by DPPC from exposure to water. The peak-to-peak distances should allow the separate estimation of the thicknesses of the DPPC and of the cholesterol within the bilayer. However, the peaks are found to be relatively broad, resulting in large errors. Instead, the thickness of DPPC was obtained from the difference in z position between PO4 and C4 beads, where the thickness of cholesterol was calculated from the difference between ROH and C2 beads. The ensemble average was obtained and the standard deviation was also calculated (see Table 4.2). Results are found to give smaller values compared with previous atomistic simulations, where a bilayer value of 4.82 ± 0.3 nm was obtained from the computed electron density profile of DPPC/CHOL (x_{chol}=0.4) at 323 K [17]. Another recent small angle neutron scattering study reported the thickness of DMPC/CHOL as 4.42 nm (x_{chol}=0.47,T=303 K) [18]. We also note that only small differences in thickness are observed between the different sterol-containing bilayers (see Table 4.2). DPPC is slightly thicker in DPPC/CHO2 than in DPPC/CHOL and in DPPC/CHO1, so that DPPC is somewhat straightened in DPPC/CHO2 bilayers. The contribution of the sterol ring (R1-R5) and tail (C1-C2) particles is represented by number density profiles calculated solely from these groups. The results shown in figure 4.7B, demonstrate that the tail group in CHO2 has the lowest probability of occupying the bilayer center. To investigate further the z positioning, the z coordinate is calculated for the center of mass of selected groups and the relative position of cholesterol with respect to DPPC was thereby deduced. The positions of the three sterols in the bilayer can be compared directly. The result, Δz_{head}, describes the difference in z position be-

tween the headgroup of DPPC (PO4 is selected) and the hydrophilic ROH group from cholesterol. The smallest difference, for DPPC/CHO2, reveals that CHO2 is found closer to the bilayer/water interface. CHO1, on the other hand, exhibits the greatest value in Δz_{head}. Therefore, CHO1 is located closer to the bilayer core. CHOL is found to adopt a behaviour in between CHO2 and CHO1. The same conclusion can be drawn by comparing the center of mass position of DPPC and cholesterol. The relative positions of DPPC and cholesterol is represented schematically in figure 4.7C.

Table 4.3: Relative z position of head group and centre of mass (COM) of cholesterol with respect to the headgroup and COM of DPPC.

Bilayer	Δz_{head}/nm	Δz_{COM}/nm
DPPC/CHOL	0.528	0.099
DPPC/CHO2	0.519	0.071
DPPC/CHO1	0.539	0.105

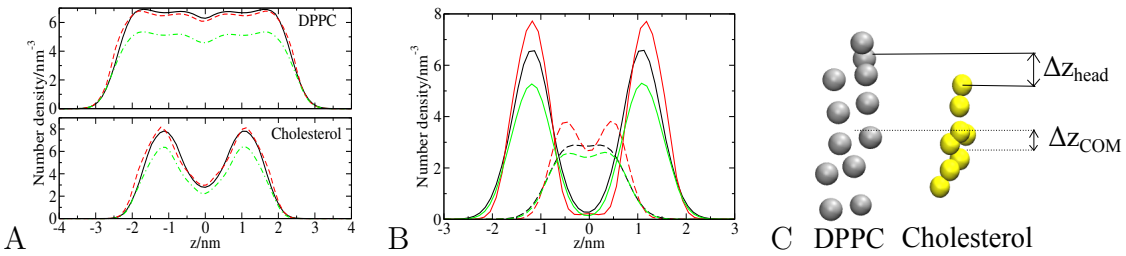

Figure 4.7: Number density functions of DPPC and cholesterol molecules (A) ; ring (solid lines) and tail (dashed lines) groups of cholesterol (B) at 313K. black: CHOL, red: CHO2; green: CHO1. Schematic representation of how results in Table 4.3 were calculated (C).

The distributions of tilt angles of the cholesterols with respect to the bilayer normal are shown in figure 4.8. The histogram of angles between the bilayer normal and the fused ring (vector connecting beads R1 and R5) at 313 K is given in figure 4.8A. Correspondingly, the calculated distribution for the angle between the bilayer normal and the sterol tail (vector connecting beads R5 and C2) is shown in figure 4.8B. For both angle distributions of ring and tail, CHOL is found

to lie on average between CHO1 and CHO2, with CHO2 aligned with the bilayer normal most closely, and CHO1 least closely. Because CHO2 is constructed with smaller van der Waals radii, it introduces less lateral perturbation than CHO1 or CHOL. In contrast, the enlarged CHO1 cannot fit into the bilayer as well as either CHOL and CHO2. The width of CHO2's angle distribution reveals that CHO2 is more dynamic. Since CHO2 is located towards the DPPC hydrophilic group where the packing is less dense, the rotational motion is less restrained.

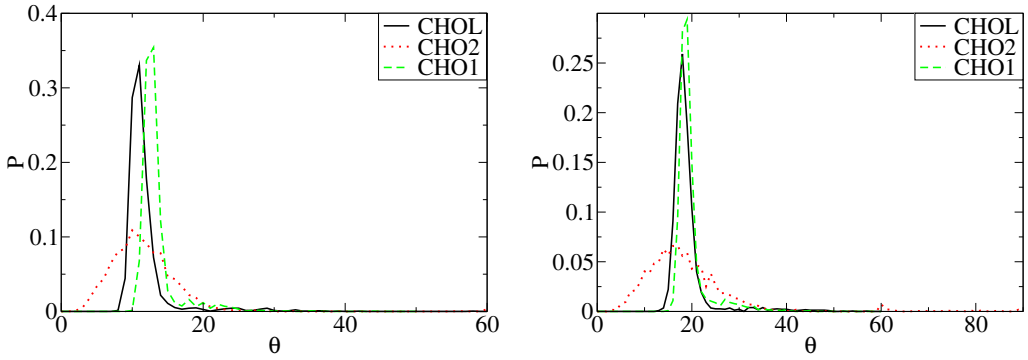

Figure 4.8: Tilt angle distribution between the bilayer normal and the vector connecting beads R1 - R5 (A) and R5 - C2 (B) at 313 K.

4.3.2 Effect on phase transition at $x_{CHOL} = 0.2$

Cholesterol has been well studied for its 'condensation effect' and impact on the gel-fluid phase transition. In this section, we report how cholesterol's size affects the phase transition of DPPC/Cholesterol bilayers.

From the work presented in chapter 3, we note that the gel-fluid transition can still be observed with 20% CHOL embedded. Features such as the cross-sectional area, RDF and orientational order parameter have been captured to identify the phase transition. A first order gel-fluid phase transition was observed, with $T_m \approx 308$ K. To understand how cholesterol's size may affect this transition, identical bilayers with CHOL replaced by CHO1 and CHO2 were simulated, and the same systematic analysis was performed.
Instead of the discontinuity shown in figure 4.9A with CHOL, linear correlations

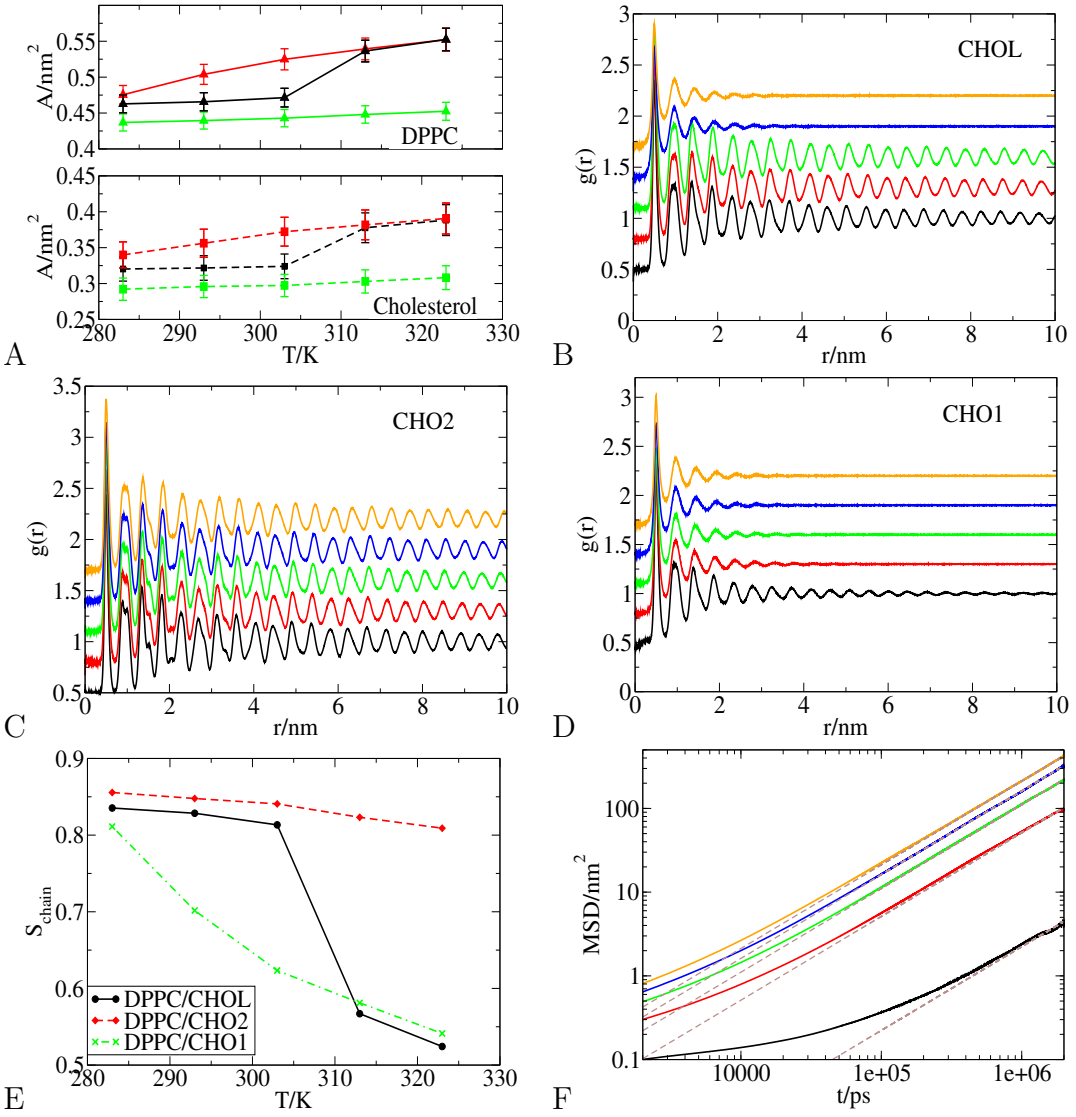

Figure 4.9: (A)Area per DPPC (solid lines) and CHOL (dashed lines) obtained from the Voronoi construction in DPPC/CHOL (black), DPPC/CHO1 (red) and DPPC/CHO2 (green) bilayers. 2D RDFs of DPPC-DPPC pair correlation computed using C2A and C2B beads at various temperatures (from bottom to top: 283 K, 293 K, 303 K, 313 K and 323 K) in DPPC/CHOL (B), DPPC/CHO2 (C) and DPPC/CHO1 (D) bilayers. RDFs are shifted vertically by 0.3 units for clarity. (E) S_{chain} obtained by averaging over all acyl beads. (F) Mean square displacement (MSD) of DPPC/CHO1 bilayers as a function of temperature, from bottom to top : 283 K, 303 K, 313 K and 323 K. Dashed lines represent the expected behavior of the MSDs in the diffusive regime.

between area per molecule and temperature were observed with DPPC/CHO1 and DPPC/CHO2 bilayers. Values obtained with CHO2 are well below those of the DPPC/CHOL bilayer. Together with the strong long range ordering shown in figure 4.9C and the high values of S_{chain}, ($\geq$ 0.8) seen in figure 4.9E, a gel phase is suggested for DPPC/CHO2 for temperatures between 283 K and 323 K. No evidence is found for any phase transition for the temperature range 283 K – 323 K. Nonetheless, a tendency for decreasing S_{chain} can be noticed at higher temperature. We increased the temperature by a further 10 K to try to observe a possible phase transition. Our Voronoi analysis shows that A_{DPPC} increases steeply to a value of 0.564 ± 0.016 nm^2 at 333 K, which is similar to the values calculated for other sterol-containing bilayers at 323 K. Furthermore, $S_{chain} = 0.423$ is consistent with the fluid phase. Examination of the 2D RDF at 333 K shows an abrupt loss of long range oscillatory behaviour (see figure 4.10A). A noticeable change in lateral packing is also seen in snapshots of half of the bilayers based on C2 beads. Only a small patch is shown with defects at 323 K (see figure 4.10B), whereas the acyl chains melt completely and lose the regular hexagonal organisation with a further 10 K increase in temperature (see figure 4.10C). Overall the main conclusion from the results reported above is that the decreased size of CHO2 molecules raises the temperature of the $S_o \rightarrow L_d$ transition to $\approx$ 328 K.

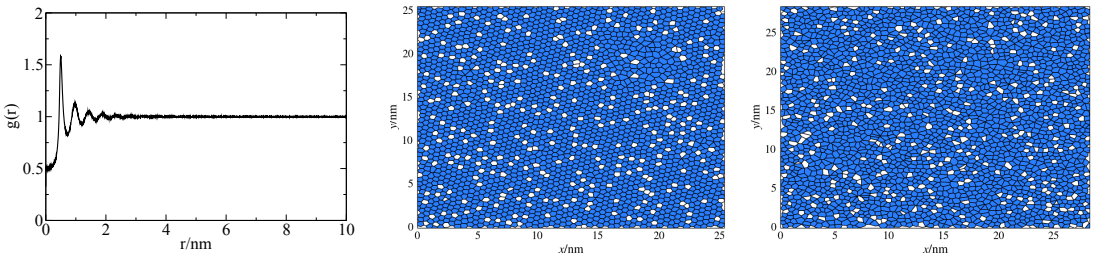

Figure 4.10: (A) 2D RDF of DPPC-DPPC pair correlation computed using C2A and C2B beads from the middle of the acyl chains at 333 K. Voronoi construction of one monolayer for DPPC/CHO2 at 323 K (B) and 333 K (C). Area occupied by DPPC is represented by polyhedra coloured in blue, and CHO2 is coloured in white.

CHO1 is found to play a more complex role on the phase transition than

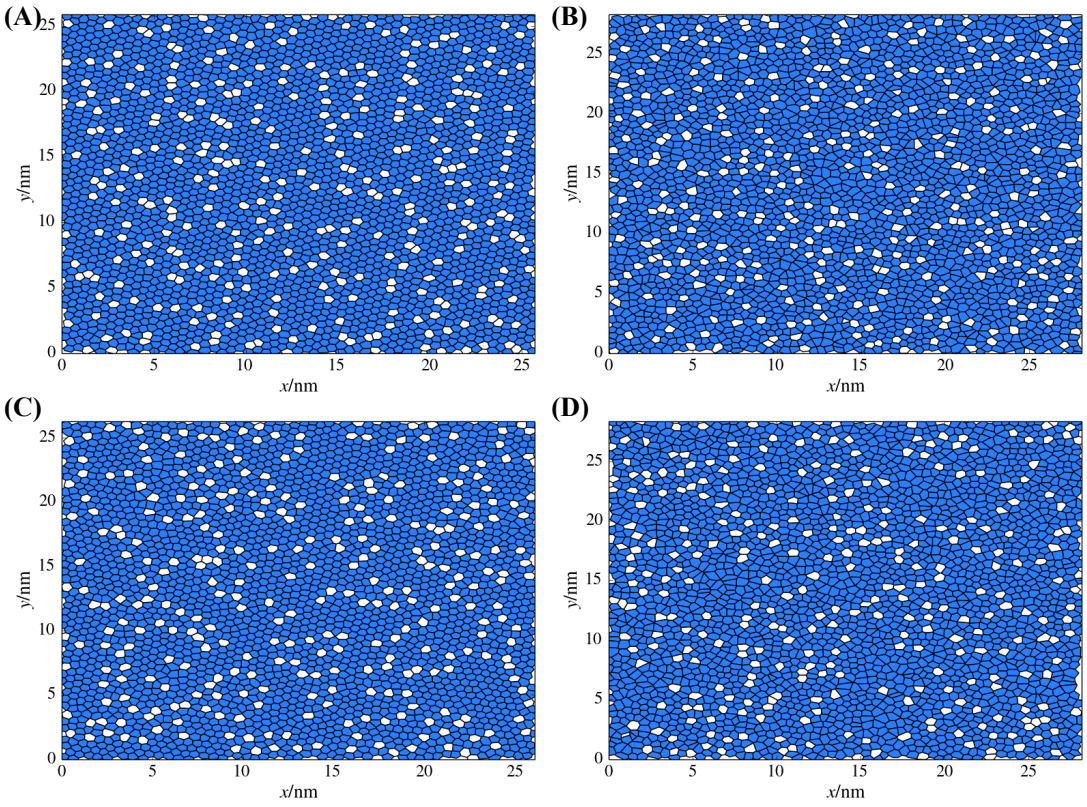

Figure 4.11: Voronoi construction of one monolayer for DPPC/CHOL ($x_{CHOL} = 0.2$) at 283 K (A) and 323 K (B); for DPPC/CHO1 at 283 K (C) and 323 K (D). DPPC is represented by areas coloured in blue, whereas white polyhedra correspond to cholesterol molecules.

CHO2. At low temperature (283 K) and high temperatures (313 K and 323 K), there is hardly any difference seen in the area and S_{chain} comparing CHO1 with CHOL. However, at intermediate temperatures, switching the cholesterol model expands the DPPC/CHO1 bilayer and gives greater values of $A_{DPPC/cholesterol}$. By checking the 2D RDFs (see figure 4.9), the nature of the translational ordering can be determined. Apart from the liquid-like, weak pair correlation present at 283 K, the DPPC/CHO1 bilayers appear to have a distinct liquid characteristic with a rapid decay of ordering from 293 to 323 K. In fluid phases, including 'L_o' and 'L_d', molecules exhibit liquid diffusive behaviour ($D \sim \times 10^{-7} cm^2/s$) [19], which differs from the gel ('S_o') phase ($D \sim \times 10^{-9} cm^2/s$)[20, 21]. D_{DPPC} is generally 2-10 times smaller in L_o than in L_d [22](see Table 4.4). Therefore, a possible $L_o \rightarrow L_d$ transition is suggested together with the evidence from the structural parameters. The sharp slope of S_{chain} (DPPC/CHO1) in figure 4.9E reveals the abrupt change in orientational order. Similar to the area per molecule, the order parameter shows good agreement between CHOL and CHO1 at high and low temperatures. The changes in the membrane in-plane structure can also be monitored by the Voronoi construction. In figure 4.11, hexagonal symmetry in the ordered phase at 283 K is clearly shown in both DPPC/CHOL and DPPC/CHO1 systems. At 323 K, they both melt and lose the hexagonal symmetry. However, the discontinuity is smeared out by the enlarged CHOL molecules. Overall, we see a continuous, possibly a second order, transition from 'L_o' to 'L_d' in DPPC/CHO1 bilayers with changing temperature.

Table 4.4: Lateral diffusion coefficient of DPPC, $D_{\mathrm{DPPC}}/10^{-7}\mathrm{cm}^2\mathrm{s}^{-1}$. The hyphen "–" represents a system for which diffusive behaviour was not reached in our simulation time scale.

T/K	DPPC/CHOL	DPPC/CHO1
283	-	0.06
293	0.02	1.28
303	0.03	2.77
313	3.79	4.04
323	5.48	5.31

4.4 Discussion and Conclusion

In this chapter, we have presented a novel study concerning the extraordinary role of cholesterol size in cluster formation and phase transitions. A number of different order parameters shown the effect of cholesterol model on the bilayer structure were computed.

With the original cholesterol model, clusters are only found with high concentrations, and so DPPC/50%CHOL was chosen in this study. The appearance of cholesterol clusters in coarse-grained simulations is a result of the smoothness of the CG cholesterol model (lack of the two off-plane methyl groups as shown in its chemical structure). From the cholesterol cluster analysis, we find that the linear cluster formation is absent by enlarging the cholesterol bead size by 15% (namely CHO1 in this chapter). CHO1 clusters are favoured in larger cluster sizes and more spherical shapes. By decreasing the area per cholesterol by 15% (namely CHO2 in this chapter), the DPPC/CHO2 bilayers are found to be more condensed. But no significant difference in preferred cluster size and shape was observed for DPPC/CHO2 bilayers compared with DPPC/CHOL bilayers.

In order to investigate the lipid-cholesterol interaction, we computed a few parameters that reveals the relative positions of cholesterol and DPPC molecules. The hydrophobic part of cholesterol molecules were found to be shielded by DPPC to avoid exposure to water. This is in agreement with the key assumption of the Umbrella model. In contrast, the structures expected for condensed complexes or superlattices models are not observed. Thus, the Condensed Complex model and the Superlattice Model are not supported by our data. In addition to the original model, we found that CHO2 condenses the membrane to a smaller cross-sectional area and results in closer lateral packing. CHO2 also allows a closer approach to itself than DPPC due to its smaller size. DPPC and CHO1 are found to occupy a similar molecular lateral area, that is greater than in DPPC/CHOL bilayers. This leads to a less effective shielding of CHO1 by the headgroups of DPPC. More neighbouring DPPC molecules are found for CHO1 due to the extended sterol-DPPC distance. Our results of tilt angle distribution follow the order CHO2 $<$ CHOL $<$ CHO1, as does the area per DPPC and cholesterol. The largest cholesterol, CHO1, induces the least tight packing in the bilayer, but is located,

on average, closest to the bilayer core. Thus, the rigid ring still straightens the DPPC acyl chains effectively. CHO2 yielded the smallest cross-sectional area with DPPC lipids, which are close to optimal packing. It is positioned closer to the bilayer/water interface with a larger cavity volume, so that has a broader distribution of tilt angles. The tilt angle follows the order CHO1 > CHOL > CHO2, which is compatible with the disrupted lateral packing on addition of the most tilted CHO2. In figure 4.12, the key differences in DPPC bilayer structure induced by different cholesterol models are schematised.

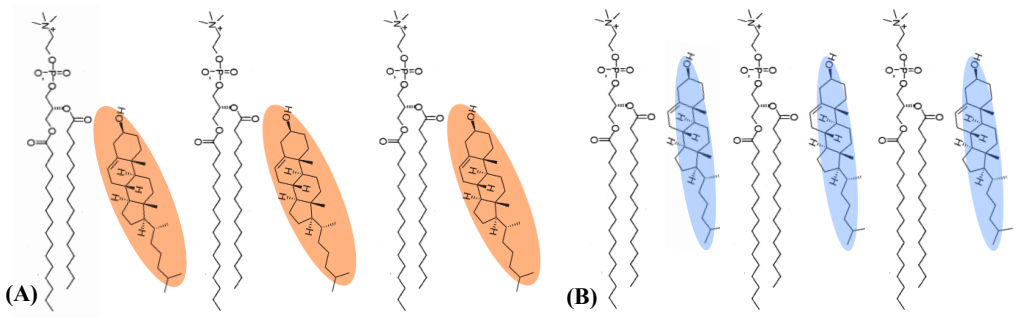

Figure 4.12: Schematic diagram showing the interaction between DPPC and CHO1(A) and CHO2(B). In DPPC/CHO1 bilayers, less condensing effect is introduced and lipids are less closely packed, although the ordering effect in the acyl chains remain. In contrast, CHO2 locates closer to the headgroup region, and is more closely aligned with the membrane normal. The bilayer packing is closer to optimal.

In agreement with observations on cholesterol cluster formation, we find that the enlarged CHO1 disrupts the translational ordering of the DPPC bilayer and destabilises the DPPC gel phase. A second order continuous $L_o \rightarrow L_d$ transition is induced together with the altered structural and dynamic parameters. Simulations with CHO2 show that the ordered phase is stabilised. Bilayers are observed with S_o characteristics in the temperature range $283 - 323$ K. Further investigation at higher temperature reveals the formation of the L_d phase at 333 K. Addition of 0.2 molar fraction of CHO2 shifts the $S_o \rightarrow L_d$ transition temperature to 328 K.

Interestingly, a high degree of similarity can be seen comparing CHO2 and CHO1

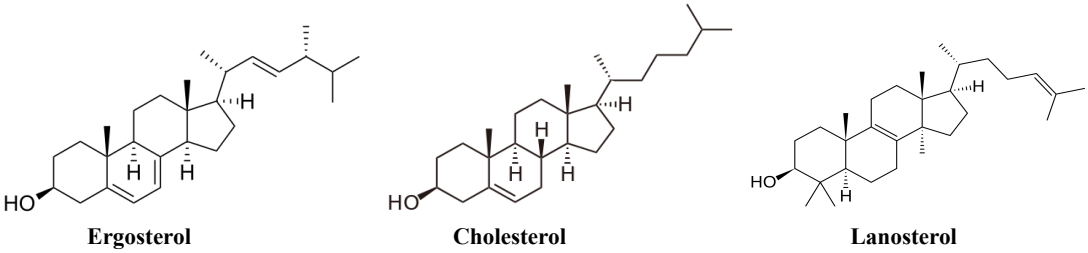

Figure 4.13: Chemical structures of ergosterol, cholesterol and lanosterol.

with some real sterols, ergosterol and lanosterol respectively. Ergosterol has a very similar chemical structure to cholesterol (see figure 4.13), which only differs in the alkyl chain. It is a common sterol found in fungi, and functions in the same way as cholesterol. Lanosterol is a slightly larger sterol, with three extra methyl groups (see figure 4.13). Previous simulations reported the van der Waals volumes for ergosterol/cholesterol/lanosterol as 0.87:1:1.1 [17, 23]. Although larger differences are observed with our cholesterol models (ratio of van der Waals volumes CHO2:CHOL:CHO1 = 0.74:1:1.4), the overall pattern agrees well. Structural studies on ergosterol in lipid bilayers found that the ordering and condensing effect of ergosterol is the highest. The smoothness of ergosterol leads to closer packing with the lipid chains, and it is found to locate closer to the bilayer/water interface. An experimental study using Fourier transform-infrared (FT-IR) spectroscopy and small-angle X-ray scattering (SAXS) investigated a p,T phase diagram of DPPC/ergosterol ($x_{ergosterol} = 0.22$) [24]. An all-fluid like L_d phase was reported at 330.5 K, which is consistent with our estimate for DPPC/CHO2 bilayers (T_m in the range of $323 - 333$ K). L_o/L_d phase coexistence is also reported in a narrow range ($314 - 330.5$ K). MD simulations at the atomistic level concluded that lanosterol induces the least effective packing within lipid bilayers, due to its bulky structure and position closer to the bilayer centre [17]. At low concentrations ($x_{lanosterol} \leq 0.2$), the DPPC acyl chains are found to be less ordered than with the same amount of cholesterol [25]. Consensus is also found in the diffusion coefficient, where results calculated for DPPC in DPPC/CHO1 bilayers match well with the data observed in a NMR study [26]. However, phase behaviour studies reveal that DPPC/lanosterol bilayers have a similar phase transition temperature as DPPC/cholesterol[26, 25]. Our observa-

tions differ from this conclusion. Nevertheless,with the very slow dynamics, the metastable state can survive for very long times, which we cannot discount.
To summarize, we have presented a detailed study that gives some insights into the mechanism of lipid-sterol interactions. We have discussed the relation between lipid packing and sterol structures with a wealth of data, including area, lipid order, radial distribution function, sterol tilt angles, and relative position of the sterol in the bilayer. The original cholesterol model adopts a behaviour between the two modified versions. Our study successfully reproduces the qualitative phase behaviour seen in experiments. Thus, the appropriate size of cholesterol is crucial for its optimal effect on the phase behaviour and orientation of the bilayer, resulting in just the right level of chain-chain interaction. A high degree of similarity is seen after comparing the effects introduced with our modified cholesterol-like molecules and some naturally existing sterols, suggesting that the influence of sterols on the bilayer structure and phase transition can be understood using relatively simple packing arguments.
Summary:

- Examined the role of sterol size on the lateral structure and phase behaviour of fully hydrated DPPC/Cholesterol bilayer mixtures using MARTINI forcefield CG-MD simulations.
- Computed several structural and dynamic properties to quantify the dependence of lateral order and phase behaviour with sterol type.
- Captured the formation of linear cholesterol clusters and observed the influence of cholesterol size on cluster formation.
- Found that the sterol size strongly influence the phase behaviour.

Future work:

- Further simulations of cholesterol analogs with bigger differences to the standard cholesterol molecule.
- More analysis of these bilayers to clarify the influence on structural and mechanical behaviours.

References

[1] M. C. Rheinstadter and O. G. Mouritsen. Small-scale structure in fluid cholesterollipid bilayers. *Current Opinion in Colloid & Interface Science*, 18(5):440 – 447, 2013. 105

[2] H. Martinez-Seara, T. Róg, M. Kartunen, I. Vattulainen, and R. Reigada. Cholesterol induces specific spatial and orientational order in cholesterol/phospholipid membranes. *PLOS one*, 5:e11162, 2010. 105, 106

[3] M. Ali, K. Cheng, and J. Huang. Assess the nature of cholesterollipid interactions through the chemical potential of cholesterol in phosphatidylcholine bilayers. *Proceedings of the National Academy of Sciences*, 104(13):5372–5377, 2007. 105

[4] P. L. Chong, W. Zhu, and B. Venegas. On the lateral structure of model membranes containing cholesterol. *Biochimica et Biophysica Acta*, 1788(1):2 – 11, 2009. 105

[5] A. Radhakrishnan and H. M. McConnell. Condensed complexes of cholesterol and phospholipids. *Biophysical Journal*, 77(3):1507–1517, 1999. 106

[6] P. L. Chong. Evidence for regular distribution of sterols in liquid crystalline phosphatidylcholine bilayers. *Proceedings of the National Academy of Sciences*, 91(21):10069–10073, 1994. 106

[7] P. J. Somerharju, J. A. Virtanen, K. K. Eklund, P. Vainio, and P. K. J. Kinnunen. 1-palmitoyl-2-pyrenedecanoyl glycerophospholipids as membrane probes: evidence for regular distribution in liquid-crystalline phosphatidylcholine bilayers. *Biochemistry*, 24(11):2773–2781, 1985. 106

[8] J. Huang. Chapter 12 model membrane thermodynamics and lateral distribution of cholesterol: From experimental data to monte carlo simulation. In J. M. Holt M. L. Johnson and G. K. Ackers, editors, *Biothermodynamics, Part A*, volume 455 of *Methods in Enzymology*, pages 329 – 364. Academic Press, 2009. 106

[9] H. Martinez-Seara, T. Róg, M. Pasenkiewicz-Gierula, I. Vattulainen, M. Karttunen, and R. Reigada. Interplay of unsaturated phospholipids and cholesterol in membranes: Effect of the double-bond position. *Biophysical Journal*, 95(7):3295 – 3305, 2008. 106

[10] H. Martinez-Seara, T. Róg, M. Karttunen, I. Vattulainen, and R. Reigada. Why is the sn-2 chain of monounsaturated glycerophospholipids usually unsaturated whereas the sn-1 chain is saturated? studies of 1-stearoyl-2-oleoyl-sn-glycero-3-phosphatidylcholine (SOPC) and 1-oleoyl-2-stearoyl-sn-glycero-3-phosphatidylcholine (OSPC) membranes with and without cholesterol. *The Journal of Physical Chemistry B*, 113(24):8347–8356, 2009. PMID: 19469492. 106

[11] O. Edholm and J. F. Nagle. Areas of molecules in membranes consisting of mixtures. *Biophysical Journal*, 89(3):1827 – 1832, 2005. 106

[12] S. J. Marrink, H. J. Risselada, S. Yefimov, D. P. Tieleman, and A. H. de Vries. The MARTINI force field: coarse grained model for biomolecular simulations. *The Journal of Physical Chemistry B*, 111(27):7812–7824, 2007. PMID: 17569554. 107, 108

[13] B. Hess, C. Kutzner, D. van der Spoel, and E. Lindahl. GROMACS 4: Algorithms for highly efficient, load-balanced, and scalable molecular simulation. *Journal of Chemical Theory and Computation*, 4:435–447, 2008. 108

[14] V. Blavatska and W. Janke. Shape anisotropy of polymers in disordered environment. *The Journal of Chemical Physics*, 133(18):184903(1)–184903(7), 2010. 109

[15] G. Wei. Asphericity and prolateness of linear and circular macromolecules. *Chinese Journal of Polymer Science (CJPS)*, 13(3):204, 1995. 109

[16] L. Guibas and J. Stolfi. Primitives for the manipulation of general subdivisions and the computation of voronoi. *ACM Transations on Graphics*, 4(2):74–123, April 1985. 113

[17] Z. Cournia, G. M. Ullmann, and J. C. Smith. Differential effects of cholesterol, ergosterol and lanosterol on a dipalmitoyl phosphatidylcholine membrane: a molecular dynamics simulation study. *The Journal of Physical Chemistry B*, 111(7):1786–1801, 2007. PMID: 17261058. 116, 125

[18] J. Pencer, M. Nieh, T. A. Harroun, S. Krueger, C. Adams, and J. Katsaras. Bilayer thickness and thermal response of dimyristoylphosphatidylcholine unilamellar vesicles containing cholesterol, ergosterol and lanosterol: A small-angle neutron scattering study. *Biochimica et Biophysica Acta (BBA) - Biomembranes*, 1720(12):84 – 91, 2005. 116

[19] S. J. Marrink, A. H. de Vries, and A. E. Mark. Coarse grained model for semiquantitative lipid simulations. *The Journal of Physical Chemistry B*, 108(2):750–760, 2004. 122

[20] S. J. Marrink, J. Risselada, and A. E. Mark. Simulation of gel phase formation and melting in lipid bilayers using a coarse grained model. *Chemistry and Physics of Lipids*, 135(2):223 – 244, 2005. 122

[21] B. Lee, S. A. Mabry, A. Jonas, and J. Jonas. High-pressure proton NMR study of lateral self-diffusion of phosphatidylcholines in sonicated unilamellar vesicles. *Chemistry and Physics of Lipids*, 78(2):103 – 117, 1995. 122

[22] G. Lindblom and G. Orädd. Lipid lateral diffusion and membrane heterogeneity. *Biochimica et Biophysica Acta*, 1788(1):234 – 244, 2009. 122

[23] J. Czub and M. Baginski. Comparative molecular dynamics study of lipid membranes containing cholesterol and ergosterol. *Biophysical Journal*, 90(7):2368 – 2382, 2006. 125

[24] M. Pühse, C. Jeworrek, and R. Winter. The temperaturepressure phase diagram of a DPPC-ergosterol fungal model membranea SAXS and FT-IR

spectroscopy study. *Chemistry and Physics of Lipids*, 152(1):57 – 63, 2008. 125

[25] D. Huster, H. A. Scheidt, K. Arnold, A. Herrmann, and P. Mller. Desmosterol may replace cholesterol in lipid membranes. *Biophysical Journal*, 88(3):1838 – 1844, 2005. 125

[26] H. A. Scheidt, D. Huster, and K. Gawrisch. Diffusion of cholesterol and its precursors in lipid membranes studied by 1H pulsed field gradient magic angle spinning NMR. *Biophysical Journal*, 89(4):2504 – 2512, 2005. 125

Chapter 5

Phase transition in DPPC/DOPC bilayers

Experiments and theoretical studies have shown the hydrophobic mismatch between DPPC and DOPC contributes to DPPC-DOPC demixing. In the present chapter, we consider the model of DPPC/DOPC binary mixtures and discuss the impact of DOPC and the effect of heterogeneity of the bilayers on the phase transitions. To do so, we study a mesoscopic model of a fully hydrated bilayer containing DPPC and DOPC. Our results showed that the initial configurations of the bilayer model strongly influence the bilayer phase transitions. A nucleation site was found to be essential to initiate the phase transitions, and a DPPC/DOPC composition-temperature phase diagram was proposed based on the model with a nucleation site.

5.1 Introduction

Naturally occurring cell membranes consist of multiple components, involving hundreds of different types of lipids, therefore complex interactions between lipids arise. There is increasing evidence that to fully understand many cellular processes, we must first understand the lipid-lipid interactions involved [1]. In the previous chapter, we have discussed the effect of the non-phospholipid component, cholesterol, on the phase behaviour of lipid membranes and on the observation of

domains of distinct phases organized laterally. Domains can create locally optimized environments for protein functions and initiate certain types of biochemical reactions [2].

The heterogeneous domains in eukaryotic cells are explained by the lipid raft hypothesis [3]. These small domains are enriched in saturated lipids and cholesterol [4, 5]. They are small in size (nano-scale), and exist as distinct liquid-ordered regions of the membrane. However, the functional roles and driving force for raft formation remain unclear. Furthermore, there are uncertainties in the size and lifetime of rafts that make relevant studies [6] difficult to implement. The common membrane model used to study lipid rafts is a mixture of simplified composition, usually saturated phospholipid/unsaturated phospholipid/cholesterol. Many ternary phase diagrams and some quaternary diagrams are reported which have shown the preferential association between certain lipid types [7, 8]. Cholesterol molecules aggregate with saturated lipid to form a liquid-ordered phase, whereas unsaturated lipids do not mix favourably with cholesterol and form the disordered phase.

1,2-dipalmitoyl-*sn*-glycero-3-phosphocholine (DPPC) as stated before, is one

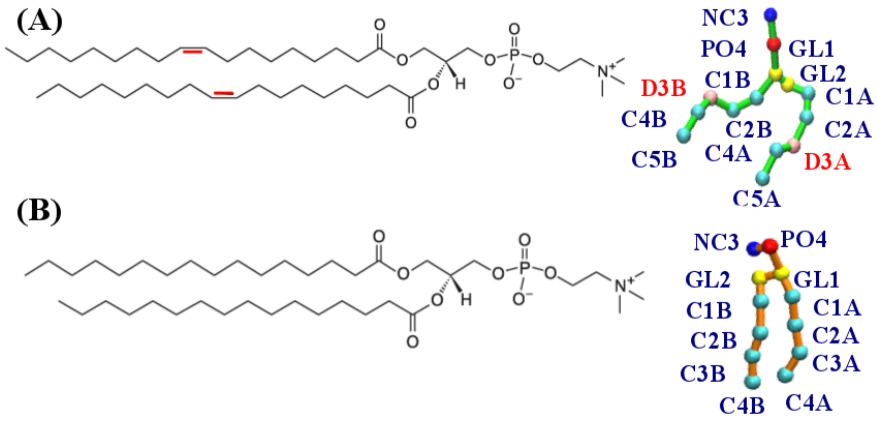

Figure 5.1: Comparison of coarse grained molecular models of DOPC (A) and DPPC (B). Beads are coloured according to interaction type. D3A and D3B represent the *cis* double bonds in the DOPC carbon tails (highlighted in red), with a smaller equilibrium angle.

of the most abundant lipids in membranes which have been well studied and is often chosen as an ingredient in multi-component mixtures. Another repre-

sentative phospholipid commonly selected for membrane models is 1,2-dioleoyol-*sn*-glycero-3-phosphocholine (DOPC), which has one double bond in the middle of each aliphatic tail (see Figure 5.1). Many studies, both experimental and computational [9, 10, 11, 12] have explored the behaviour of ternary mixture-DPPC/DOPC/cholesterol as a model for membrane lipid rafts. The study of partial phase diagrams of binary mixtures, including DPPC/cholesterol, DOPC/cholesterol and DOPC/DPPC is the starting point for the investigation of the multi-dimensional phase digram. DPPC/cholesterol, which we have discussed in detail in chapter 3, has drawn much more attention than the other two mixtures. The literature contains little information about the DOPC/cholesterol and DPPC/DOPC mixtures. The partial phase diagram of DPPC-d_{62}/cholesterol of Vist et al. [13] shows that cholesterol is miscible in DOPC up to 40 mol%. Before the study present by Schmidt et.al [14](see Figure 5.2C), only a rough temperature composition phase diagram of the DPPC/DOPC bilayer is given [15, 16] (see Figure 5.2A-B). Moreover, some theoretical [17] and experimental studies (e.g. scattering[18, 16], fluorescence [15] and NMR [14]) on DPPC/DOPC mixtures have been reported. However, there are comparatively few computational investigations. This chapter presents a careful study of the phase equilibria of DOPC/DPPC mixtures using molecular dynamics simulation.

The phase behaviour of single component DOPC bilayers is expected to be similar to that of pure DPPC bilayers: a first order transition should be observed as the temperature is increased above T_m. The DOPC molecule has longer carbon chains than DPPC (18 versus 16, see figure 5.1) and contains a *cis* double bond in the middle of each tail, whereas DPPC is fully saturated ($T_m = 41.2\,^{\circ}\mathrm{C}$ [19, 20]). The presence of the *cis* double bond results in poor packing of the lipid chains (see figure 5.1). DOPC bilayers exhibit a low main phase transition temperature, $T_m = -16.5\,^{\circ}\mathrm{C}$ for the gel-fluid transition [21]. The lower T_m enables the bilayers to maintain their flexibility, compressibility and fluidity at physiological temperatures. For DPPC/DOPC mixtures, a clear demixing (two-phase gel/fluid coexistence) is expected due to the large difference in the main phase transition temperatures of DPPC and DOPC lipid bilayers.
The same MARTINI CG force-field used for the DPPC/cholesterol study in chap-

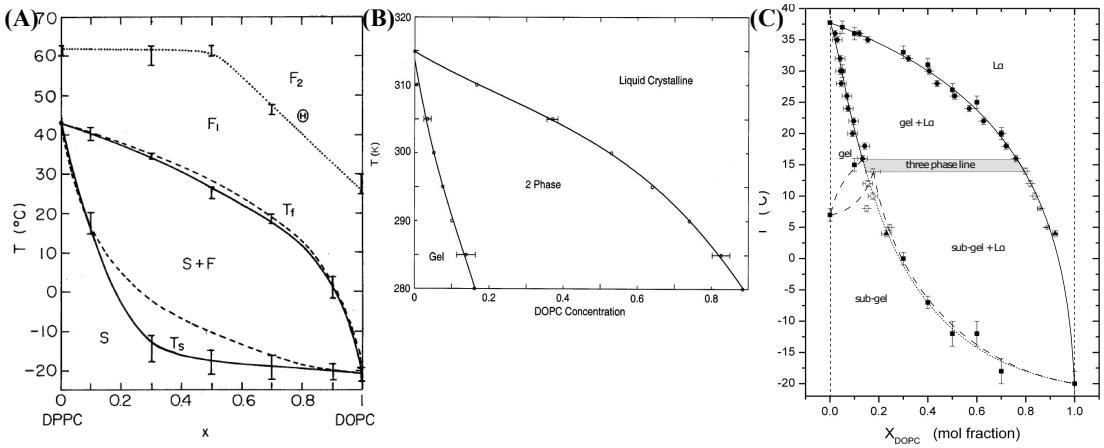

Figure 5.2: Three representative phase diagrams for a DPPC/DOPC system. (A) Phase diagram reported by Furuya and Mitsui determined with X-rays (solid lines) and calculated on the basis of thermodynamics (dashed lines) [16]. S represents for ordered state, where F stands for the disordered phase. In the S+F region, phase coexistence is observed. (B) A calculated phase digram derived from a molecular model of DPPC/DOPC bilayer which is solved with self-consistent field theory [17]. (C) The temperature-composition phase diagram of DOPC/DPPC-d_{62} in excess water [14]. The filled squares was obtained by inspection of the ^{2}H NMR spectra, and the filled circles was obtained by spectral subtraction. The firmly established phase boundaries are plotted with solid lines, while the solidus curve derived from the metastable gel date is shown in dotted line and the proposed phase boundaries are present with dashed lines. A three-phase coexistence is also reported here.

ter 3 is also applied in this study, which allows the use of longer time-scales together with larger system sizes (thousands of molecules for several microseconds). We begin this chapter by considering two different pure bilayers, those composed of only DPPC or DOPC lipids. The structural and dynamic properties of DPPC/DOPC mixtures over a wide range of temperatures and compositions is then monitored. The gradual change in DOPC composition is achieved using several different approaches, and we find that the initial arrangement of the bilayer strongly influences the final outcome seen in its phase behaviour. A complete DPPC/DOPC phase diagram evaluated from various quantitative analyses is then proposed and discussed at the end of the chapter.

5.2 Methodology

5.2.1 Force-field and simulation details

The standard MARTINI CG model with MARTINI 2.0 force field is used for all the simulations in this chapter, including DPPC, DOPC and water molecules. The same simulation conditions are applied here as described in chapter 3. The initial bilayer configurations consisting of 128 DPPC (T = 325 K) and 128 DOPC (T = 300 K) lipids were taken from the simulation work of Marrink and co-workers [22] (available on-line at: http://md.chem.rug.nl/cgmartini/). The bilayers were replicated in the xy dimensions and fully hydrated configurations of 2048 DPPC or DOPC molecules with 32000 water CG molecules were generated [23]. Unlike of 16 methylene/methyl units in each chain as found within the DPPC molecule, the DOPC molecule is longer by two methylene units and is modelled with one more CG bead in the MARTINI force-field. 'D' beads are introduced in the DOPC molecules to represent the *cis* double bond within the carbon tail. The 'D' bead is categorised as a type 'C_3' interaction site (see Figure 5.1). Differently from the 'C_1' site which is used to describe the aliphatic chains, the equilibrium angle is reduced to 120° from 180° with 'C_3'.

The DPPC/DOPC binary mixtures are obtained in three ways, but all of them are given a typical simulation box of dimensions $\{L_x, L_y, L_z\} = \{25, 25, 10\}$ nm with 4×10^4 particles including 2048 phospholipid molecules.

Asymmetric bilayers: Configurations with different compositions of DOPC were generated by randomly substituting the appropriate number of DPPC molecules within a single monolayer of a pure DPPC bilayer in the fluid phase into DOPC molecules. These asymmetric bilayer is also achievable using experimental techniques, e.g. Langmuir Blodgett/Langmuir Schaeffer [24]. The resulting bilayers consist of a mixed DPPC/DOPC monolayer and a pure DPPC monolayer (see Table 5.1).

Self-assembled bilayers: Configurations were obtained by self-assembling

Table 5.1: Asymmetric bilayers obtained with different concentrations of DOPC. The heterogeneity between the two leaflets can be seen from the side view snapshots of the DPPC/DOPC bilayer. orange:DPPC, green:DOPC, blue:choline group, red:phosphate group, yellow: glycerol ester group, water molecules were removed for clarity.

x_{DOPC}	N_{DOPC}	N_{DPPC}	Snapshot
0	0	2048	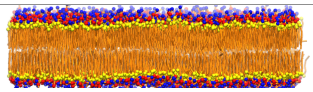
0.05	102	1946	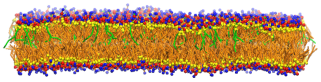
0.125	256	1792	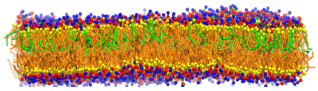
0.25	512	1536	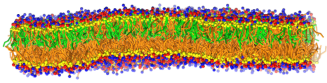
0.5	1024	1024	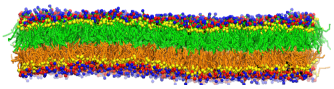
1	2048	0	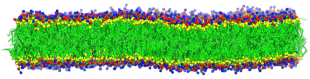

Table 5.2: Equi-molar DPPC/DOPC bilayer obtained by self-assembly. orange:DPPC, green:DOPC, blue:choline group, red:phosphate group, yellow: glycerol ester group, water molecules were removed for clarity.

x_{DOPC}	N_{DOPC}	N_{DPPC}	Snapshot
0.5	1024	1024	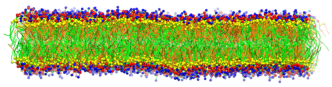

a small DPPC/DOPC bilayer from a random configuration of DPPC, DOPC and water in the simulation box. Configurations of single DPPC and DOPC molecules were extracted from the pre-equilibrated bilayers at 285 K (DPPC:gel phase, DOPC: fluid phase). 64 DPPC and 64 DOPC molecules together with 768 CG water sites were placed randomly in a simulation box of dimensions $\{L_x, L_y, L_z\} = \{7.5, 7.5, 7.5\}$ nm and set to move freely. A bilayer was formed after a short simulation run, resulting in roughly $x_{DOPC} = 0.4$ and 0.6 in the upper

and bottom monolayers respectively. It was then replicated in the xy dimensions to create a larger system used for further analysis. The resulting bilayer consisted of 1024 DPPC, 1024 DOPC and 28000 CG water molecules (see Table 5.2).

Symmetric bilayers: The configuration was obtained by combining two pure DPPC and DOPC bilayers side-by-side within a simulation box, with a gap of $\approx$ 0.3 nm to avoid overlaps. The two pure bilayers were pre-equilibrated at 285 K to obtain a gel phase for DPPC and fluid phase DOPC. The resulting two monolayers were constructed with the same composition, containing 2048 phospholipids in total and 29000 water beads.

Table 5.3: Symmetric bilayers constructed by combining gel phase DPPC bilyer and fluid phase DOPC bilayers. orange:DPPC, green:DOPC, blue:choline group, red:phosphate group, yellow: glycerol ester group

x_{DOPC}	N_{DOPC}	N_{DPPC}	Snapshot
0	0	2048	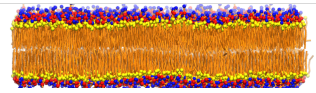
0.125	256	1792	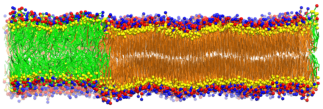
0.25	512	1536	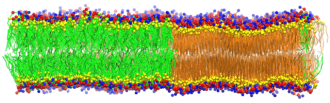
0.5	1024	1024	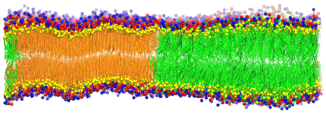
1	2048	0	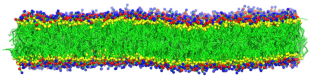

After energy minimization of the initial configuration, the bilayers were equilibrated and simulated for 1 μs at low temperature (285 K). The final configurations obtained after the simulations at low temperature were used as the starting configurations for higher temperature runs (295-325 K). The trajectories were saved every 5000 steps (0.1 ns). The first 900 ns in the trajectory is considered as an

equilibration stage and was discarded when computing ensemble averages.

5.3 Results and Discussions

5.3.1 Phase behaviour of pure DOPC bilayers

The gel-fluid phase transition of pure DPPC bilayers has been discussed in chapter 3. A sharp first order transition was observed and the transition temperature was determined to be in the range of 295-315 K. The unsaturated phospholipid DOPC remains in the fluid phase above the freezing temperature of the MARTNI water model ($T_m = 256.5\ K$ for gel-fluid transition[21]), therefore no gel-fluid phase transition is expected for DOPC bilayers in this simulation work.

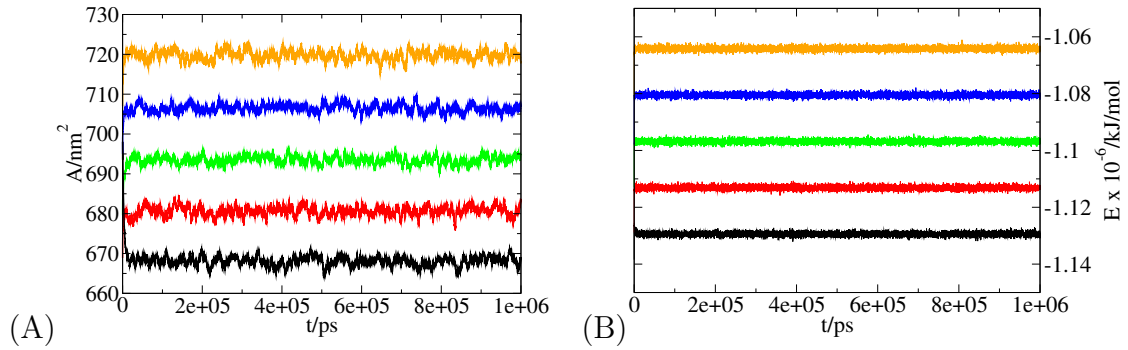

Figure 5.3: Evolution of the cross-sectional area of the simulation box (A) and potential energy (B), from bottom to top :285 K, 295 K, 305 K, 315 K and 325 K.

The equilibration process was monitored by computing the cross-sectional area of the simulation box and the potential energy for the DOPC bilayer from 285 K to 325 K (see Figure 5.3 A-B for the time dependence of both parameters). Unlike in DPPC bilayers, the DOPC bilayers studied here were in the fluid phase for all temperatures investigated. Hence, they reached the equilibration state within a much shorter time-scale.

We show in figure 5.4 that the area per DOPC and S_{chain} increase linearly with the increase in temperature, from 285 K to 325 K. Our simulations predict

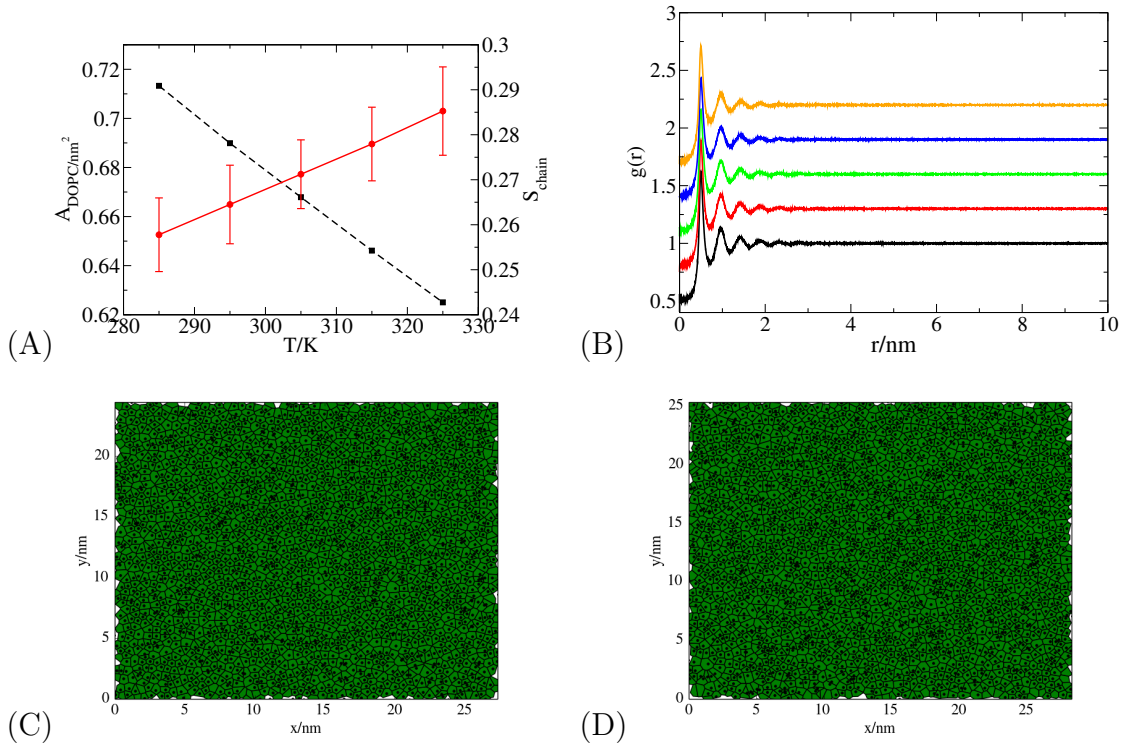

Figure 5.4: Simulation results for a pure DOPC bilayer at various temperatures. (A) Area per DOPC molecule (solid red lines)Average chain order parameter (dashed black lines) (B) RDFs computed using the C2A and C2B beads in the middle of each acyl chain. From bottom to top, 285 K, 295 K, 305 K, 315 K and 325 K. Voronoi construction of one monolayer at 285 K (C) and 325 K (D). The beads employed for the Voronoi construction C2A and C2B are represented by black dots and the corresponding area is colored green.

a cross-sectional area per lipid of 0.677 $\pm$ 0.03 nm^2 at T = 305 K. The area per lipid value is about 6.5% smaller than the experimental value [25], but agreed better with the previous atomistic simulation result for the same system (0.6915 $\pm$ 0.0127 nm^2) [26]. The average chain order parameters (S_{chain} , see Figure 5.4A) of DOPC are in the range of 0.24-0.29, which reveals a low orientational ordering in the lipid acyl chains and correspondingly a L_d phase as discussed in chapter 3. This numerical value agrees quantitatively with that of $2S_{CD}$ for DOPC at 298 K and wide-angle x-ray scattering averaged orientational order parameters (S_{x-ray}), where S_{CD} is the ^{2}H-NMR segmental order parameter [27]. The rapidly decaying radial distribution functions (see Figure 5.4B) are characteristic

of the fluid phase behaviour of DOPC bilayers. The fluidity is confirmed by the lack of regular packing in Voronoi polyhedra of monolayer (see Figures 5.4 C-D). Overall, all the structural parameters examined here indicate the existence of a liquid-disordered phase.

$$S_{\text{bond}} = \frac{1}{2}(3\langle\cos^2\theta\rangle - 1) \tag{5.1}$$

$$S_{\text{chain}} = 1/N_{bond} \sum_{i=1}^{N_{bond}} S_{\text{bond},i} \tag{5.2}$$

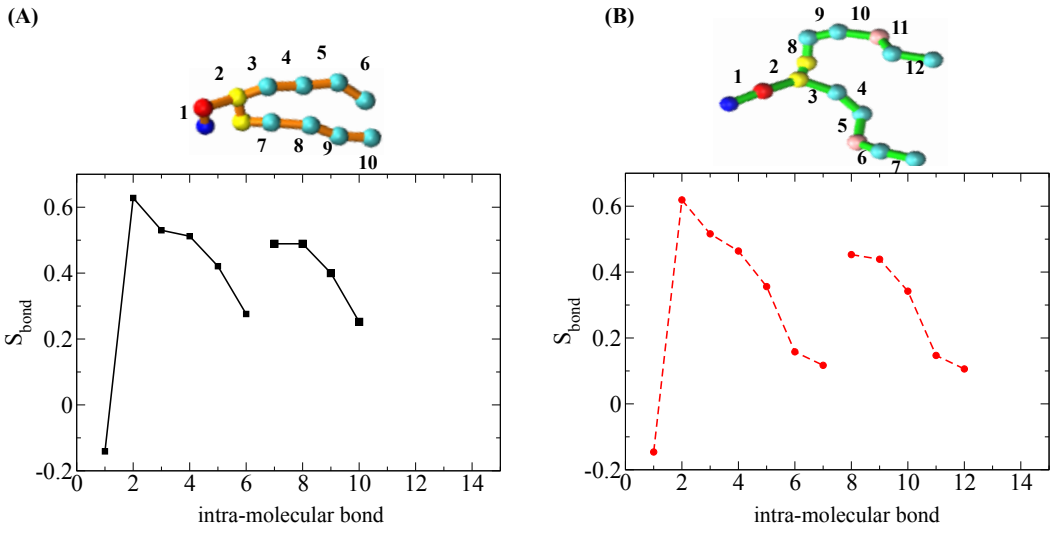

Figure 5.5: The orientational order parameter of intra-molecular bonds for the DOPC bilayer at 305 K(B) and the DPPC bilayer at 315 K(A). The intra-molecular bond numbers shown on the horizontal axis are indexed in the DPPC and DOPC coarse-grained models present on the top.

As discussed in chapter 2, the orientational order parameter of lipid acyl chain, S_{chain}, is averaged over the orientational order parameters of all CG bonds within the lipid tails (see equation 5.2). The orientational order parameter of each lipid bond, S_{bond}, is defined as a measurement of the lipid alignment with respect to

the bilayer normal (see equation 5.1). Figure 5.5 shows the S_{bond} values for all the intra-molecular bonds of DPPC and DOPC. Negative values were observed for the CG bonds within the lipid headgroup region, which means that these bonds are tend to align perpendicularly to the bilayer normal. A drop in the value of S_{bond} is expected for the unsaturated hydrocarbon tails compared to fully saturated chains, and this is captured by the MARTINI CG model.

5.3.2 Phase behaviour of asymmetric DPPC/DOPC bilayers

Lipid asymmetry is a common feature of all eukaryotic membranes, which is a consequence of many factors, such as the spontaneous "flip-flop" through the membrane interior and the presence of transporters (enzymes). Asymmetric distribution of plasma membranes has been found to have many important consequences on cell functions (more details can be found in this review [28]). To study the influence of DOPC and the impact of membrane composition heterogeneity on the phase behaviour of DPPC bilayers, the composition was varied systematically and the appropriate number of DOPC molecules were added to one monolayer. The composition remained stable within the time-scale of the simulation. No trans-membrane (flip-flop) motion of either DPPC or DOPC was found. In order to observe the gel-fluid phase transition, the mixed bilayers were quenched down to 285 K first, then allowed to heat up slowly to 325 K at 10 K intervals. Bilayers with x_{DOPC} =0.05 were simulated with a heating-cooling loop from 285 K to 275 K. It was cooled down further than the other system ($x_{DOPC} >$ 0.05) in order to observe the phase transition. 5% of the total water beads were substituted with anti-freeze particles to prevent the freezing of water in the system containing x_{DOPC} =0.05 at 275 K [22].

The area per DPPC and DOPC was computed as an ensemble average over the final 100 ns simulation trajectories using the Voronoi tessellation method (see Figure 5.7). The variation of $a_{DPPC}(x_{DOPC})$ and $a_{DOPC}(x_{DOPC})$ with temperature for different compositions of DOPC is shown. The area per DPPC

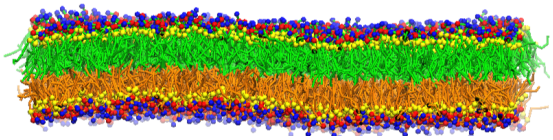

Figure 5.6: An example of asymmetric DPPC/DOPC bilayer, x_{DOPC} =0.5. orange:DPPC, green:DOPC, blue:choline group, red:phosphate group, yellow: glycerol ester group, water molecules were removed for clarity.

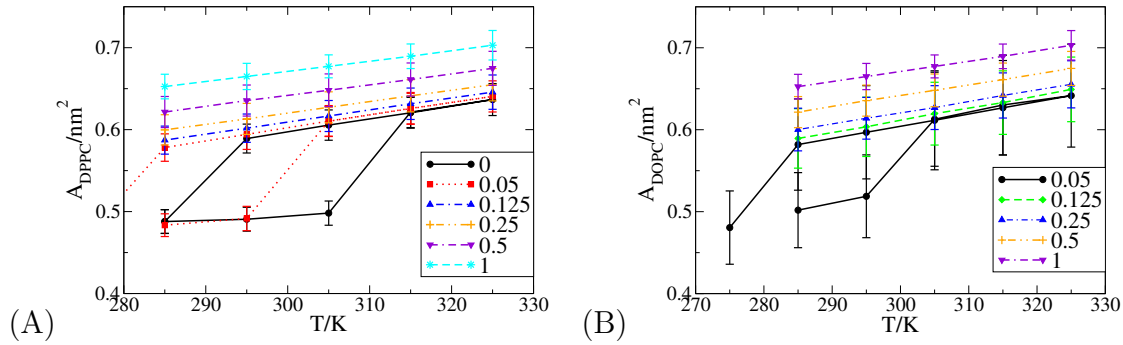

Figure 5.7: Area per DPPC(A) and DOPC(B) lipid versus temperature for different molar fractions of DOPC from 0 to 1.

and DOPC increases linearly with increasing temperature with more than 5% of DOPC embedded. Similar trend can be concluded for both $a_{DPPC}(x_{DOPC})$ and $a_{DOPC}(x_{DOPC})$ versus temperature. DPPC/DOPC bilayers with 5% of DOPC embedded in one monolayer behave in a similar way as the pure DPPC bilayer. A clear discontinuity is observed between 285 K and 305 K which is attributed to the $S_o \rightarrow L_d$ transition. The hysteresis loop is shifted down by 10 K with respect to pure DPPC bilayers. However, the area per lipid increases linearly with temperature at higher concentrations of DOPC ($x_{DOPC} \geq 0.05$).

The same trend is seen in the average chain order parameter S_{chain} (see Figure 5.8). The values for both DPPC and DOPC with molar fraction equal to 5% are halved by increasing the temperature from 295 K to 305 K, which is compatible with the existence of a gel-fluid transition. A minor decrease in S_{chain} is observed for bilayers with molar fraction greater than 5%. The distribution of S_{chain} over the whole bilayer system can be used to indicate possible phase coexistence, as the difference in S_{chain} is relatively large between gel and fluid lipids.

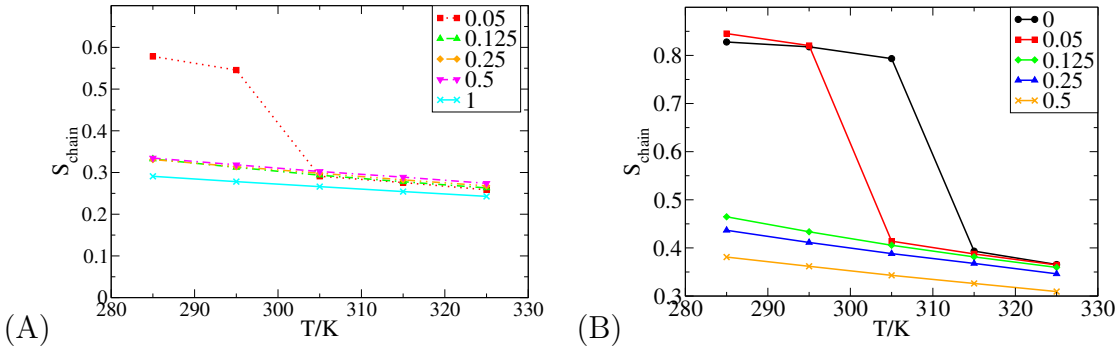

Figure 5.8: Average chain order parameter of DOPC(A) and DPPC(B) as a function of DOPC molar fraction and temperature.

Figure 5.9 shows the probability of the average chain order parameter of pure DPPC and DOPC bilayers in the gel and fluid phases. The long tail observed in the gel phase DPPC bilayer corresponds to the a small disordered region of DPPC molecules as discussed in chapter 3. Results for DPPC/DOPC mixtures are reported in figures 5.10 and 5.11. As shown in figures 5.10A and 5.11A, single peaks are observed for DPPC molecules in all the mixtures, where peaks found either around S_{chain} =0.9 or 0.4 correspond to the gel or fluid phase behaviours (see figure 5.10A). At higher concentrations, both DPPC and DOPC are in the fluid phase. The behaviour of DOPC molecules at $x_{\mathrm{DOPC}} = 0.05$ (see figure 5.10B) is more complicated. A single phase is observed for higher temperature. However, the orientational ordering of DOPC molecules seems to be distributed uniformly across all the values corresponding to the gel and fluid phase at 285 and 295 K. Hence, DOPC molecules are observed in both gel and fluid phases.

The C2A and C2B beads (see figure 5.1 for the labelling of CG beads) which are present in both DOPC and DPPC lipids in the middle of the hydrocarbon chains were selected to compute the RDFs. As seen in figure 5.12A ($x_{DOPC} = 0.05$), we find an abrupt loss of long range ordering between 285 K and 295 K, which is connected to the $S_o \rightarrow L_d$ phase transition. Bilayers with higher DOPC content ($x_{DOPC} \geq 0.05$, see figure 5.12B-E) also feature a sudden loss of long ranged ordering at all temperatures, which is indicative of the L_d phase.

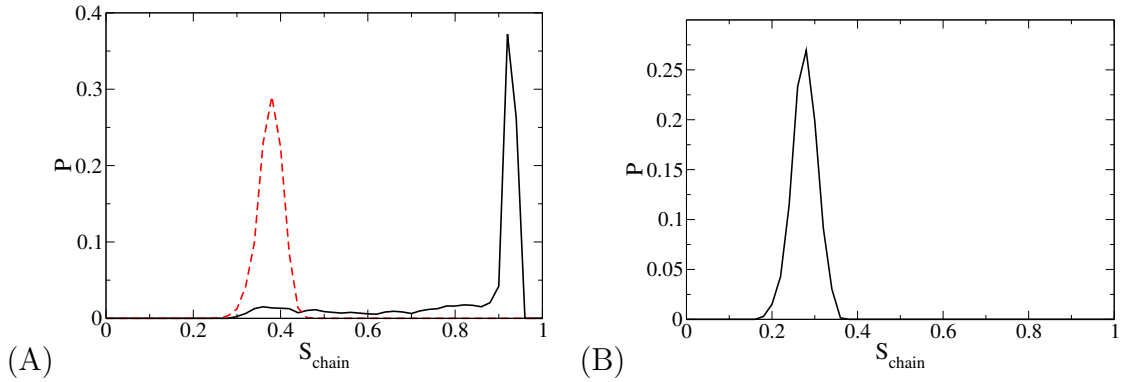

Figure 5.9: Probability of the average chain order parameter in pure DPPC bilayers(A) (black-solid:gel phase; red-dashed:fluid) and in pure DOPC bilayers (fluid phase).

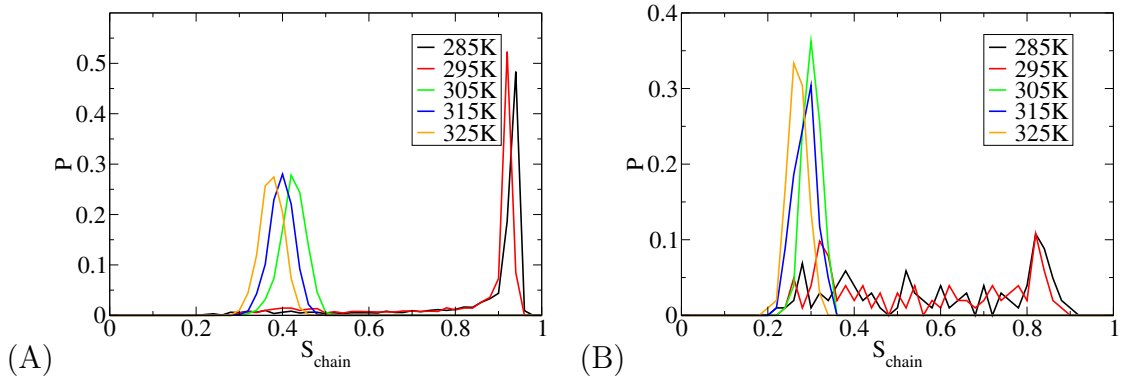

Figure 5.10: Probability of the average chain order parameter of DPPC (A) and DOPC(B) in the bilayers where $x_{\mathrm{DOPC}} = 0.05$.

The snapshots of monolayers obtained from the Voronoi construction do also provide information on the lipid chain lateral packing. With 5% of DOPC embedded in one monolayer, a loss of hexagonal order for both leaflets is seen as the temperature was increased (see figure 5.13 A-D). DOPC molecules pack well within the bilayer and the hexagonal packing remains undisturbed at low temperature (285 K). These observations reflect the loss of translational symmetry upon an increase of the temperature. In contrast, at higher concentrations of DOPC, the bilayer features is poor hexagonal ordering at all temperatures (see figure 5.13E-H), which is compatible with the absence of a gel phase at these temperatures.

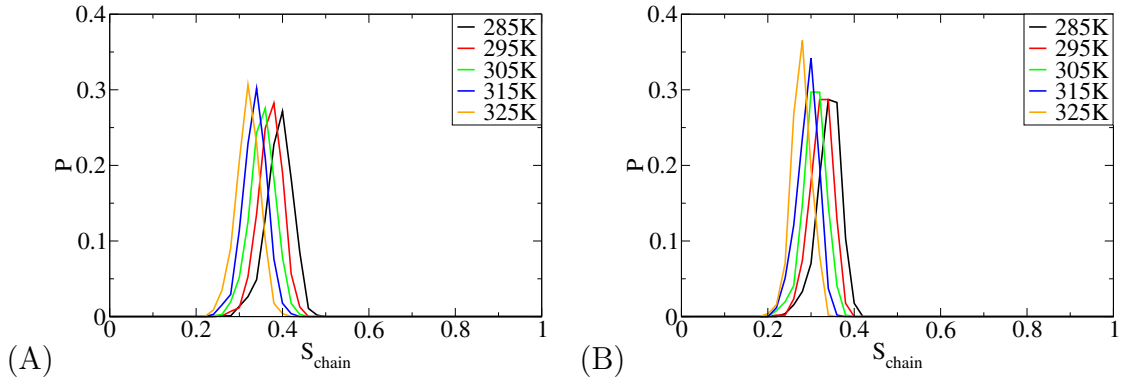

Figure 5.11: Probability of the average chain order parameter of DPPC(A) and DOPC(B) in DPPC/DOPC bilayers with $x_{\mathrm{DOPC}} = 0.25$.

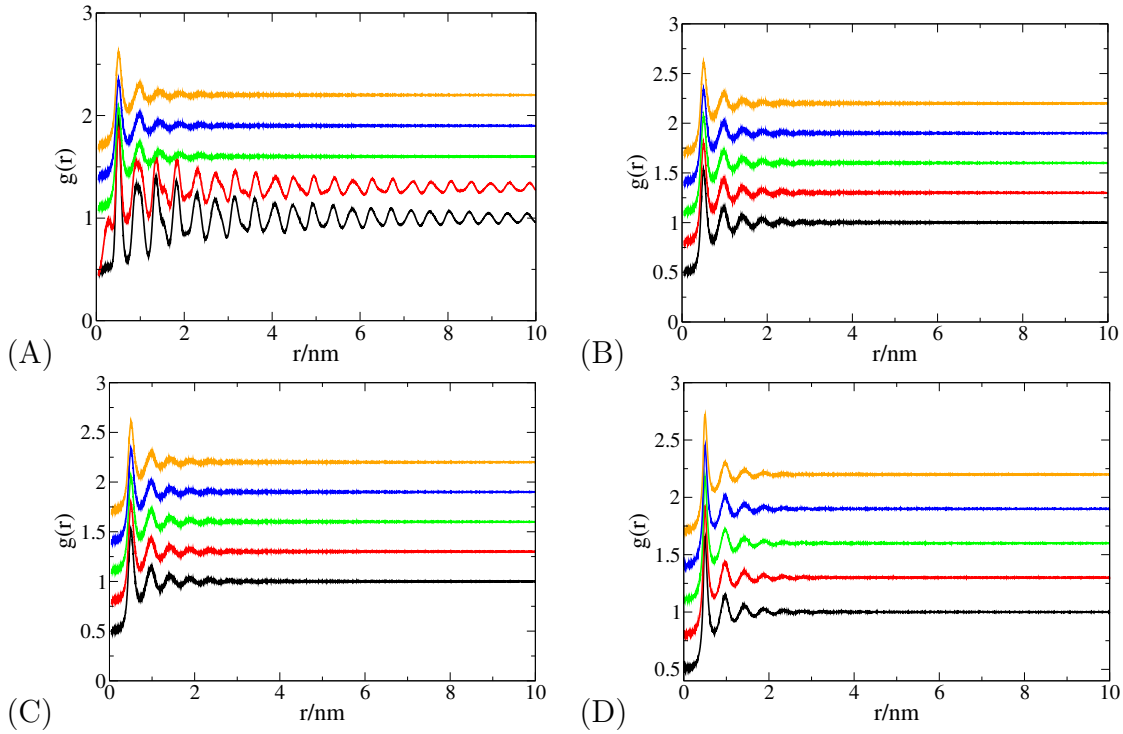

Figure 5.12: RDFs of the central beads (C2A and C2B) of each phospholipid chain. From bottom to top, 285 K, 295 K, 305 K, 315 K and 325 K at $x_{\mathrm{DOPC}} = 0.05$ (A), $x_{\mathrm{DOPC}} = 0.125$ (B), $x_{\mathrm{DOPC}} = 0.25$ (C),$x_{\mathrm{DOPC}} = 0.5$ (D).The RDFs have been shifted by 0.3 units vertically for better clarity.

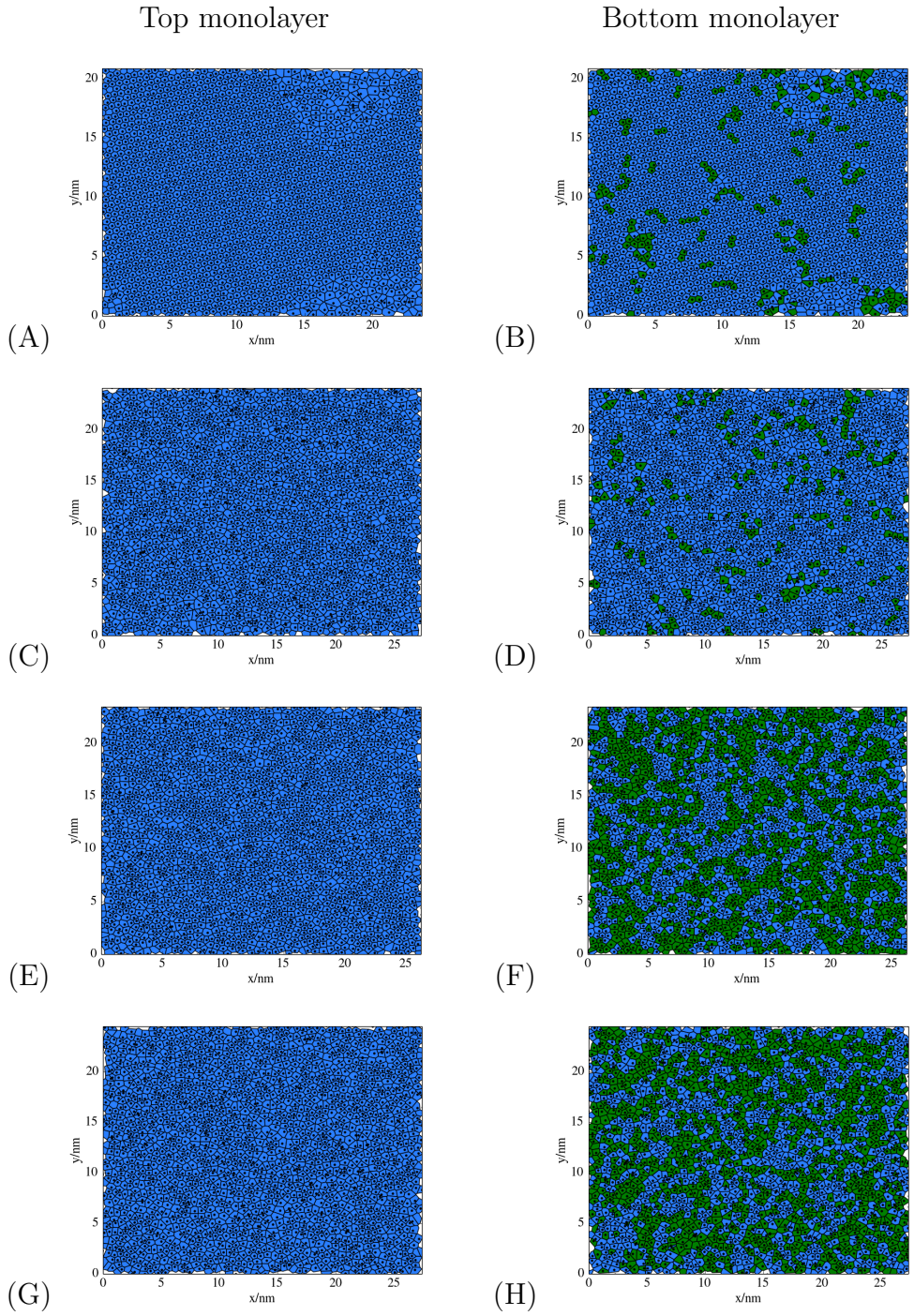

Figure 5.13: Snapshots with the same number denotation represent the corresponding Voronoi construction plots for half of bilayer at 285K (A-B and E-F) and 323K (C-D and G-H) with $x_{\mathrm{DOPC}} = 0.05$ (A-D) and $x_{\mathrm{DOPC}} = 0.25$ (E-H). The beads employed for the Voronoi construction C2A and C2B are represented by black dots, the corresponding polyhedra of DPPC and DOPC are coloured blue and green respectively.

5.3.2.1 Lipid dynamics of asymmetric DPPC/DOPC bilayers

The dynamic properties of the lipids within the mixture bilayer can also reveal the effect of DOPC addition. The lateral diffusion coefficients of DPPC and DOPC are computed from the mean square displacement (MSD) (see figures 5.14 and 5.15) and numerical results are reported in Tables 5.4 and 5.5. The resulting diffusion coefficients are comparable with those reported in experiments of lipids in the L_d phase [29], of the order of $10^{-7}\mathrm{cm}^2\mathrm{s}^{-1}$. We note that the lateral diffusion coefficients fluctuate only slightly with the composition of DOPC at a given temperature, and DPPC phospholipids are found to diffuse slightly more rapidly than DOPC due to the large head-group area of the latter.

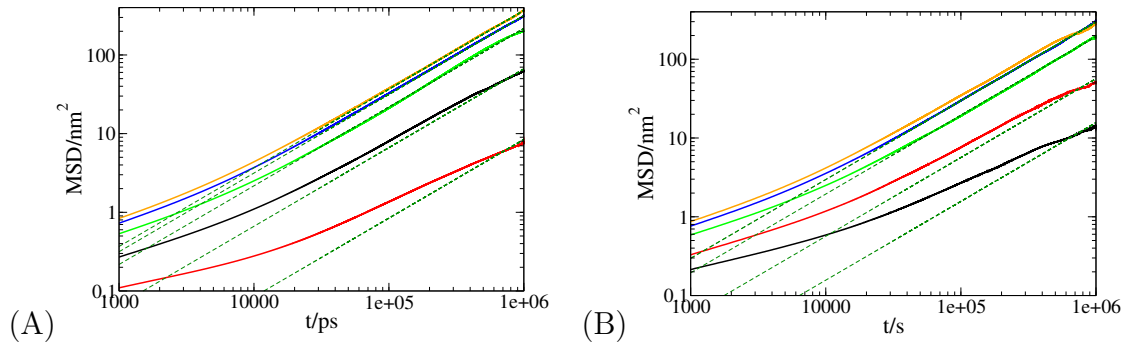

Figure 5.14: Lateral mean square displacement (MSD) of the DPPC (A) and DOPC (B) molecules in DPPC/DOPC bilayers as a function of temperature at $x_{\mathrm{DOPC}} = 0.05$, from bottom to top 285 K, 295 K, 305 K, 315 K and 325 K. Dashed lines represent the expected behavior of the MSDs in the diffusive regime.

Table 5.4: Lateral diffusion coefficient of DPPC, $D_{\mathrm{DPPC}}/10^{-7}\mathrm{cm}^2\mathrm{s}^{-1}$. The hyphen "–" represents systems for which diffusive behaviour was not reached in our simulation time scale.

x_{DOPC}	285	295K	305K	315K	325K
0	–	–	–	7.81	9.28
0.05	–	–	5.43	7.88	9.19
0.125	3.41	4.54	6.72	7.81	9.07
0.25	3.54	4.78	6.21	7.96	9.05
0.5	3.92	4.48	4.95	7.70	9.87

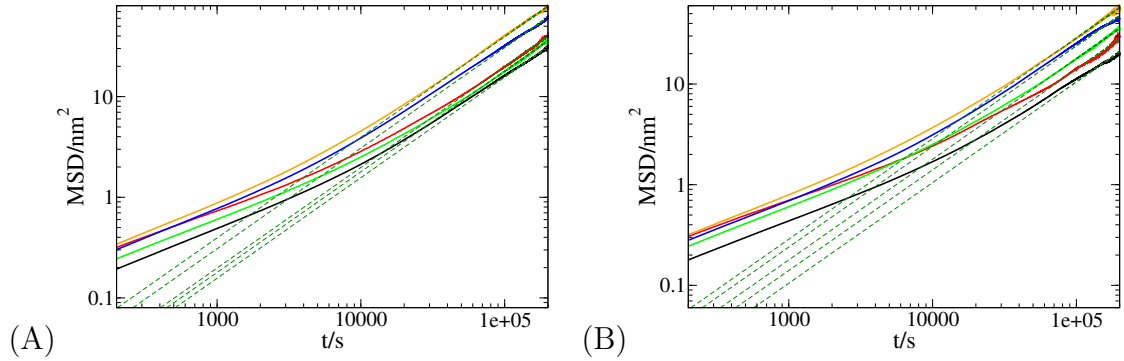

Figure 5.15: Temperature dependence of the MSD of DPPC (A) and DOPC (C) at $x_{\mathrm{DOPC}} = 0.5$, from bottom to top 285 K, 295 K, 305 K, 315 K and 325 K. Dashed lines represent the expected behavior of the MSDs in the diffusive regime.

Table 5.5: Lateral diffusion coefficient of DOPC, $D_{\mathrm{DOPC}}/10^{-7}\mathrm{cm}^2\mathrm{s}^{-1}$. The hyphen "–" represents systems for which diffusive behaviour was not reached in our simulation time scale.

x_{DOPC}	285	295K	305K	315K	325K
0.05	–	–	4.86	7.44	7.41
0.125	3.30	3.59	6.24	6.76	8.74
0.25	2.96	3.91	4.98	6.84	8.25
0.5	2.62	3.51	4.48	6.00	7.18
1	2.93	3.88	5.00	6.62	8.94

The overall conclusions that can be drawn by combining the information given from the parameters reported above, is that the addition of DOPC to one monolayer is enough to inhibit the first order $S_o \rightarrow L_d$ melting transition and the transition temperature. For $x_{\mathrm{DOPC}} = 0.05$, the melting temperature is reduced to $\sim$ 300 K. We did not observe a transition for bilayers containing more than 5% DOPC, where DPPC/DOPC binary mixture bilayers feature only a pure fluid phase between 285 and 325 K. This is in disagreement with the general demixing theory of phospholipids and previous experimental results [16, 17, 14], where clear gel/fluid coexistence should be observed over a broad range of temperatures and compositions. Further investigation is required to examine the applicability of MARTINI CG models to reproduce the phase behaviour of DPPC/DOPC bilayers.

5.3.3 Self-assembled DPPC/DOPC bilayer at $x_{DOPC} = 0.5$

A self-assembled DPPC/DOPC bilayer was constructed to investigate the effect of bilayer heterogeneity on its phase behaviour (see figure 5.19). The initial configuration was obtained by mixing the gel phase DPPC and fluid phase DOPC molecules freely in order to minimise the time-scale for the possible gel phase formation.

This self-assembled bilayer behaves in a similar way to the asymmetric bilayer

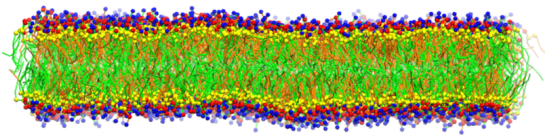

Figure 5.16: Self-assembled equi-molar DPPC/DOPC bilayer, $x_{DOPC} = 0.5$. orange:DPPC, green:DOPC, blue:choline group, red:phosphate group, yellow: glycerol ester group, water molecules were removed for clarity.

(one pure DOPC monolayer and one pure DPPC monolayer) at $x_{DOPC} = 0.5$. The area per DPPC and DOPC increases gradually upon increasing the temperature (see figure 5.17B), but no discontinuity can be seen. The area per lipid approaches to the same value compared with the asymmetric bilayer. The 2D RDFs plotted in figure 5.17A reveal the loss of the long range ordering.

The disordering in the hydrocarbon tails was quantified from the values of S_{chain}. Like in the asymmetric bilayer at the same composition, only single peaks are observed when analysing the probability distribution of all the molecules across the whole bilayer (see figure 5.18). Therefore, there is no indication of phase coexistence.

Since there is hardly any difference in the structural parameters between the asymmetric and self-assembled DPPC/DOPC bilayers (see figures 5.18 and 5.17), we can conclude that the two monolayers within the DPPC/DOPC bilayer couple strongly. From the results reported above, we can conclude that self-assembled DPPC/DOPC bilayers at $x_{\mathrm{DOPC}} = 0.5$ exhibits only a fluid phase in the temper-

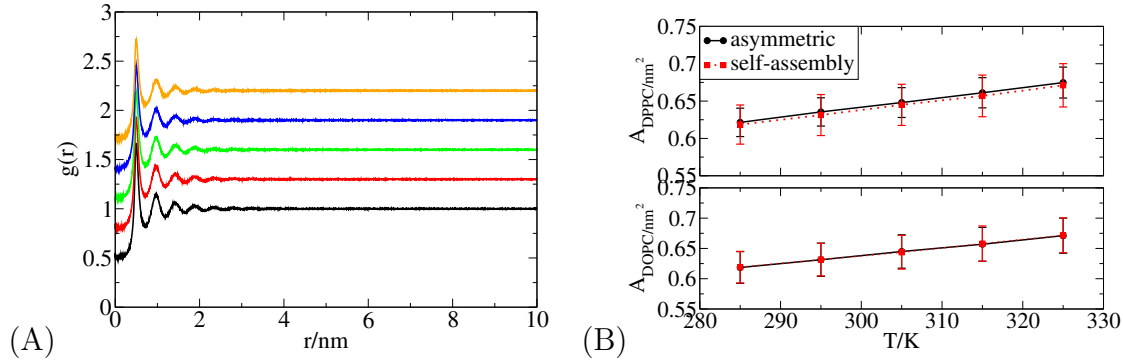

Figure 5.17: RDFs of the central beads (C2A and C2B) of self-assembly bilayers at $x_{\mathrm{DOPC}} = 0.5$ (A), from bottom to top, 285 K, 295 K, 305 K, 315 K and 325 K . The RDFs have been shifted by 0.2 units vertically for better clarity. Comparison of area per lipid between self-assembly and asymmetric bilayers (B).

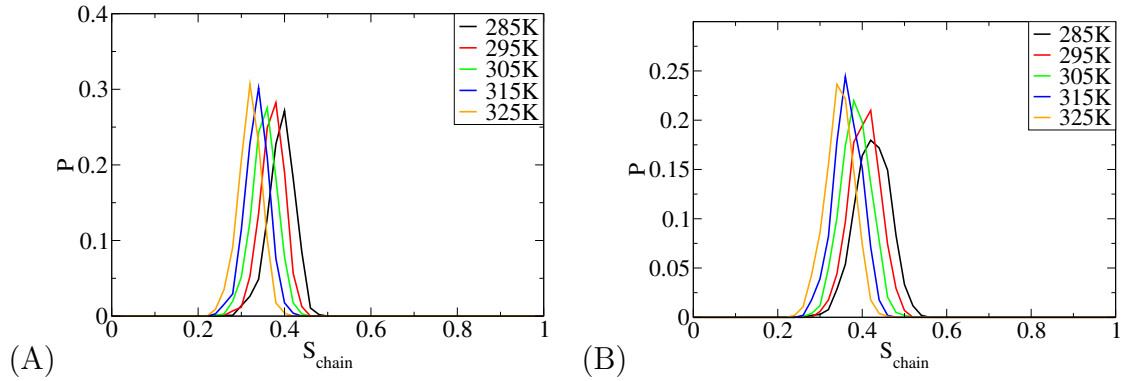

Figure 5.18: Probability of the average chain order parameter of DPPC in DPPC/DOPC bilayers with $x_{\mathrm{DOPC}} = 0.5$ in asymmetric bilayer(A) and self-assembly bilayer(B)

ature range from 285 K to 325 K. Overall, no evidence of phase coexistence was found for the self-assembled bilayers.

5.3.4 Phase behaviour of symmetric DPPC/DOPC bilayers

A further investigation was made with symmetric DPPC/DOPC bilayers, which were obtained by merging gel phase DPPC and fluid phase DOPC configuration

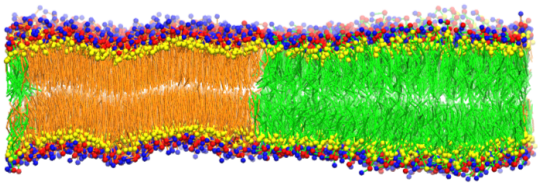

Figure 5.19: An example of symmetric equi-molar DPPC/DOPC bilayer, $x_{DOPC} = 0.5$. orange:DPPC, green:DOPC, blue:choline group, red:phosphate group, yellow: glycerol ester group, water molecules were removed for clarity.

side by side. Such a method of configuration construction has been applied in a united-atom simulation study for accurate main phase transition temperature determination and can minimize the effect of slow kinetics of the gel-transition [30]. The gel phase DPPC bilayer can also provide a nucleation site which can initiate gel formation within the binary mixture.

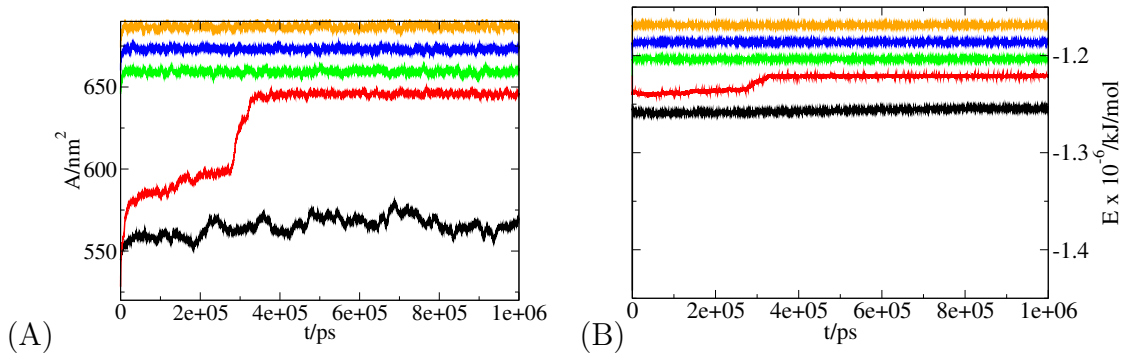

Figure 5.20: Evolution of the cross-sectional area of the simulation box (A) and potential energy (B) with $x_{DOPC} = 0.5$, from bottom to top :285 K, 295 K, 305 K, 315 K and 325 K.

The equilibration process was monitored by checking the cross-sectional area of the simulation box and potential energy of the system (see figure 5.20). The bilayer system at 295 K reaches its thermodynamically stable state after $\approx$ 400 ns with a clear jump seen in cross-sectional area and the potential energy of the system, which indicates a possible phase change at this point. More information of the change in structural properties is given below.

5.3.4.1 $S_o \rightarrow L_d$ transition and domain formation

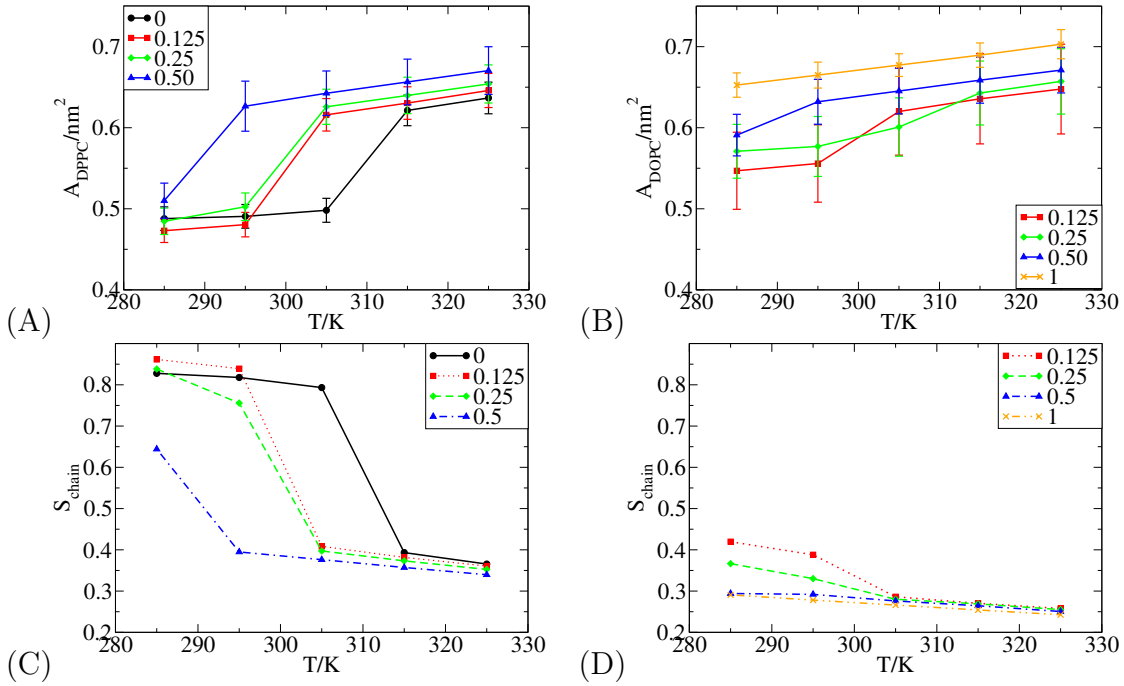

Figure 5.21: Area per DPPC (A) and DOPC (B) across temperature with different compositions of DOPC. Average chain order parameter of DPPC (C) and DOPC (D) molecules versus temperature for different concentrations of DOPC.

Figures 5.21A-B show the area per DPPC and DOPC computed separately using the Voronoi tessellation method. Unlike in the asymmetric bilayer cases, clear jumps in the $a_{DPPC}(x_{DOPC})$ and $a_{DOPC}(x_{DOPC})$ were still observed at high DOPC concentrations (x_{DOPC}=0.5), which can be attributed to the $S_o \rightarrow L_d$ transition. The 'turning point' in area per lipid is shifted to 10 K lower with x_{DOPC} = 0.125 and 0.25, and 20 K lower with x_{DOPC}=0.5 comparing with pure DPPC bilayer (see figure 5.21A). As the T_m of DPPC differs from that of DOPC, the melting temperature of the DPPC/DOPC mixture should fall in the range between T_m(DPPC) and T_m(DOPC). A similar trend is present in the variation of $a_{DOPC}(x_{DOPC})$ with temperature, apart from the case of x_{DOPC}=0.25 where the discontinuity is less obvious and broader. Differences can still be observed between the results seen from pure DOPC bilayers where $a_{DOPC}(x_{DOPC})$ varies linearly.

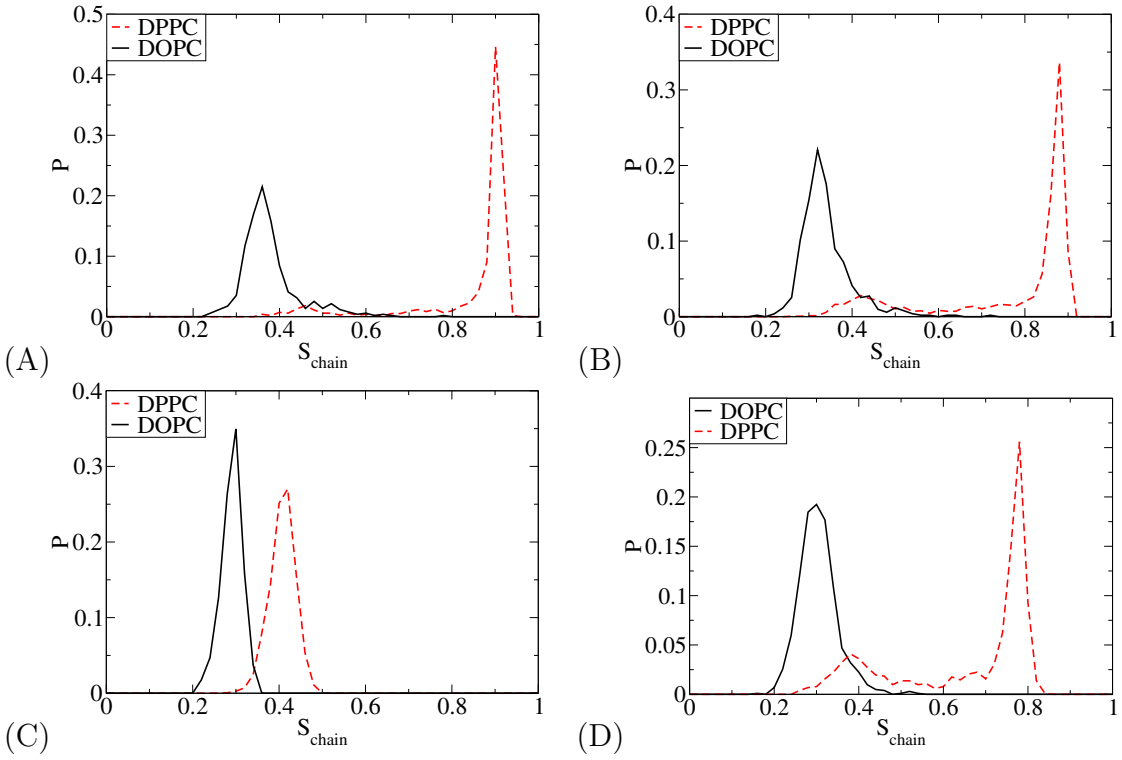

Figure 5.22: Probability distribution S_{chain} for all the lipids within the bilayer that $x_{DOPC} = 0.25$ at 285 K (A), 295 K (B), 305 K (C) and that $x_{DOPC} = 0.5$ at 285K (D). DPPC: dashed red line; DOPC: solid black line.

Plots of S_{chain} versus temperature at different compositions (see figures 5.21C-D) mirror what we have seen with the area per lipid change. A clear drop in S_{chain}(DPPC) reveals that the acyl chains have melted, and clear gel-fluid phase transitions can be seen in the range from 285 K to 305 K for all binary mixtures (see figure 5.21C). The higher values of S_{chain}(DOPC) at low temperatures ($\leq$ 295 K) with low concentrations of DOPC ($x_{DOPC} \leq 0.25$) suggest an increased degree of orientational ordering (see figure 5.21D). The intermediate values of S_{chain} lead to the possibility of gel/fluid phase coexistence, which can be confirmed by considering the probability distribution of S_{chain} over all the lipids from the bilayer. Figures 5.22A& B& D show that most of the DPPC molecules retain a high degree of ordering as in the gel phase ($S_{chain} \approx 0.8$) while a small number of DPPC molecules melt, forming the fluid phase ($S_{chain} \approx 0.4$) at low

temperatures ($\leq$ 295 K). In contrast, DOPC remains in the fluid phase ($S_{chain} \approx$ 0.3). The single peak distributions of DPPC and DOPC in figure 5.22C prove the absence of gel domains.

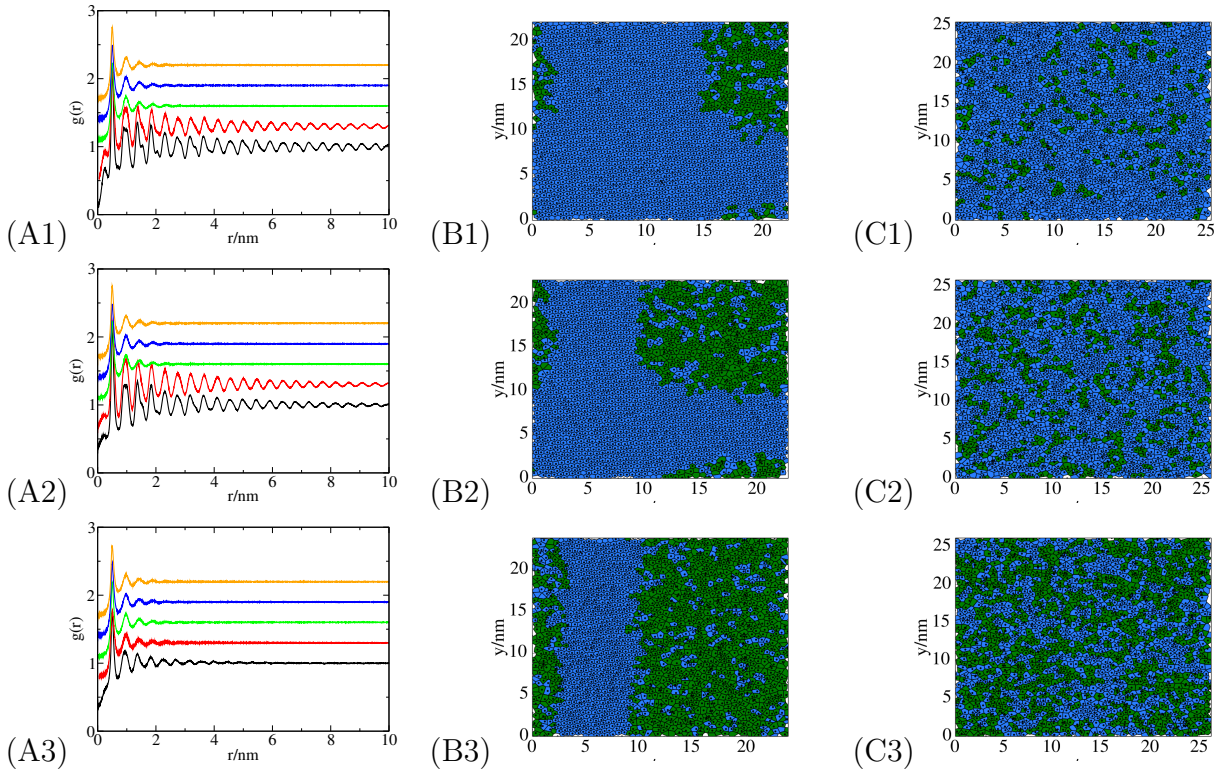

Figure 5.23: 2D RDFs calculated using the middle beads (C2A and C2B) from DPPC and DOPC acyl chains at x_{DOPC} = 0.125 (A1), x_{DOPC} = 0.25 (A2), x_{DOPC} = 0.5 (A3). From bottom to top: 285 K, 295 K, 305 K, 315 K, 325 K. RDFs have been shifted vertically by 0.3 units for better clarity. Snapshots with the same letter denotation (A/B/C) represent the corresponding Voronoi construction plots for half of bilayer at 285K (B1-3) and 325K (C1-3). The beads employed for the Voronoi construction C2A and C2B are represented by black dots, the corresponding polyhedra of DPPC and DOPC are coloured blue and green respectively.

The loss of long range oscillatory order in the 2D radial distribution functions (see Figure 5.23A) characterises the absence of translational ordering due to the $S_o \rightarrow L_d$ phase transition as the temperature increases from 295 K to 305 K ($x_{DOPC} \leq 0.25$), or from 285 K to 295 K ($x_{DOPC} = 0.5$). However, bilayers at low

temperatures feature liquid-like behaviours in the RDFs which is longer ranged than the ones observed in the L_d phase, but weaker in the intensity of peaks than those of gel phase (see figure 5.24A). Voronoi constructions performed on monolayers are consistent with the existence of phase coexistence. At low temperatures (see figure 5.23B), a clear hexagonal packing is seen in some regions of the bilayer, whereas part of the bilayer appears disordered. There is evidence for the presence of lipids in both gel and fluid phases. In contrast, the Voronoi construction reveals a lack of hexagonal order at high temperature, which is compatible with the L_d phase behaviour. The RDFs shown in figure 5.24B also reveal that no major differences can be observed between the DPPC/DOPC bilayers and fluid phase DPPC bilayers at high temperature.

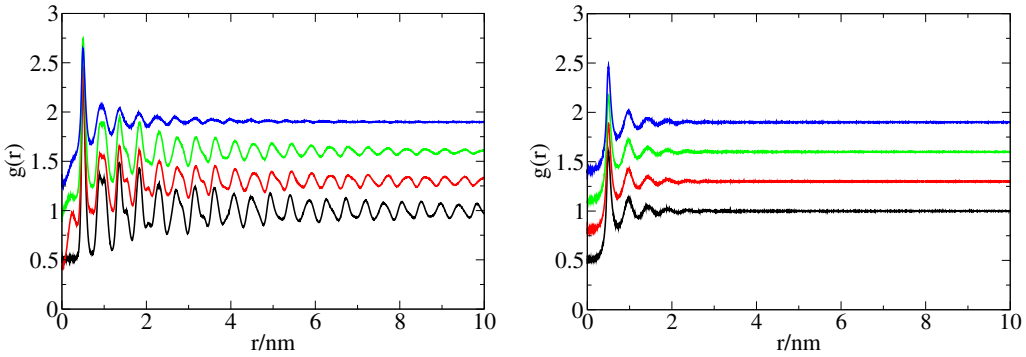

Figure 5.24: RDFs of the central beads (C2A and C2B) in the phospholipid chains. From bottom to top, $x_{DOPC} = 0$, 0.125, 0.25, 0.5 at 285 K (A) and 315 K (B). The RDF's have been shifted by 0.3 units vertically for better clarity.

Our results for the lipid diffusion coefficient show the influence of the lipid mole fraction in difference phases (see table 5.6). The behaviour of the diffusivity is compatible with previous structural analyses. Diffusive behaviour cannot be observed within our simulation time when a large fraction of lipids are in the gel phase. Overall, it is clear that the addition of DOPC tends to lower the transition temperature of $S_o \rightarrow L_d$ compared to pure DPPC. Moreover, a gel/fluid mixture is identified across the temperature range 285 K to 295 K. Hence, we suggest a phase transition from the S_o/L_d coexisting phase to the L_d phase for DPPC/DOPC bilayers where $0.5 \geq x_{DOPC} \geq 0.25$.

Table 5.6: Properties of lipid bilayers with phase coexistence. C_o is lipid concentration in the ordered phase. Lipids are grouped according to their chain order parameter, that is ordered lipids are classified with S_{chain} values greater than 0.6. $D_{\mathrm{DPPC}}/10^{-7}\mathrm{cm}^2\mathrm{s}^{-1}$ is the lateral diffusion coefficient of DPPC. The hyphen "−" represents systems for which diffusive behaviour was not reached in our simulation time scale.

x_{DOPC}	T/K	phase	C_o	$D_{\mathrm{DPPC}}/10^{-7}\mathrm{cm}^2\mathrm{s}^{-1}$
0.125	285	S_o/L_d	0.85	−
0.125	295	S_o/L_d	0.82	−
0.125	305	L_d		3.38
0.125	315	L_d		8.01
0.125	325	L_d		8.98
0.25	285	S_o/L_d	0.69	−
0.25	295	S_o/L_d	0.60	−
0.25	305	L_d		5.85
0.25	315	L_d		6.95
0.25	325	L_d		8.85
0.5	285	S_o/L_d	0.35	0.39
0.5	295	L_d		3.59
0.5	305	L_d		5.62
0.5	315	L_d		7.29
0.5	325	L_d		8.79

5.3.4.2 Exploring the S_o/L_d coexistence regions

As noted in the introduction, DPPC/DOPC bilayers should exist with clear gel/fluid phase coexistence, which was confirmed in our study. To explore the coexistence region and determine the limits of lipid mole fractions forming the pure gel/fluid phases, we analysed the local molar fraction of DOPC using the method described in chapter 3.

The analysis of the phase boundaries was performed on systems that were confirmed by both structural and dynamic studies to exhibit phase coexistence. The local concentration was computed from both monolayers independently. The coordinates of the C2 beads from both lipids were projected onto the xy plane which was then divided into a 3×3 square grid. The molar fraction of DOPC within each grid was calculated and averaged over 900 ns with $\sim$ 1000 configurations. Histograms of molar fractions were then used to compute the probability of finding a particular concentration of DOPC in the bilayer plane. A bi-normal distribution is expected for bilayers under coexistence conditions, where both DOPC-poor (gel) and DOPC-rich (fluid) regions exist.

Two distinctive peaks are observed in figure 5.25A appearing at $x_{DOPC} \approx 0.2$ and ≈ 0.8. The phase boundaries for S_o and L_d coexistence are indicated. The histograms feature three peaks in figure 5.25B, including a very intense one at zero. This may be due to the extremely slow dynamics of the lipid molecules. Therefore, the lipid molecules cannot diffuse much within the simulation time and many of the grids remain DOPC-free or DPPC-free. One possible solution is to start with a uniformly distributed DPPC/DOPC mixture rather than having only single lipids on each side. The other two maxima were found at x_{DOPC} $\sim$0.17 and x_{DOPC} $\sim$0.68. These results are compatible with S_o/L_o coexistence as seen from their Voronoi constructions, and we will use them below to construct the phase diagram of the DPPC:DOPC:water mixture. Above 303 K, the interface between gel and fluid phases quickly disappeared and an almost homogeneous distribution of DOPC was found (see figure 5.25C).

A DPPC/DOPC temperature-composition phase diagram (see figure 5.26) was

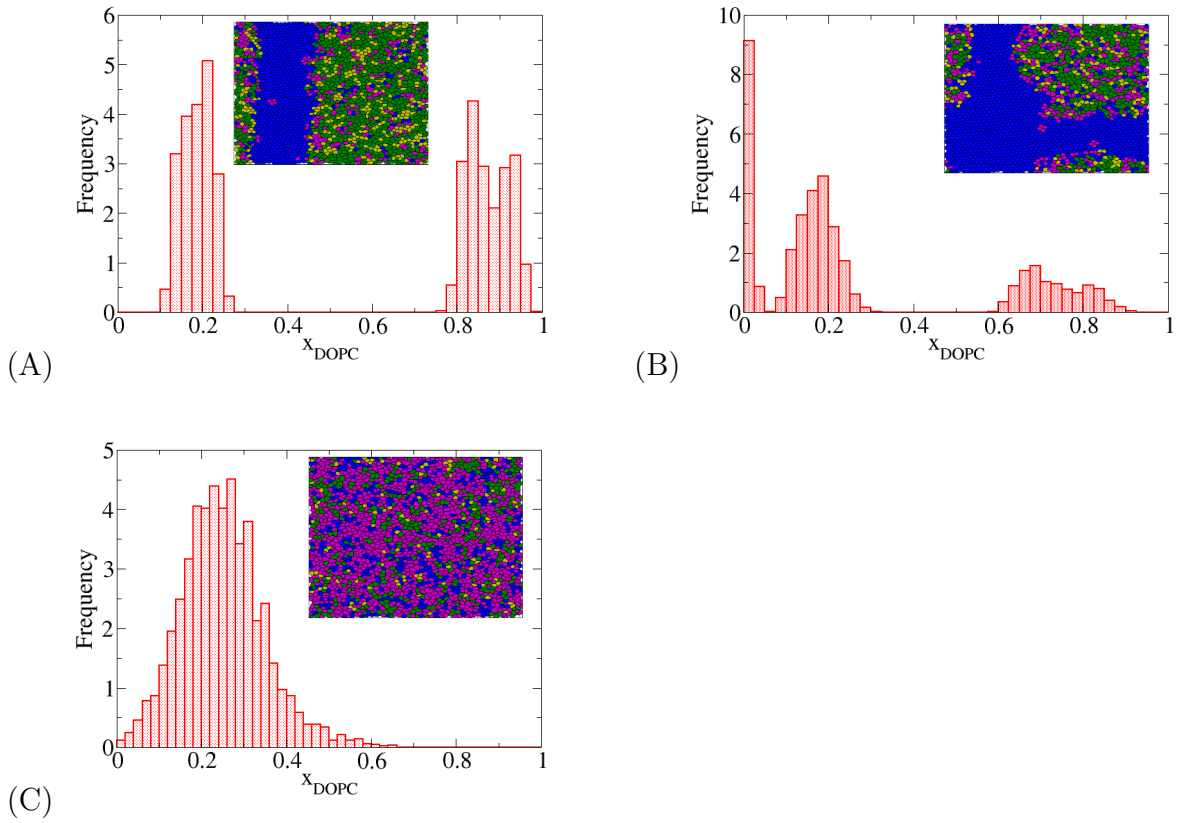

Figure 5.25: Histograms of DOPC concentration obtained with $x_{DOPC} = 0.5$ at 285 K (A), $x_{DOPC} = 0.25$ at 295 K (B) and $x_{DOPC} = 0.25$ at 305 K (C). Insets: Voronoi constructions of the corresponding monolayers. Beads in the ordered or disordered phases as defined by R_{cut} and nearest neighbours (more details are given in chapter 2) are coloured in blue and magenta for DPPC, yellow and green for DOPC respectively.

construed using the observations and data reported above, including structural, dynamic, and examination of representative snapshots. We are aware of the current limitations of simulation models and methods, which lead to restrictions in the precision of tie-lines. Consequently, uncertainties in the coexistences lines have been included. A broad range of S_o/L_o coexistence is shown in the proposed phase diagram below the pure DPPC bilayer melting temperature. With increasing amount of DOPC, L_d behaviour starts to dominate. Good agreement is found by comparing the proposed phase diagram with previous theoretical (see

figure 5.27) [17] and experimental studies [14].

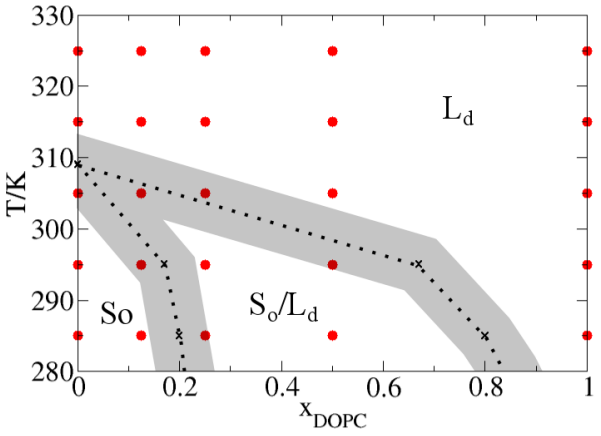

Figure 5.26: DPPC/DOPC phase diagram proposed in this work. The S_o/L_d coexistence lines were estimated from the analysis of the DOPC concentration histograms, and the S_o/L_d transition is based on the analysis of the structural parameters of DPPC. The grey areas give an indication of the estimated uncertainties in the coexistence lines.

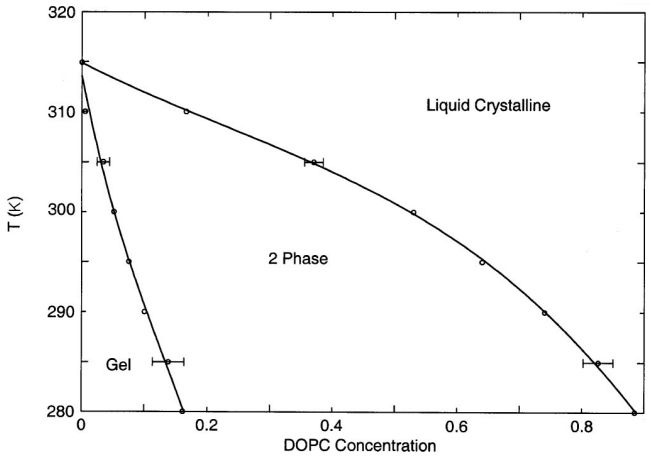

Figure 5.27: A calculated phase digram derived from a molecular model of DPPC/DOPC bilayer which is solved with self-consistent field theory [17].

5.4 Conclusions

In this chapter a comprehensive investigation of the phase behaviour of fully hydrated DPPC/mono-unsaturated DOPC mixtures is described. Several order parameters were reported to give insight into the phase behaviour of DPPC/DOPC mixtures.

Results from the studies on asymmetric and self-assembled bilayers reveal that pure fluid phase bilayers were observed with more than 5% DOPC embedded and gel domains did not form spontaneously. Similar problems have been reported by Baoukina et.al [9] with the application of the MARTINI force-field. This may be related to the original MARTINI parametrization, which was devised to target the properties of the fluid phase. Consequently, a nucleation site is essential for the studies of gel phase behaviour with restricted simulation time.

Good agreement is found with previous observations from experiments and simulations for symmetric bilayers with a gel-fluid boundary region. The $S_o \rightarrow L_d$ phase transition upon increasing the concentration of DOPC was successfully reproduced by the MARTINI model. The S_o/L_d phase coexistence was observed below T_m(DPPC) for a wide range of DOPC composition. A small number of DOPC molecules ($x_{DOPC} \leq 0.125$) was found to have little impact on the structure of gel phase DPPC. At high concentrations ($x_{DOPC} \geq 0.25$), DOPC starts to disrupt the regular packing of DPPC and the fluid phase domain grows. No phase change was observed above the melting temperature of pure DPPC. The tie-lines of S_o/L_d phase coexistence were explored and reported, but we cannot discount at this point the formation of long lived metastable domains. Greater simulation time is required to extend the study with greater sampling of the lipid dynamics. Overall, our DPPC/DOPC phase diagram provides clear insights into the binary mixture phase behaviour.

Summary:

- Examined the influence of unsaturated phospholipids DOPC on saturated phospholipid DPPC bilayers using MARTINI force-field CG-MD simulations.

- Understood the structural and dynamic properties of symmetric, asymmet-

ric and self-assembled DPPC/DOPC bilayers quantitatively.

- Investigated the effect of membrane heterogeneity on phase behaviour of DPPC/DOPC mixture bilayers.
- Explored the possible phase coexistences of the mixture bilayers.
- Proposed a temperature-composition DPPC/DOPC phase diagram.

Future work:

- Longer simulations to reduce the uncertainties of S_o/L_d tie-lines in the proposed phase diagram.
- Construction of the asymmetric DPPC/DOPC bilayers with different number of lipids in each monolayer, in order to retain the ordered structure of DPPC lipids.
- Discussion on the possible more accurate methods of investigating phase coexistences.

References

[1] M. R. Ali, K. H. Cheng, and J. Huang. Assess the nature of cholesterol-lipid interactions through the chemical potential of cholesterol in phosphatidylcholine bilayers. *Proceedings of the National Academy of Sciences*, 104(13):5372–5377, 2007. 131

[2] D. M. Engelman. Membranes are more mosaic than fluid. *Nature*, 438(7068):578580, 2005. 132

[3] D. Lingwood and K. Simons. Lipid rafts as a membrane-organizing principle. *Science*, 327(5961):46–50, 2010. 132

[4] K. Simons and E. Ikonen. Functional rafts in cell membranes. *Nature*, 387(6633):569572, 1997. 132

[5] L. J. Pike. Lipid rafts: bringing order to chaos. *Journal of Lipid Research*, 44(4):655–667, 2003. 132

[6] L. J. Pike. Rafts defined: a report on the keystone symposium on lipid rafts and cell function. *Journal of Lipid Research*, 47(7):1597–1598, 2006. 132

[7] G. W. Feigenson. Phase diagrams and lipid domains in multicomponent lipid bilayer mixtures. *Biochimica et Biophysica Acta (BBA) - Biomembranes*, 1788(1):47 – 52, 2009. 132

[8] S. L. Veatch and S. L. Keller. Seeing spots: Complex phase behavior in simple membranes. *Biochimica et Biophysica Acta (BBA) - Molecular Cell Research*, 1746(3):172 – 185, 2005. 132

[9] S. Baoukina, E. Mendez-Villuendas, W. F. D. Bennett, and D. P. Tieleman. Computer simulations of the phase separation in model membranes. *Faraday Discuss.*, 161:63–75, 2013. 133, 160

[10] P. Uppamoochikkal, S. Tristram-Nagle, and J. F. Nagle. Orientation of tie-lines in the phase diagram of DOPC/DPPC/cholesterol model biomembranes. *Langmuir*, 26(22):17363–17368, 2010. 133

[11] J. Juhasz, F. J. Sharom, and J. H. Davis. Quantitative characterization of coexisting phases in DOPC/DPPC/cholesterol mixtures: Comparing confocal fluorescence microscopy and deuterium nuclear magnetic resonance. *Biochimica et Biophysica Acta (BBA) - Biomembranes*, 1788(12):2541 – 2552, 2009. 133

[12] J. de Joannis, P. S. Coppock, F. Yin, M. Mori, A. Zamorano, and J. T. Kindt. Atomistic simulation of cholesterol effects on miscibility of saturated and unsaturated phospholipids: Implications for liquid-ordered/liquid-disordered phase coexistence. *Journal of the American Chemical Society*, 133(10):3625–3634, 2011. 133

[13] M. R. Vist and J. H. Davis. Phase equilibria of cholesterol/dipalmitoylphosphatidylcholine mixtures: deuterium nuclear magnetic resonance and differential scanning calorimetry. *Biochemistry*, 29(2):451–464, 1990. 133

[14] M. L. Schmidt, L. Ziani, M. Boudreau, and J. H. Davis. Phase equilibria in DOPC/DPPC: Conversion from gel to subgel in two component mixtures. *The Journal of Chemical Physics*, 131(17):–, 2009. 133, 134, 148, 159

[15] B. R. Lentz, Y. Barenholz, and T. E. Thompson. Fluorescence depolarization studies of phase transitions and fluidity in phospholipid bilayers. 2. two-component phosphatidylcholine liposomes. *Biochemistry*, 15(20):4529–4537, 1976. 133

[16] K. Furuya and T. Mitsui. Phase transitions in bilayer membranes of dioleoyl-phosphatidylcholine/dipalmitoyl-phosphatidylcholine. *Journal of the Physical Society of Japan*, 46(2):611–616, 1979. 133, 134, 148

[17] R. Elliott, K. Katsov, M. Schick, and I. Szleifer. Phase separation of saturated and mono-unsaturated lipids as determined from a microscopic model. *The Journal of Chemical Physics*, 122(4):–, 2005. 133, 134, 148, 159

[18] T. T. Mills, J. Huang, G. W Feigenson, and J. F Nagle. Effects of cholesterol and unsaturated DOPC lipid on chain packing of saturated gel-phase DPPC bilayers. *General physiology and biophysics*, 28(2):126139, 2009. 133

[19] T. Schubert, E. Schneck, and M. Tanaka. First order melting transitions of highly ordered dipalmitoyl phosphatidylcholine gel phase membranes in molecular dynamics simulations with atomistic detail. *The Journal of Chemical Physics*, 135(5):055105, 2011. 133

[20] S. Tristram-Nagle and J. F. Nagle. Lipid bilayers: thermodynamics, structure, fluctuations, and interactions. *Chemistry and Physics of Lipids*, 127(1):3 – 14, 2004. 133

[21] A. S. Ulrich, M. Sami, and A. Watts. Hydration of DOPC bilayers by differential scanning calorimetry. *Biochimica et Biophysica Acta (BBA) - Biomembranes*, 1191(1):225 – 230, 1994. 133, 138

[22] S. J. Marrink, H. J. Risselada, S. Yefimov, D. P. Tieleman, and A. H. de Vries. The MARTINI force field: coarse grained model for biomolecular simulations. *The Journal of Physical Chemistry B*, 111(27):7812–7824, 2007. PMID: 17569554. 135, 141

[23] J. F. Nagle and S. Tristram-Nagle. Structure of lipid bilayers. *Biochimica et Biophysica Acta (BBA) - Reviews on Biomembranes*, 1469(3):159 – 195, 2000. 135

[24] J. Yuan, C. Hao, M. Chen, P. Berini, and S.F Zou. Lipid reassembly in asymmetric Langmuir-Blodgett/Langmuir-Schaeffer bilayers. *Langmuir*, 29(1):221–227, 2013. PMID: 23215148. 135

[25] H. I. Petrache, S. Tristram-Nagle, K. Gawrisch, D. Harries, A. Parsegian, and J. F. Nagle. Structure and fluctuations of charged phosphatidylserine

bilayers in the absence of salt. *Biophysical Journal*, 86(3):1574 – 1586, 2004. 139

[26] A. Liu and X. Qi. Molecular dynamics simulations of DOPC lipid bilayers: The effect of lennard-jones parameters of hydrocarbon chains, 2012. 139

[27] T. T. Mills, G. E.S. Toombes, S. Tristram-Nagle, D. Smilgies, G. W. Feigenson, and J. F. Nagle. Order parameters and areas in fluid-phase oriented lipid membranes using Wide Angle X-Ray Scattering. *Biophysical Journal*, 95(2):669 – 681, 2008. 139

[28] B. Fadeel and D. Xue. The ins and outs of phospholipid asymmetry in the plasma membrane: roles in health and disease. *Critical reviews in biochemistry and molecular biology*, 44(5):264–277, 2009. 141

[29] A. Filippov, G. Oradd, and G. Lindblom. Lipid lateral diffusion in ordered and disordered phases in raft mixtures. *Biophys. J.*, 86:891–896, 2004. 147

[30] P. S. Coppock and J. T. Kindt. Determination of phase transition temperatures for atomistic models of lipids from temperature-dependent stripe domain growth kinetics. *The Journal of Physical Chemistry B*, 114(35):11468–11473, 2010. 151

Chapter 6

Conclusions

In this PhD thesis, I have presented a simulation study of a coarse-grained model consisting of DPPC and other lipid components. I employed the MARTINI coarse-grained force-field to simulate mesoscopic systems consisting of several thousand phospholipids and covering timescales of tens of microseconds. The biological functions of cell membranes are strongly related to the thermodynamic state of the membranes, and for this reason my discussion has been restricted mainly to the investigation of phase transitions. Moreover, since phosphocholine is the predominant phospholipid in most mammalian membranes ($> 50\%$), the focus of my work has been primarily on the bilayers containing saturated 1,2-dipalmitoyl-*sn*-glycero-3-phosphocholine (DPPC), and mixtures with cholesterol or unsaturated 1,2-dioleoyol-*sn*-glycero-3-phosphocholine (DOPC).

6.1 DPPC/cholesterol bilayer

In a first stage, I investigated the validity of MARTINI CG model with simple DPPC bilayers to predict the gel-fluid phase transition temperature through a few structural parameters.

The first conclusion is that the study of gel-fluid melting temperature ($305 - 315\ K$) reveals a good agreement with previous experimental ($\approx 314.2\ K$) and simulation studies generally. However, the MARTINI coarse-grained (CG) model predicts a main transition temperature ($295 - 315\ K$) that is lower than the

experimental ones. Overall, the simulation results of structural and dynamic parameters are in a good agreement with those reported experimentally.
In a second stage, we have introduced a model of DPPC and cholesterol to study the effect of cholesterol on the bilayer structure. In this model, cholesterol is represented by a bulky hydrophobic core, a small hydrophilic head, and a short hydrophobic tail. The reduced degree of coarse graining of cholesterol compared to the phospholipids allows the MARTINI cholesterol molecule to keep its ring geometry.
Our DPPC/cholesterol bilayer model agrees well with experimental data on structural and dynamic properties of the bilayer, as well as with all-atom simulation results. The addition of cholesterol to DPPC bilayers has been proposed to lead to the formation of the liquid ordered (L_o) phase where the movement of lipid tails is restricted by cholesterol molecules. We also find that cholesterol destabilises the DPPC gel phase and stabilises the liquid ordered phase. The addition of cholesterol, upto 30 mol%, is found to have little impact on the melting temperature of the gel-fluid transition. At high temperatures the bilayer can accommodate up to 50 mol% of cholesterol without significantly disrupting its structure. We observe a triple point at $x_{chol} \approx 0.3$ which signals the formation of the liquid ordered (L_o) phase. Only an L_o phase is observed at high concentrations of cholesterol ($x_{chol} > 0.5$) within the temperature range of our study, $283 < T < 323\ K$. These observations agree with the results of many experimentally studied DPPC/cholesterol bilayers. The main result of the DPPC/cholesterol bilayer study is the temperature-composition phase diagram. Our results support S_o/L_o coexistence but not L_d/L_o coexistence. We have performed an analysis to examine the latter transition that has been reported in some experimental and simulated works. However, a second order transition scenario seems to be the most likely for the L_d/L_o transition within the MARTINI model. Notwithstanding the limited time scale and the simplicity of the MARTINI model, our proposed phase digram provides insight into the phase behaviour of DPPC/cholesterol bilayers and gives a wealth of information on the molecular organisation of the molecules at different phases.

6.2 Modified MARTINI cholesterol model

In a third stage, I further investigated in detail some interesting features of MARTINI CG cholesterol molecules observed in chapter 3. The size of original MARTINI CG beads was either increased or decreased by 15%. These two modified CG cholesterol types were simulated in a bilayer together with DPPC to investigate the induced specific spatial order and influence on the $S_o \rightarrow L_d$ phase transition. The study of modified CG cholesterols is of great interest since the structural organization of the cholesterol molecules in the L_o phase shows very interesting features. The strong mismatch in cross-sectional area between cholesterol and phospholipid is thought to disrupt the lateral packing within the bilayer. Therefore, the simulation of DPPC with different sized cholesterol models is of particular interest. Several papers suggest that the formation of 'thread-like' linear cluster is due to the asymmetric planar structure of cholesterol molecules where two off-plane methyl groups are attached to one side of its tetracyclic ring system. Being one of many artefacts of the MARTINI CG model, whereby the asymmetric planar structure of cholesterol is not parametrised. Preliminary simulations of CG DPPC/cholesterol-like sterols a show strong relation between lateral packing and cholesterol size.

We find in our simulations that the linear cluster pattern disappears in the simulations using CG cholesterol beads that are bigger than standard MARTINI ones by 15 % (namely CHO1). The enlarged cholesterol (CHO1) packs less effectively with DPPC acyl chains. In addition, CHO1 is found to position itself closer to the bilayer core and appear to tilt more at the bilayer/water interface. A second order continuous $L_o \rightarrow L_d$ transition is observed with enlarged cholesterol such as CHO1. In contrast, the lipids are packed more closely and the water-sterol contacts are also reduced by decreasing the cholesterol bead size to 85% of the original CG bead (namely CHO2). CHO2 appears to locate closer to itself than to DPPC, allowing optimal packing. The gel phase bilayer with CHO2 is found to be stable from 283 K to 323 K. The observations on the interactions between DPPC and CHO1 or CHO2 suggest that these modified sterol-like molecules act in a similar way to naturally occurred lanosterol and ergosterol in the phase transitions.

6.3 DPPC/DOPC bilayer

In the final stage, I explored the effects of mixing unsaturated lipid with saturated DPPC lipids on the phase behaviour of the bilayer. DOPC was selected as the other components in the bilayers since it is one of the most typical cell membrane lipids. We constructed the mixture bilayers by three methods, namely:

- **asymmetric bilayer** was constructed with a pure DPPC monolayer and a mixed DPPC/DOPC monolayer in a fluid phase to study the effect of bilayer heterogeneity which is a common feature of all eukaryotic membranes.
- **self-assembled bilayer** was obtained using configurations from low temperature simulations which were obtained by simulating randomly placed lipids molecules freely,
- **symmetric bilayer** was built by 'sticking' a gel phase DPPC bilayer and a fluid phase DOPC bilayer side by side.

From the simulations of asymmetric bilayers, the $S_o \rightarrow L_d$ phase transition was not observed with the addition of more than 5 mol% DOPC. Instead, bilayers with more than 5 mol% DOPC embedded were found to exhibit in a pure fluid phase between 283 K and 323 K. Self-assembled bilayers were found to behave in the same way as the asymmetric bilayers, and a strong coupling between two the monolayers was found. Differently, a clear phase transition from ordered to disordered phase can still be observed from the simulations of the symmetric bilayers at high DOPC concentrations ($x_{DOPC} = 0.5$). Unsaturated lipids such as DOPC are known to have a much lower transition temperature than the saturated lipid DPPC. The addition of DOPC to a DPPC bilayer has been found to lower the phase transition temperature. We also find that S_o/L_d coexistence occurs over a wide range of DOPC compositions and temperatures by checking the quantitative results and visual observations. This conclusion supports the data reported by previous experimental and theoretical works. A temperature-composition phase

diagram showing the S_o/L_d coexistence was proposed based on the simulation results of the symmetric bilayers.

6.4 Limitations

This work also illustrates some of the limitations associated with the use of the MARTINI coarse-grained model on phospholipid membrane simulations. In general the MARTINI model allows long simulation times and larger system sizes, but is still subjected to the highly coarse grained structures of the molecules, and the MARTINI force-field is parametrised to reproduce the properties of the liquid phase but not the solid phase. For instance, we observed the formation of linear clusters at high cholesterol concentrations ($x_{chol} \geq 0.4$) which is not supported by atomistic simulations. Despite these limitations, the MARTINI coarse-grained model is a powerful model that can be used to study the phase behaviour of lipid membranes. With fast and simple simulations better understanding of phase transitions can be obtained on the biological membranes. Our results show that the MARTINI model can capture quantitatively the effects of lipids on phase transitions, and can predict structural parameters in good agreement with experimental observations.

6.5 Future work

This thesis up to now suggests a few possible extensions.

1. First of all, the simulations on exploring the phase coexistence regions gives an idea of phase boundaries, but more extensive computations, are needed to ensure sufficient sampling of the lipid dynamics. Metastable domains can be long lived due to the very slow dynamics of lipids. As noted in Chapters 3 and 5, this gives rise to uncertainties in proposed results: the tie-lines shown in phase diagrams are given with quite big error bars. The obvious

solution to this would be to extend the simulation study to a microscopic system size over a simulation time of the order of 100 μs. However, this requires extensive computational power. To keep computational costs low, a possible solution could be improving the current method used to investigate the lipid domains. Instead of splitting the bilayer into a few square grids, the phase boundaries could be defined more precisely according to the differences of order parameters in different phases.

2. Apart from the structural and dynamic properties of lipid bilayers I reported in this thesis, there are quite a few other macroscopic properties, such as heat capacity, compressibility and bending moduli, can be investigated. Compressibility and bending moduli will provide understandings of the mechanical properties of the bilayers simulated. Such investigations on L_o phase lipid bilayers are of my interest for future work especially.

3. I should also mention some of the issues in reproducing membrane heterogeneity. I noted at the end of Chapter 5 that many open questions remained on the matter. The ordered structure of lipids in the initial asymmetric bilayers melt immediately. Therefore, there is no chance to investigate the melting process by adding low melting temperature lipids to high melting temperature bilayers with the effect of membrane heterogeneity. Additional work should therefore be undertaken to study the asymmetric bilayers with different number of lipids, so that the ordered structure of lipids in the initial configuration can retain.

4. Amongst other possible future objectives is the back-mapping to atomistic models from the coarse-grained ones studied in this thesis. MARTINI CG force-field allows us to extend the simulation scale extensively. However, the detailed structures of lipids are lack of understanding and some properties can not be compared with experiments directly. After applying back-mapping from pre-equilibrated bilayers under CG force-field, the atomistic

bilayers that are unachievable from direct simulations can be obtained and are readily to use for further investigations.

5. We have performed extensive investigations of phase transitions of binary mixtures. My results provide insights into the general phase transition and phase coexistence features. However, real biological systems contain thousands of components including a wide variety of lipids and proteins. Future work in the simulation of ternary or quaternary mixtures is therefore needed. Beyond the common lipids, bilayers containing proteins are also of great interest. Once the study of ternary or quaternary systems is completed and better understood, it can be used for extensive investigations of lipid-protein interactions and functions in bio-membranes.

6. Currently, the bilayers simulated in this work were pre-assembled into lamellar phases. However, depending on the combination of various factors, non-lamellar structure can exist. As a function of water content and temperature, different aggregates structures can form, such as micelle, tubular and bilayer. It would also be interesting to investigate non-lamellar phases self-assembled from different lipid compositions.